MODELLING AND EXPERIMENTAL EVALUATION OF AN ELECTROHYDRAULIC PITCH TRIM SERVO ACTUATOR

A THESIS SUBMITTED TO
THE GRADUATE SCHOOL OF NATURAL AND APPLIED SCIENCES
OF
MIDDLE EAST TECHNICAL UNIVERSITY

BY

AHMET ÖZTURAN

IN PARTIAL FULFILLMENT OF THE REQUIREMENTS
FOR
THE DEGREE OF MASTER OF SCIENCE
IN
MECHANICAL ENGINEERING

FEBRUARY 2012

Approval of the thesis:

MODELLING AND EXPERIMENTAL EVALUATION OF AN ELECTROHYDRAULIC PITCH TRIM SERVO ACTUATOR

submitted by **AHMET ÖZTURAN** in partial fulfillment of the requirements for the degree of **Master of Science in Mechanical Engineering Department, Middle East Technical University** by,

Prof. Dr. Canan ÖZGEN _____
Dean, Graduate School of **Natural and Applied Sciences**

Prof. Dr. Süha ORAL _____
Head of Department, **Mechanical Engineering**

Prof. Dr. Tuna BALKAN _____
Supervisor, **Mechanical Engineering Dept., METU**

Examining Committee Members:

Prof. Dr. Y. Samim ÜNLÜSOY _____
Mechanical Engineering Dept., METU

Prof. Dr. Tuna BALKAN _____
Mechanical Engineering Dept., METU

Asst. Prof. Dr. Yiğit YAZICIOĞLU _____
Mechanical Engineering Dept., METU

Asst. Prof. Dr. Gökhan O. ÖZGEN _____
Mechanical Engineering Dept., METU

Lt. Col. Teoman ÖZMEN, M.Sc. _____
5th Main Maintenance Center

Date: 08.02.2012

I hereby declare that all information in this document has been obtained and presented in accordance with academic rules and ethical conduct. I also declare that, as required by these rules and conduct, I have fully cited and referenced all material and results that are not original to this work.

Name, Last name : Ahmet ÖZTURAN

Signature :

ABSTRACT

MODELLING AND EXPERIMENTAL EVALUATION OF
AN ELECTROHYDRAULIC PITCH TRIM SERVO ACTUATOR

ÖZTURAN, Ahmet

M. Sc., Department of Mechanical Engineering

Supervisor: Prof. Dr. Tuna BALKAN

February 2012, 107 pages

The pitch trim actuator is a hydraulic powered electro-mechanical flight control device of UH-60 helicopters which converts a mechanical input and an electrical command into a mechanical output with trim detent capabilities. In this thesis study, pitch trim actuator is investigated and a mathematical model is developed. From these mathematical equations, the actuator is modeled in MATLAB Simulink environment.

While constructing the mathematical model, pressure losses in hydraulic transmission lines and compressibility of hydraulic oil are considered. To achieve a more realistic model for valve torque motor, particular tests are carried out and the torque motor current gain and the stiffness of torque motor flexure tube and the flapper displacement are obtained.

Experimental data to verify the Simulink model is acquired with KAM-500 data acquisition system. A test fixture is designed for acquiring the experimental data. This test fixture can also be used to test the pitch trim actuator during depot level maintenance and overhaul.

To verify the consistency of Simulink model, acquired experimental data is implemented in Simulink environment. The output of Simulink model simulation and the experimental data are compared. The results of comparison show that the model is good enough to simulate the steady state behavior of the actuator.

Keywords: Fluid power control, Valve torque motor, Electrohydraulic actuator, Hydraulic modeling

ÖZ

YUNUSLAMA HAREKETİ DENGE KONUMU
ELEKTROHİDROLİK SERVO EYLEYİCİSİNİN
MODELLENMESİ VE DENEYSEL DEĞERLENDİRMESİ

ÖZTURAN, Ahmet
Yüksek Lisans, Makina Mühendisliği Bölümü
Tez yöneticisi: Prof. Dr. Tuna BALKAN
Şubat 2012, 107 sayfa

Yunuslama hareketi denge konumu eyleyicisi, aldığı mekanik ve elektriksel girişi denge konumu sabitleme yeteneğine sahip mekanik çıkışa çeviren UH-60 helikopterlerine ait hidrolik ile çalışan elektromekanik bir uçuş komuta aygıtıdır. Bu tez çalışmasında yunuslama hareketi denge konumu eyleyicisi araştırılmış ve matematiksel modeli elde edilmiştir. Elde edilen matematiksel model kullanılarak eyleyicinin MATLAB Simulink ortamında analizi yapılmıştır.

Matematiksel model oluşturulurken hidrolik hatlardaki basınç kayıpları ve hidrolik sıvısının sıkışabilirliği dikkate alınmıştır. Eyleyicinin tork motorunun daha gerçekçi modelini oluşturmak için ilave testler yapılmış ve tork motorunun akım kazancı, esnek borunun yay sabiti ve tork motor üzerindeki plakanın hareketi belirlenmiştir.

Simulink modelini doğrulamak için KAM-500 veri toplama sistemi kullanılarak deneysel çalışmalar yapılmıştır. Deneysel çalışmalar için bir test mastarı tasarlanmıştır. Bu test mastarı kapsamlı bakım ve yenileştirme sonrası yunuslama hareketi denge konumu eyleyicisini test etmek için de kullanılmaktadır.

Simulink modelinin doğrulanması için toplanan deneysel veriler Simulink ortamına aktarılmıştır. Simulink modelinin benzetim sonuçları ile deneysel sonuçlar

karşılaştırılmıştır. Karşılaştırma sonuçları, Simulink modelinin eyleyicinin sürekli rejim tepkisini belirlemek için yeterli olduğunu doğrulamıştır.

Anahtar Kelimeler: Akışkan gücü kontrolü, Valf tork motoru, Elektro-hidrolik eyleyici, Hidrolik modelleme

To my daughter,

to my wife and

to my parents.

ACKNOWLEDGEMENTS

I would like to express my sincere gratitude to my supervisor Prof. Dr. Tuna Balkan for his precious support and guidance through the thesis. This thesis wouldn't have been possible without his encouragement.

I would like to special thanks to Hakan Çalışkan for his support, valuable discussion and for his time through my visits at his office.

Special thanks to Lt. Col. Dilek Özer, whom shows me a tolerance about finishing this study, instead of workload in 5th Main Maintenance Command.

I would like also thanks to Necati Yılmaz, Seçkin Karakuş, Teoman Özmen and other hydraulic workshop personnel for their support during experimental study. I am also thankful to my colleague Nurettin Özkök, Erhan Bayat, Mahir Ali Koç, Harun Önce, Murat Çakıcı, Bülent Burçak, Onur Yıldırım, Muhammet Yılmaz and Ozan Aktaş for their precious support, and discussion.

I would like to sincerely thank to my wife Aysun Tezel Özturan for her love and patience. I am grateful that I have such a great wife. I also thank to my parents who made all of this possible, for their endless love and support.

This study could not be realized without the support of 5th Main Maintenance Command (5th MMC).

Any opinion sited in this thesis does not reflect the official view of Turkish Armed Forces.

TABLE OF CONTENTS

LIST OF FIGURES

FIGURES

LIST OF TABLES

TABLES

LIST OF SYMBOLS

A_a	cross-sectional area of air gap (m^2)
A_m	sum of cross-sectional areas of permanent magnets (m^2)
A_o	area of fixed orifices (m^2)
A_p	the cross-sectional area of pistons (m^2)
B_r	residual magnetic flux density of permanent magnet (T)
C_{C1}	hydraulic capacitance for the hydraulic line of first cylinder
C_{C2}	hydraulic capacitance for the hydraulic line of second cylinder
C_{dn}	discharge coefficient of variable orifices
C_{do}	discharge coefficient of fixed orifices
$F_{P_{C1}}$	force due to first cylinder pressure (N)
$F_{P_{C2}}$	force due to second cylinder pressure (N)
F_{P_r}	force due to return pressure (N)
F_1	reaction force acting on first piston (N)
F_2	reaction force acting on second piston (N)
F_{spr1}	spring force acting on first piston (N)
F_{spr2}	spring force acting on second piston (N)
I_1	hydraulic inertia for the hydraulic line of first cylinder
I_2	hydraulic inertia for the hydraulic line of second cylinder
J_{tl}	mass moment of inertia of rotating trim lever, gradient spring and input arm ($N.m.s^2/rad$)
J_α	mass moment of inertia of rotating armature ($N.m.s^2/rad$)
K_i	torque motor current gain (N.m/A)
K_m	torque motor electromagnetic spring constant (N.m/rad)
K_p	spring constant of piston spring (N/m)
K_t	the rotational stiffness of flexure tube (N.m)
L_a	distance between poles at both ends of a yoke (m)
L_f	the length of flapper (m)
L_t	the length of flexure tube (m)

L_{tl}	the half length of trim lever (m)
M_m	magneto motive force of permanent magnets
N	number of coil turns
R_1	hydraulic resistance for the hydraulic line of first cylinder
R_2	hydraulic resistance for the hydraulic line of second cylinder
R_a	reluctance of air gap at null
R_m	permanent magnet reluctance
T_m	torque generated by electromagnetic forces (N.m)
T_p	torque due to the pressure difference (N.m)
T_t	torque due to flexure tube (N.m)
V_1	the volume of fluid in hydraulic line of first cylinder (m^3)
V_2	the volume of fluid in hydraulic line of second cylinder (m^3)
V_o	the volume of the cylinder at null position (m^3)
b_j	damping coefficient caused by visco jet (N.s/m)
b_p	viscous damping coefficient of pistons (N.s/m)
d_f	nozzle diameter of flapper nozzle valve (m)
d_f	nozzle diameter of flapper nozzle valve (m)
f_{tl}	damping coefficient of rotating parts (N.m.s/rad)
f_α	damping coefficient of armature (N.m.s/rad)
i	input current to torque motor (A)
k_l	coefficient of leakage flux, i.e. the flux through free space
k_r	magnetic reluctance constant
l_m	length of the permanent magnet (m)
m_p	mass of the pistons (kg)
p_1	pressure at the right side of the flapper (Pa)
p_1	pressure at the inlet of 1st hydraulic line (Pa)
p_2	pressure at the left side of the flapper (Pa)
p_2	pressure at the inlet of 2nd hydraulic line (Pa)
p_{C1}	pressure at the 1st cylinder inlet (Pa)
p_{C1}	pressure in the 1st cylinder(Pa)
p_{C2}	pressure at the 2nd cylinder inlet (Pa)
p_{C2}	pressure at the 2nd cylinder (Pa)
p_r	return pressure (Pa)

p_s	supply pressure (Pa)
ΔP_{I1}	pressure loss due to hydraulic inertia
ΔP_{I2}	pressure loss due to hydraulic inertia
ΔP_{R1}	pressure loss due to resistance of first hydraulic line
ΔP_{R2}	pressure loss due to resistance of second hydraulic line
ΔP_{T1}	total pressure loss at first hydraulic line
ΔP_{T2}	total pressure loss at second hydraulic line
q_1	volumetric flow rate through fixed office at the left (m^3/s)
q_2	volumetric flow rate through fixed office at the right (m^3/s)
q_3	volumetric flow rate through variable office at the left (m^3/s)
q_4	volumetric flow rate through variable office at the right (m^3/s)
q_{C1}	flow rate to the 1st cylinder (m^3/s)
q_{C1}'	flow rate due to the compressibility of hydraulic fluid (m^3/s)
q_{C2}	flow rate to the 2nd cylinder (m^3/s)
q_{C2}'	flow rate due to the compressibility of hydraulic fluid (m^3/s)
x_a	length of air gap (m)
x_f	the displacement of flapper at the tip of the nozzles (m)
x_f	the flapper displacement at the tip of the nozzles (m)
x_i	the initial flapper distance to nozzle and flapper displacement limit (m)
y_i	initial compression of piston spring (m)
y	the displacement of the pistons (m)
y	piston displacement (m)
α	angular displacement of armature (rad)
μ	Dynamic viscosity of hydraulic fluid (Pa.s)
μ_0	permeability of free space (= $4\pi/10^7$) (T.m/A)
μ_m	permeability of permanent magnet (T.m/A)
θ	angular displacement of trim lever (rad)
$\dot{\theta}$	angular velocity of trim lever (rad/s)
$\ddot{\theta}$	angular acceleration of trim lever (rad/s^2)

CHAPTER 1

INTRODUCTION

1.1. Background and Motivations

Helicopters are known as rotary-wing aircrafts, as opposed to fixed-wing aircraft such as airplanes. The helicopter's ability to maneuver in and out of hard-to-reach areas and to hover efficiently for long periods of time makes it valuable for operating in places where airplanes cannot land. These helicopters can perform important military tasks such as ferrying troops directly into combat areas or quickly transporting wounded soldiers to hospitals. The helicopter cannot fly as fast as the airplanes and has a poor cruising performance, but it is the obvious choice for tasks where vertical flight is necessary [1].

In 1907, a French bicycle make named Paul Cornu constructed a vertical flight machine that was reported to have carried a human off the ground for the first time [2]. In 1935, Sikorsky was issued a patent [3], which showed a relatively modern looking single rotor/tail rotor helicopter design with flapping hinges and a form of cyclic pitch control. Although Sikorsky encountered many technical challenges, he tackled them systematically and carefully. Sikorsky's first helicopter, the VS-300, was flying by May 1940 [4].

Today, the helicopter design is more complex and larger helicopters are being designed and manufactured. As the helicopter is becoming larger, the force to operate the flight control is becoming higher, i.e. beyond the handling capability of pilot. So, hydraulic power is utilized to operate the flight controls of helicopters.

Hydraulic fluid power is widely used in airborne applications specifically to operate the flight controls and landing-gear systems due to its compact size, high response

rates, high load holding capabilities and excellent power to weight ratio. Modern helicopters are no exceptions in this regard due to the adaptation of advanced rotor systems calling for higher control loads, fast response requirements and use of retractable landing gear systems [5].

Hydraulic flight control components, such as pitch trim actuator, are flight safety critical aircraft parts, i.e. containing a critical characteristic whose failure, absence or malfunction could cause a catastrophic failure resulting in loss or serious damage to the aircraft. Because of this, the maintenance, repair or overhaul of flight control parts must be done carefully in accordance with the technical manuals and prior to installation on aircraft, it must be tested to be sure that it is working properly in the limits.

To understand the working principles of such flight safety critical parts is important while testing, maintaining or repairing. Technical manuals give instruction to do routine maintenance or repair. Some technical manuals include some troubleshooting issues. During the tests of components, when a trouble or malfunction is found which does not exist in these troubleshooting instructions, the technician or the engineer must know the working principles of the component to fix the trouble without making a lot of trial and error process, which is time consuming and expensive.

Modeling and simulation are very important tools of systems engineering that have now become a central activity in all disciplines of engineering and science. Not only do they help us gain a better understanding of the functioning of the real world, they are also important for the design of new systems as they enable us to predict the system behavior before the system is actually built. Modeling and simulation also allow us to analyze systems accurately under varying operating conditions. Due to advancements in systems engineering for handling complex systems, modeling and simulation have, of late, become popular [6].

Simulink is software for modeling, simulating, and analyzing dynamic systems. Simulink enables users to pose a question about a system, model it, and see what happens. With Simulink, users can easily build models from scratch, or modify

existing models to meet their needs. Simulink supports linear and nonlinear systems, modeled in continuous time, sampled time, or a hybrid of the two [7].

The motivation of this thesis depends on the studies on gaining the overhaul and maintenance capability of pitch trim actuator. The best way to understand the working principles of a system is modeling it mathematically. After constructing the mathematical model, Simulink is a good tool to simulate the dynamic model. In this study, the actuator part of the pitch trim assembly is modeled.

1.2. Literature Survey

1.2.1. Electrohydraulic Servo Valves

In [8], Merritt describes the working principles of electrohydraulic servovalves and gives the theory for torque motor of servovalves.

The input to an electrohydraulic (EH) servovalve is typically a current or a differential current that powers an electromagnetic torque motor. The differential current Δi is typically supplied by an amplifier to avoid excess loading of the interface to the computer or controller. The single stage or direct acting EH valve is limited to low rates of flow (small valves) [8].

In order to achieve higher flow rates, a two or three stage servovalve may be necessary. In this case the torque motor controls the first stage valve that actuates the spool on the second stage. The first stage valve is typically not a spool valve but either a flapper nozzle valve or a jet pipe valve. The flapper-nozzle is more common. For these valves flow passes from the nozzle through a cylindrical area between the nozzle and the flat flapper that is near to it. As shown in

Figure 1-1 from [8], the EH valve uses one flapper between two nozzles to produce a differential pressure that is applied to each side of the spool.

The displacement of the flapper from a neutral position is powered by the torque motor and resisted by a torsional spring. The “fixed upstream orifice” in both types of valve is important to allow the pressure on either end of the spool to be below the

supply pressure. A small flapper motion creates an imbalanced pressure in one direction or the other on the ends of the spool of the second stage.

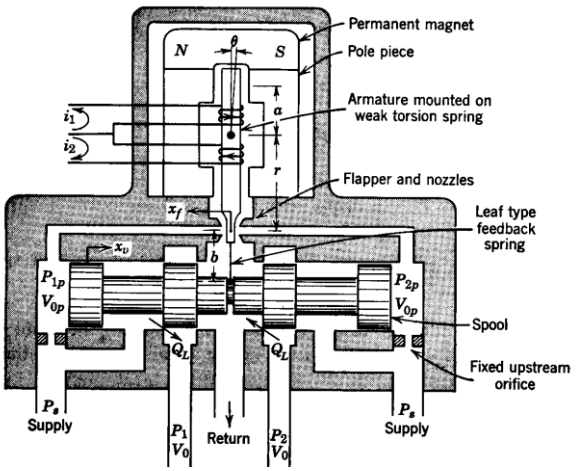

Figure 1-1 Schematic of typical two-stage electrohydraulic servovalve with force feedback [8]

Obviously the spool will tend to move in response to this imbalance and allow flow Q_L to the actuator. Since continued imbalance in pressure would quickly move the spool to its limits of travel, a form of feedback connects the motion of the spool to the effective displacement of the flapper. A very small spool displacement will result in a large flow at high pressures typically used [8].

Figure 1-1 shows the force feedback arrangement in which a feedback leaf spring applies a force to the flapper to restore equilibrium. The ratio between the spring constant of this spring and the torsional spring on the torque motor determine the ratio between motion of the flapper and the spool.

1.2.2. Modeling Studies on Flapper-Nozzle Servovalve

In [9], Gordic creates a detailed mathematical model of the servovalves based on the comprehensive theoretical analysis of all functional parts of two-stage

electrohydraulic servovalves with a spool position feedback (a current amplifier, a torque motor, the first and the second stage of hydraulic amplification).

In [10], Rabie analyzes the static and dynamic performance of electrohydraulic servo actuators (EHSA). In this book, the equations describing the behavior of the basic elements of EHSAs are deduced and the steady-state performance of these elements is discussed, mainly, the electromagnetic torque motor and the flapper valve. A mathematical model describing the dynamic behavior of the whole electrohydraulic servo actuator is deduced.

In [11], Dongie proposed a new approach based on input-output linearization for mathematical modeling of twin flapper nozzle servovalve. In [12], Zhang works on the influence of temperature on null position pressure characteristics of flapper-nozzle servo valve. Many other researchers work on modeling servovales [13-17].

1.2.3. Electromagnetic Torque Motor

The electromagnetic torque motor converts an electric input signal of low-level current (usually within 10 mA) into a proportional mechanical torque. The motor is usually designed to be separately mountable, testable, interchangeable, and hermetically sealed against the hydraulic fluid. The net torque depends on the effective input current and the flapper rotational angle [10]. Electromagnetic Torque Motor is an electro-mechanical transducer commonly used with the input stage of a servovalve. Displacement of the armature of the torque motor is generally limited to a few thousandths of an inch [18].

In Figure 1-2, typical components of electromagnetic torque motor is shown. This figure belongs to a permanent magnet type torque motor. There are the upper and lower yoke, between these yokes there are permanent magnets. There is armature at the middle. There are coils to magnetizing the armature. The armature is seated on flexure tube which works as rotational spring. The displacement of the flapper is proportional to current and rotation of armature.

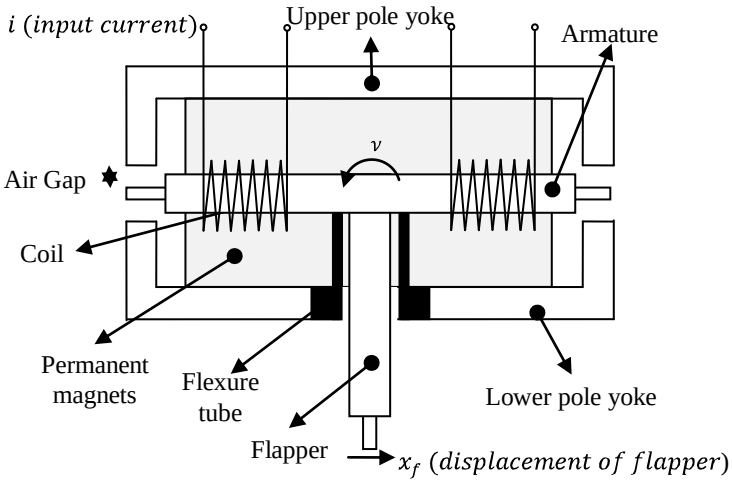

Figure 1-2 Schematic drawing of electromagnetic torque motor

In the design of the servo valve torque motor, the valve manufacturer is confronted with necessity of providing a wide range of differential current inputs to satisfy users' requirement. To accomplish this, manufacturers may vary the number of turns in the torque motor, the width of the air gaps, the bias flux created by the permanent magnet etc. The latter particularly provides an effective way of varying the differential current requirements. In fact, the differential current input can be theoretically reduced to a very low value by increasing the size of the permanent magnet, since the force output of the torque motor is proportional to the product of the permanent magnetic and differential current produced fluxes. However, if the differential current is reduced to too low a value, the output force becomes too dependent on the characteristics of the permanent magnets, which may be quite temperature sensitive, thus presenting a serious null shift problem. There probably is an optimum compromise between minimum controlling power and the susceptibility to external disturbances creating null shift [19].

Theory of electromagnetic torque motor using permanent magnets is developed by Merritt in [8] and this theory is widely used by authors of books and research paper, but Urata [20] states that the theory of Merritt gives totally erroneous results because it ignores the magnetic reluctance of permanent magnets and accompanying leakage flux. Urata also investigates the influence of unequal air-gap thickness in servo valve torque motors in [21].

Gordic [22] investigates the effects of variation of few torque motor electromagnetic parameters (air-gap length (thickness) at null, residual magnetic flux density (magnetic inductivity) of permanent magnet and number of turns of each coil) on dynamic performance of servovalve. His analysis showed that the biggest influence on servovalve dynamic characteristics has variation of air-gap length at zero.

1.2.4. Discharge Coefficient of Flapper Nozzle

In [23], Lichtarowicz explained that depending on the relation between the distances flapper nozzle and flat end of the nozzle, two kinds of flow can appear, and so, two different discharge coefficient tendencies. These tendencies are shown in Figure 1-3.

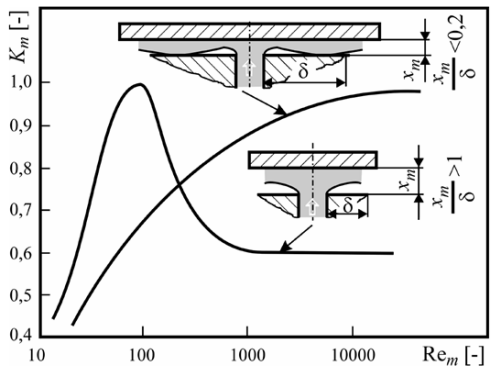

Figure 1-3 Flow coefficient of variable orifices (flapper-nozzle type) [24]

In [25], Bergada experimentally determined discharge coefficient values for the most frequent working fluid flow regimes through flapper-nozzle servovalve shown in Figure 1-4. In [24], it is justified presumption that flow coefficients of left and right variable orifice are equal. One should be careful with the choice of values for flow coefficients of constant orifices. According to [24], to analyze the transient response of flapper nozzle valve the variation of discharge coefficient with Reynolds number must be taken in account. In this study [24], the steady values of discharge coefficient for variable orifices is given as 0.64 and it is given as 0.783 for fixed orifices.

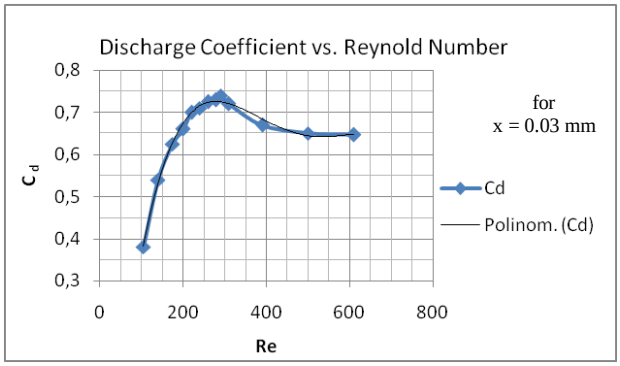

Figure 1-4 Discharge coefficients when flow from nozzle to flapper [25]

1.2.5. Studies on UH-60 Helicopter

United Technologies Inc. patented the algorithm and the principle ideas on auto flight system of UH-60 [26-32]. In literature, there are many studies on flight stability and handling quality of UH-60 helicopter. Howlett [33, 34] constructs the mathematical model of UH-60 helicopter for NASA. However, no study is found on hydraulic component or hydraulic system of UH-60 helicopter.

1.3. Objective of the Thesis

The main objectives of this thesis study are to investigate electrohydraulic pitch trim actuator, to achieve mathematical model for this actuator, to model pitch trim actuator in MATLAB Simulink environment and validate this model with experimental study.

To understand the basic operation principle of pitch trim actuator, the hydraulic circuit is determined. By using Autodesk® Inventor software, the 3D model of the actuator's hydraulic lines and spool assembly is drawn. Once the operation principle is understood, pitch trim actuator is modeled mathematically. Experimental studies are performed to find the values of physical and mechanical parameters of the actuator.

In order to obtain detailed Simulink model, the sub-assemblies of pitch trim actuator are modeled separately. To achieve realistic Simulink model of components,

particular experiment is performed for electromagnetic torque motor. However, these experiments do not lead up to valuable results. Instead of particular experiment for electromagnetic torque motor, it is realized that if the torque motor and fixed orifices are tested together by forming hydraulic Wheatstone bridge circuit, the results are more convenient as the fixed orifices and torque motor are calibrated together to form a bridge circuit without null shift.

For experimental comparison, a test fixture is designed and experimental setup is equipped. The designed test fixture is manufactured at 5^{th} Main Maintenance Center (5^{th} MMC). The pitch trim actuator is tested with no load condition. The data such as current input, pressures, and displacement outputs are acquired by using KAM-500 data acquisition system.

The other objective is to validate the constructed Simulink model. The acquired current inputs are transferred to Simulink model as inputs. The resultant measured input arm displacements and the outputs of Simulink model simulation for these current inputs are compared. The model is modified and some parameters are tuned to achieve more accurate output. Some unknown parameters are estimated by using the parameter estimation tool of MATLAB. Finally, Simulink model is developed for simulating the steady state response of the pitch trim actuator.

1.4. Scope of the Thesis

Pitch Trim Assembly consists of three main parts; pitch trim actuator, pitch boost actuator and pitch SAS actuator. This thesis study deals with mathematical modeling and experimental evaluation of electrohydraulic pitch trim actuator. The thesis has five principal parts: the first part includes general information on helicopter flight control system, UH-60 flight control and general information about pitch trim actuator, the second part includes mathematical modeling of pitch trim actuator, the third part includes the developed Simulink model, the fourth part concerns with the performance and components tests, the fifth part deals with the validation of Simulink model and final tune-up. These parts are organized as six chapters as summarized below.

In Chapter 2, general information about flight control system of UH-60 helicopter and its related systems are given.

In Chapter 3, some general features of pitch trim actuator are described. Investigation on actuator, methods for determination of hydraulic lines, and the CAD drawings are presented.

In Chapter 4, the detailed mathematical model of pitch trim actuator is presented. The free body diagrams of systems are illustrated. The flow rate, pressure and motion equations for the actuator are developed and explained in detail.

In Chapter 5, the experimental setup, some brief information about data acquisition system, the experiments to determine the unknown system parameters, the results of these tests and the experimental data acquisition to verify the model and are presented.

In Chapter 6, the structure of Simulink model, models of particular components, whole system model and the results of parameter estimation is given.

In Chapter 7, the result of comparison between the output of Simulink model simulation and experimental results are given as plots, and validated model with the test results are also presented.

In Chapter 8, the whole study is summarized and the conclusions achieved from the study are presented.

CHAPTER 2

FLIGHT CONTROL FUNDAMENTALS

2.1. Helicopter Axes of Flight

The helicopter is free to rotate about three body axes that are fixed to the centre of gravity. The axes systems is no different to that of a fixed wing aircraft and are; the longitudinal axis also known as the rolling axis, lateral axis also known as the pitching axis and vertical axis also known as the yawing axis [35]. In Figure 2-1, the helicopter axes of flight is shown.

Movement along the longitudinal axis is conducted by a combination of forward or rearward movement of the cyclic pitch control, together with sufficient collective pitch application to prevent the helicopter losing or gaining altitude. To promote pitching movement about the lateral axis the cyclic pitching control is moved forward or rearward.

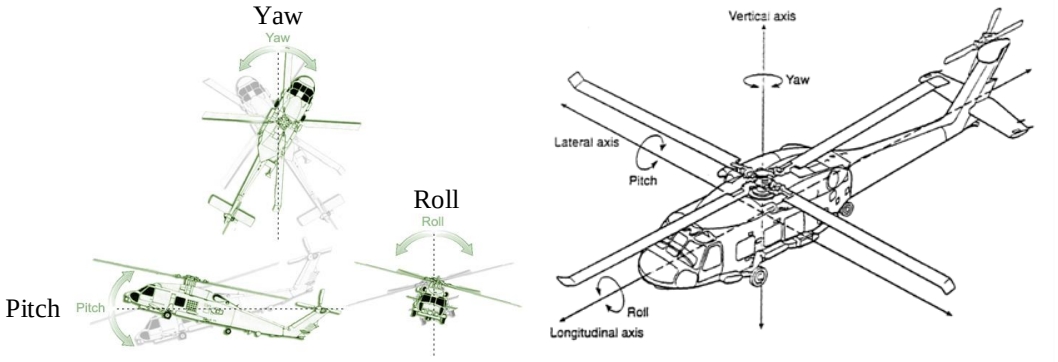

Figure 2-1 Helicopter axes of flight [35, 36]

2.2. Flight Control System of Helicopters

Typical controls of helicopter are described in [37]. There are four basic controls used during flight. These are the collective pitch control, the throttle, the cyclic pitch control, and the anti-torque pedals.

2.2.1. Collective Pitch Control

The collective pitch control, located on the left side of the pilot's seat, changes the pitch angle of all main rotor blades simultaneously, or collectively, as the name implies. This is done through a series of mechanical linkages and the amount of movement in the collective lever determines the amount of blade pitch change. Changing the pitch angle on the blades changes the angle of attack on each blade.

2.2.2. Throttle Control

The function of the throttle is to regulate engine rpm. Most of the helicopters have governor system to maintain the desired rpm when the collective is raised or lowered. Pilot can also control the throttle manually with the twist grip in order to maintain rpm.

2.2.3. Cyclic Pitch Control

The cyclic pitch control is usually mounted vertically between the pilot's knees. The cyclic can pivot in all directions. The cyclic pitch control tilts the main rotor disc by changing the pitch angle of the rotor blades in their cycle of rotation. When the main rotor disc is tilted, the horizontal component of lift moves the helicopter in the direction of tilt. The rotor disc tilts in the direction that pressure is applied to the cyclic pitch control.

2.2.4. Anti-torque Pedals

The anti-torque pedals, located on the cabin floor by the pilot's feet, control the pitch, and therefore the thrust, of the tail rotor blades. The main purpose of the tail rotor is to counteract the torque effect of the main rotor. Besides counteracting

torque of the main rotor, the tail rotor is also used to control the heading of the helicopter while hovering or when making hovering turns.

2.3. Helicopter Hydraulic System

Helicopters above 3,000 kg all up weight category using modern rotor concepts like semi-rigid or rigid rotors will result in control loads beyond pilot's handling capability, positively calls for fully powered flight control system and hydraulic power is invariably used to operate the flight controls. Requirement of high response characteristics under high operating load conditions needed for the flight control operations has resulted in extensive use of hydraulic systems in helicopters [5].

A typical hydraulic system consists of actuators, also called servos, on each flight control, a pump which is usually driven by the main rotor gearbox and a reservoir to store the hydraulic fluid. A switch in the cockpit can turn the system off, although it is left on under normal conditions. A pressure indicator in the cockpit may also be installed to monitor the system [37].

When pilot make a control input, the servo is activated and provides an assisting force to move the respective flight control, thus lightening the force required. These boosted flight controls ease pilot workload and fatigue. In the event of hydraulic system failure, pilots are still able to control the helicopter, but the control forces will be very heavy. In those helicopters where the control forces are so high that they cannot be moved without hydraulic assistance, two or more independent hydraulic systems may be installed. Some helicopters use hydraulic accumulators to store pressure, which can be used for a short period of time in an emergency if the hydraulic pump fails. This gives pilot enough time to land the helicopter with normal control [37].

Hydraulic fluid used in helicopters hydraulic system, a kerosene-like petroleum product, has good lubricating properties, as well as additives to inhibit foaming and prevent the formation of corrosion. It is chemically stable, has very little viscosity change with temperature, and is dyed for identification [37].

2.4. Helicopter Auto Flight

In [37], the basics of helicopter auto flight concept are summarized. Most helicopters incorporate stability augmentations systems (SAS) to aid in stabilizing the helicopter in flight and in a hover. The SAS may be overridden or disconnected by the pilot at any time. The SAS reduce pilot workload by improving basic aircraft control harmony and decreasing disturbances.

Helicopter autopilot systems are similar to stability augmentations systems except they have additional features. An autopilot can actually fly the helicopter and perform certain functions selected by the pilot. These functions depend on the type of autopilot and systems installed in the helicopter. The most common functions are altitude and heading hold. Some more advanced systems include a vertical speed or indicated airspeed (IAS) hold mode, where a constant rate of climb/descent or indicated airspeed is maintained by the autopilot.

The autopilot system consists of electric actuators or servos connected to the flight controls. These servos move the respective flight controls when they receive control commands from a central computer. This computer receives data input from the flight instruments for attitude reference and from the navigation equipment for navigation and tracking reference. An autopilot has a control panel in the cockpit that allows pilots to select the desired functions, as well as engage the autopilot.

2.5. General Information About Sikorsky UH-60 Helicopter

In the technical manual [38], the introductory information about UH-60 helicopter is given. The primary mission of Sikorsky UH-60 Black Hawk helicopter is the transportation of personnel and equipment. The crew consists of a pilot, copilot, and helicopter technician. UH-60 helicopters are powered by twin turbo shaft engines mounted above the mid-fuselage. The main rotor group consists of a four-bladed, fully-articulated, elastomeric rotor. The tail rotor group consists of a canted crossbeam tail rotor with two continuous composite spars running from blade tip to blade tip, crossing each other at the hub to form the four tail rotor blades. Forward, rear, lateral, and vertical flight is done by the main rotor system, while the tail rotor

system counteracts torque from the main rotor and provides directional control. Power to drive the main rotor is supplied from engine torque transmitted by drive shafting to the input module of the main transmission. The tail rotor is driven by drive shafting extending from the main module of the main transmission through the intermediate gear box to the tail gear box. Three separate hydraulic systems are used in the helicopter. The No. 1 and No. 2 hydraulic systems provide power for the main rotor servos and the pilot-assist servos. The No. 3 or backup, hydraulic system provides backup power for the No. 1 and No. 2 hydraulic systems and recharges the APU start subsystem. Basic electrical power is supplied by two AC generators mounted on the accessory module. AC power is converted to DC power for operation of certain systems. In Figure 2-2, the main components of UH-60 helicopter are shown.

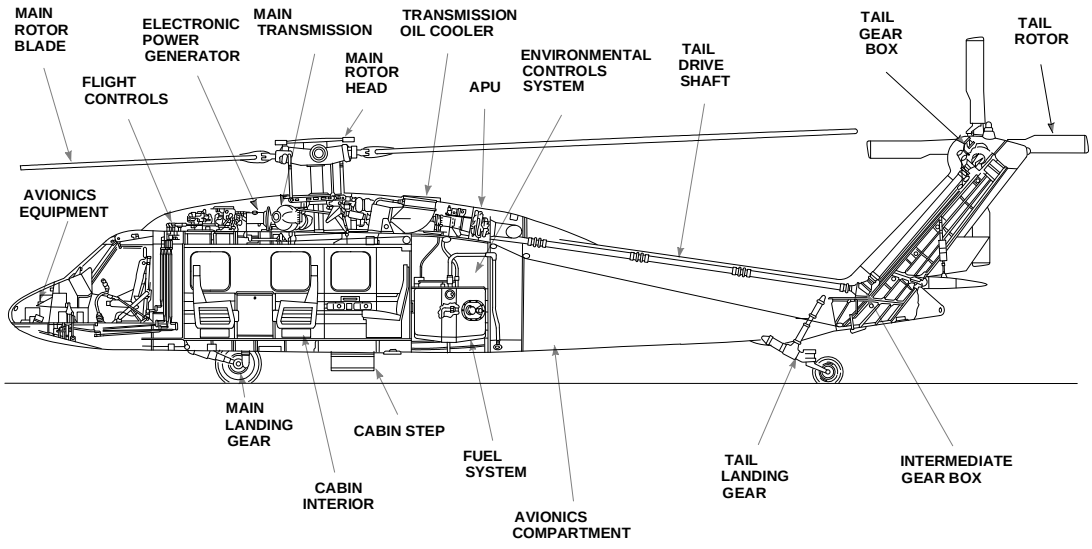

Figure 2-2 UH-60 helicopter [38]

In Table 2-1, general specifications of UH-60 helicopter is listed. The maximum takeoff weight of UH-60 helicopters is 9,173 kg, maximum useful power is 2,301 kW, and the main rotor radius is 8.18 m.

Table 2-1 UH-60A general specifications [39]

Operating Weights and Engine Power		
Empty Weight	5,238 kg (11,563 lbs)	
Fuel Weight, Typical	1,108 kg (2,446 lbs)	
Takeoff Weight, Typical	6,618 kg (14,609 lbs)	
Maximum Takeoff Weight	9,173 kg (20,250 lbs)	
Maximum Takeoff Rating	2,301 kW (3,086 shp)	
Maximum Useful Power	2,109 kW (2,828 shp)	
Rotor Parameters	Main Rotor	Tail Rotor
Radius	8.18 m (26.83 ft)	1.68 m (5.5 ft)
Chord	0.53 m (1.73 ft)	0.247 m (0.81 ft)
Solidity Ratio	0.082	0.188
Number of Blades	4	4
Rotor Rotational Speed	27.02 rad/s	124.54 rad/s
Tip Speed	221 m/s (725 ft/s)	209 m/s (685 ft/s)

2.6. Flight Control System Components of UH-60 Helicopter

The flight control system of UH-60 helicopter is hydraulically power-boosted mechanical control system. The flight control system consists of the collective, cyclic, and tail rotor (directional) control subsystems as usual. These subsystems use a series of push-pull rods, bellcranks, cables, pulleys, and servos that transmit control movements from cockpit to the main and tail rotors. The pilot and copilot have dual controls. Cyclic sticks control forward, rearward, and lateral helicopter movements; collective sticks control vertical helicopter movements; and tail rotor pedals control helicopter headings. Assistance for the pilot or copilot in pitch, roll, and yaw control is provided by the stability augmentation system (SAS), flight path stabilization (FPS), and electro-mechanical trim [38].

In Figure 2-3, the block diagram for flight control system of UH-60 helicopter is given. The movement in any control input to the mixing unit will result in a coordinated output to the main rotor and/or tail rotor servos. There are three primary

servos; lateral, aft, and forward. The primary servos change the orientation or level of swashplate.

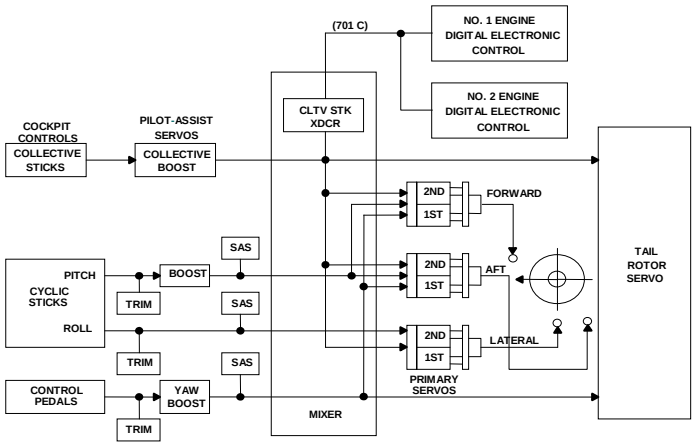

Figure 2-3 Flight control system block diagram [40]

Mechanical flight controls shown in Figure 2-4 provide means for the pilot or copilot to control the rotor systems and the direction of the helicopter flight. The pilot and copilot have dual controls.

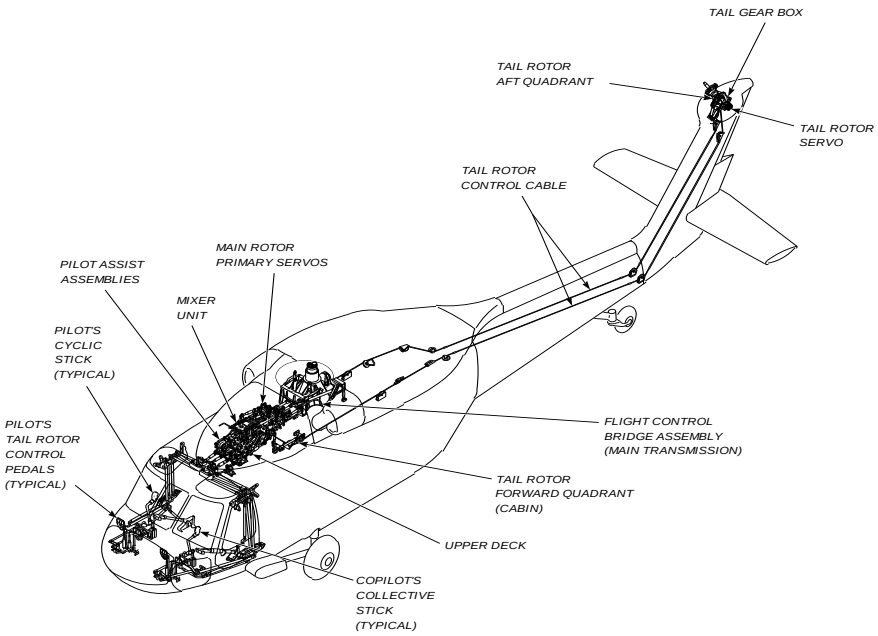

Figure 2-4 Flight control system components [41]

2.6.1. Pilot Assist Assembly

In pilot assist assembly shown in Figure 2-5, there are four assist servos; named as collective boost servo, yaw boost servo, roll SAS actuator and pitch trim assembly. There are two trim actuator; name roll trim actuator and yaw trim actuator. These servos change Auto Flight Computer Set (AFCS) electrical input signals into mechanical motion and provide boost to the flight control system, except for the roll SAS actuator. Roll and yaw trim actuators are electro-mechanical where pitch trim actuator is electro-hydro-mechanical. Pitch trim assembly refers the assembly of pitch trim servo actuator, pitch boost actuator and pitch channel SAS actuator. The scope of this thesis is pitch trim servo actuator only.

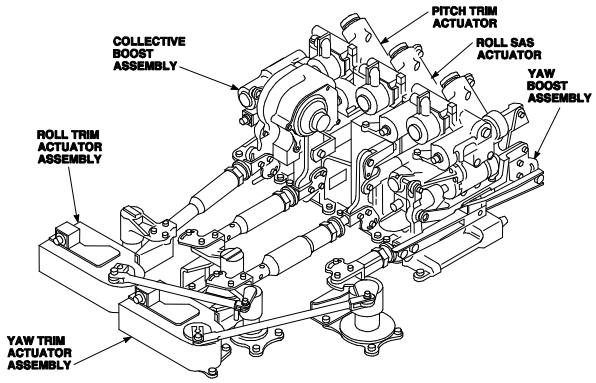

Figure 2-5 Pilot assist assembly [38]

2.6.2. Cyclic Control System of UH-60 Helicopter

This system provides forward, rearward, and lateral control of the helicopter. The cyclic sticks are mechanically-coupled, lever-type controls for both pilot and copilot. The cyclic sticks are connected through a torque shaft, a series of control rods, bellcranks, pitch trim assembly, roll assembly SAS actuator and a mixing unit, to the primary servos. These control movement of the main rotor blades. The servos are powered by the first stage and second stage hydraulic systems.

The cyclic stick assembly consists of a grip assembly shown in Figure 2-6, tube assembly, socket assembly, and associated wiring. The grip assembly has a stick trim thumb switch, radio-ICS rocker switch, trim release pushbutton, panel lights kill switch, go around enable pushbutton, cargo hook release. The cyclic stick also houses a manual slew-up switch.

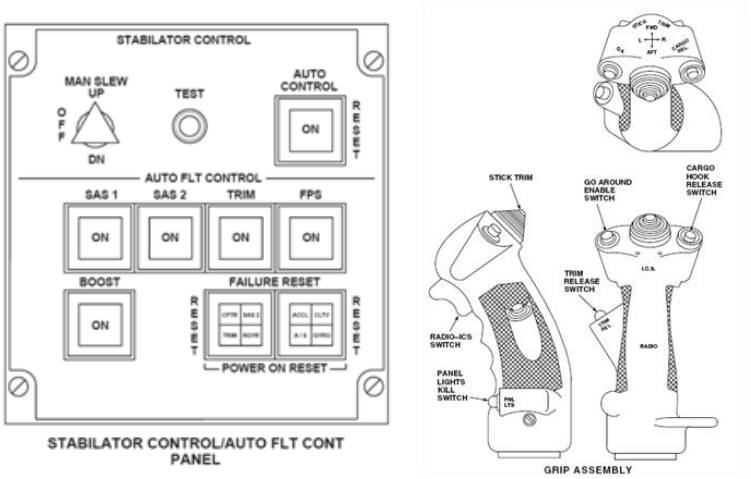

Figure 2-6 Auto flight control panel and cyclic stick grip [38]

2.6.3. Pitch Channel Trim Operation

Trim of a helicopter is the situation in which all the forces, inertial and gravitational, as well as the overall moment vectors are in balance in the three mutually perpendicular axes. So, trim of helicopter in lateral axis is referred as pitch trim.

Trim switch at Auto Flight Control panel shown in Figure 2-6 provides cyclic (pitch and roll), pedal (yaw) flight control position reference, and control gradient to maintain the cyclic stick and pedals at a desired position.

Trim is engaged by pressing the control panel's TRIM switch. With trim engaged, 28 VDC is fed from the control panel to the computer, pitch turn on valve in the pilot assist module, and both cyclic stick grips. The ground path to the pitch turn on valve is completed through the computer, and the pitch turn on valve opens applying hydraulic pressure at 6.89 MPa (1,000 psi) to the pitch trim servo. A trim piston

within the servo is held in place by the hydraulic pressure to establish pitch trim reference and is connected to the cyclic pitch control through a force gradient spring. The gradient spring gives either pilot the authority to override trim while still maintaining trim reference.

With the trim engaged 28 VDC is also applied to the Trim Release and Stick Trim command switches shown in Figure 2-6. The Trim Release switch allows either pilot to momentarily disengage pitch and roll cyclic trim to establish a new attitude reference. In Figure 2-7, the pitch motion flight controls block diagram is shown. The pitch motion of UH-60 helicopter is controlled by pilots with the components shown in the figure.

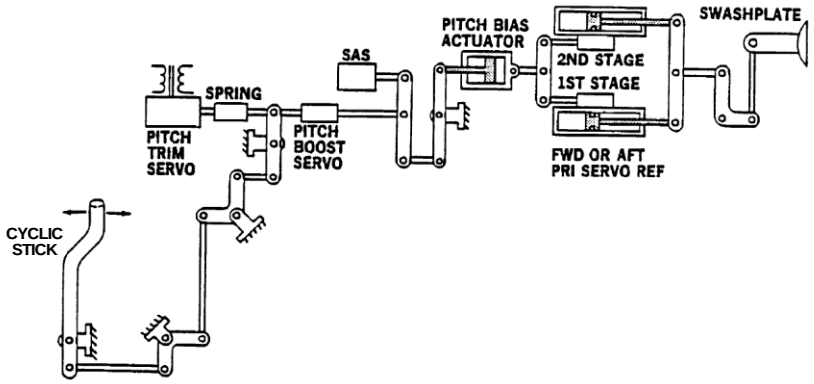

Figure 2-7 Pitch flight controls block diagram [34]

The computer maintains pitch trim by applying a ground signal to the pitch turn on valve. When the Trim Release switch is pressed, the 28 VDC signal is removed from the computer, which disables the signals to the pitch turn on valve. The pitch turn on valve closes, removing hydraulic pressure from the trim piston. This action permits unrestricted cyclic stick movement to the new reference position.

The Stick Trim switch gives either pilot another means of selecting a new cyclic trim reference. The switch provides cyclic trim command signals that result in pitch (FWD or AFT position) movements of the cyclic stick. The stick command signals are applied to the computer which produces pitch drive voltage output. The pitch

drive voltage is applied to a solenoid in the pitch trim servo that controls hydraulic flow to the trim piston. As the piston moves, the mechanical connection through the force gradient spring repositions the cyclic stick. The piston also moves a potentiometer that develops a feedback signal proportional to trim position to cancel the drive voltage in the computer and stop piston travel when the desired position is reached. The detailed block diagram of AFCS is given in Appendix A and pitch channel trim operation is highlighted.

2.6.4. Flight Path Stabilization (FPS)

FPS maintains helicopter pitch and roll attitudes, airspeed, and heading during cruise flight, and provides a coordinated turn feature at airspeeds >60 knots. The computer provides FPS command signals to the pitch trim servo which in turn repositions the flight controls. FPS command signals maintain the cruise flight attitude established by the trim reference. The pitch attitude/airspeed hold function controls the helicopter pitch attitude necessary to maintain a desired airspeed. This hold function uses the vertical gyro pitch signal to sense helicopter pitch attitude and uses the pitch rate signal from the stab amp to sense rate of change in pitch attitude. The signals are processed together in the computer and added to the airspeed signal (airspeed transducer). The resultant signal is compared with the pitch trim position signal, and the difference is applied to the pitch trim servo as a pitch FPS command signal. As shown in Figure 2-8, FPS is a module of Auto Flight Computer System (AFCS).

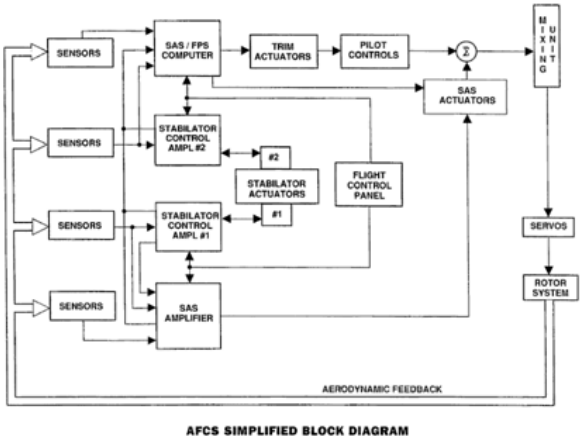

AFCS SIMPLIFIED BLOCK DIAGRAM

Figure 2-8 AFCS simplified block diagram [40]

2.7. Hydraulic System of UH-60 Helicopters

The hydraulic systems provide between 3000 and 3100 psi of hydraulic pressure to operate the primary servos, tail rotor servos, pilot-assist servos, and APU starter motor. There are three hydraulic systems:

(1) First stage hydraulic system
(2) Second stage hydraulic system
(3) Backup hydraulic system

The second stage hydraulic system supplies pressure from the No. 2 pump module to the No. 2 transfer module. From the transfer module, pressure is supplied to the second stage of the primary servos (lateral, forward, and aft) and the pilot-assist module. From the pilot-assist module, pressure is supplied to the pilot-assist servos (collective boost assembly; yaw boost servo; yaw SAS actuator mounted on the yaw boost servo; roll actuator; roll SAS actuator mounted on the roll actuator; pitch trim assembly; and pitch SAS actuator mounted on the pitch trim assembly). The pitch trim assembly is supplied pressure at a reduced rate of 1000 psi by means of a pressure regulating valve. In Figure 2-9, the hydraulic system block diagram of UH-60 helicopters is shown.

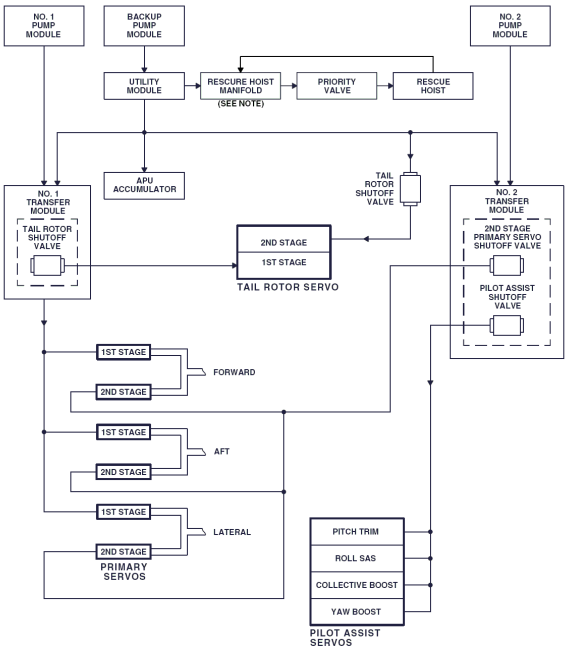

Figure 2-9 Hydraulic systems block diagram [38]

CHAPTER 3

PITCH TRIM ACTUATOR ASSEMBLY

3.1. General Information

In the maintenance work requirement [42], the introductory information about pitch trim actuator is given. The pitch trim actuator shown in Figure 3-1, is a flight control device which converts a mechanical input, an electrical command, and a hydraulic power supply into a mechanical output with trim detent capabilities. A mechanical input to the input arm of the actuator drives the output arm of the actuator through the aid of a boost actuator which in turn drives the primary pitch actuator of the helicopter. The boost actuator is also used to prevent the output arm from back driving the input arm. An electrical command to the hydraulic amplifier of the actuator converts a hydraulic power supply into a resulting output flow. The output flow acts on a "push-push" assembly which sets a trim detent position. The input arm and "push-push" assembly are mechanically connected via a preloaded spring. Movement of the input arm relative to the "push-push" assembly will cause the spring to break out at a preset detent force and continue to open at a preset spring gradient. A dual element rotary potentiometer provides feedback of the input and trim detent positions. The actuator also contains a bypass valve assembly and thermal relief valve/vent valve assembly. The bypass valve assembly isolates the "push-push" assembly from the hydraulic power supply and interconnects the pistons of the "push-push" assembly through a damping orifice when the hydraulic power supply falls below a preset pressure. The thermal relief valve assembly bleeds off pressure in the return line when the return line reaches a preset pressure.

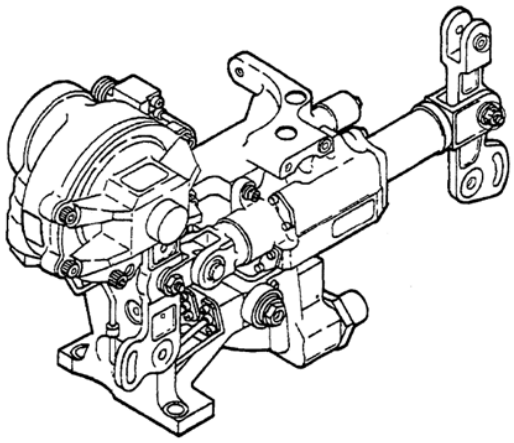

Figure 3-1 Pitch trim assembly [42]

The pitch trim assembly controls the longitudinal axis and attitude of the helicopter. The actuator is controlled by the SAS 1, SAS 2, TRIM and FPS (flight path stabilization) switches on the automatic flight control panel. The pitch trim assembly maintains the position of the cyclic stick in the longitudinal axis.

The pitch trim assembly contains a SAS servo assembly, boost actuator, and pitch trim actuator. The pitch trim actuator is an electro-hydro-mechanical actuator. It provides a trim reference to the cyclic stick in the longitudinal axis by positioning a hydraulic piston controlled by an electrohydraulic servo valve.

3.2. Components of Pitch Trim Actuator

There are eight main components of pitch trim actuator assembly (Figure 3-2).

1. Structural body and pressure lines (Figure 3-2)
2. Electromagnetic torque motor (Figure 3-3) and fixed orifices (Figure 3-4)
3. Sleeve and Spool Assembly (Figure 3-5)
4. Pistons (Figure 3-6)
5. Gradient Spring and Trim Lever Assembly (Figure 3-7)
6. Input Arm (Figure 3-7)
7. Trim and Input rotary potentiometer
8. Pitch Boost Actuator (Figure 3-8)
9. Output Arm (Figure 3-2)

3.2.1. Structural Body and Pressure Lines

The frame of pitch trim actuator includes pressure lines. The frame is also support for pistons, trim lever, gradient spring, input arm, trim and input rotary potentiometer, electromagnetic torque motor, spool assembly, pitch boost actuator, pitch SAS actuator and the output arm. In Figure 3-2, the components of pitch trim actuator is shown.

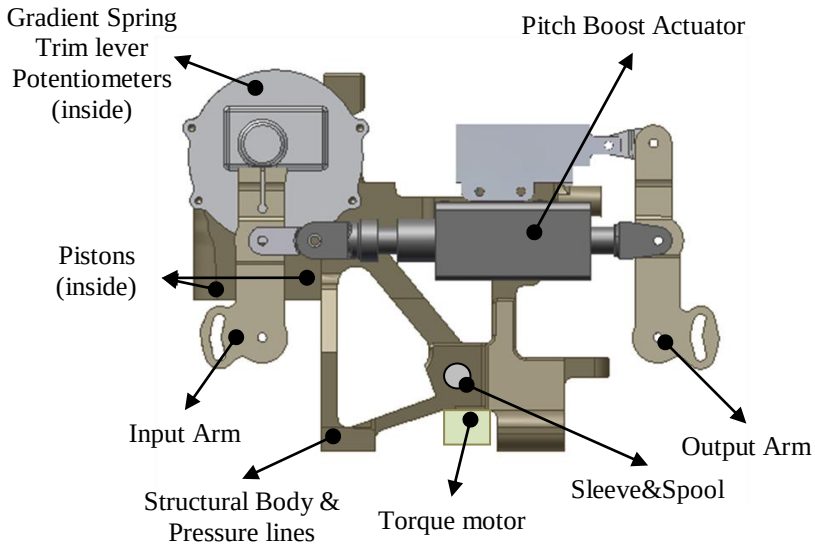

Figure 3-2 Components of pitch trim assembly

3.2.2. Electromagnetic Torque Motor and Fixed Orifices

The electromagnetic torque motor of pitch trim actuator shown in Figure 3-3 is flapper-nozzle type. The manufacturer of torque motor is Moog Inc. The current input is ± 4 mA. It is named as hydraulic amplifier in [42]. It converts the electrical current signal into mechanical displacement of flapper. Thus, it works as variable orifice. An electrical command to the hydraulic amplifier of the actuator converts a hydraulic power supply into a resulting output flow. The torque motor is calibrated with fixed orifices shown in Figure 3-4 and without null shift they work properly in hydraulic bridge circuit.

Figure 3-3 Electromagnetic torque motor of pitch trim actuator

Figure 3-4 Fixed orifices and filter

3.2.3. Sleeve and Spool Assembly

Sleeve and spool assembly of pitch trim actuator works as hydraulic switch. In Figure 3-5, the 3-D solid model of sleeve and spool assembly drawn by using Autodesk® Inventor software is shown. The figure shows position of the spool when the actuator is pressurized.

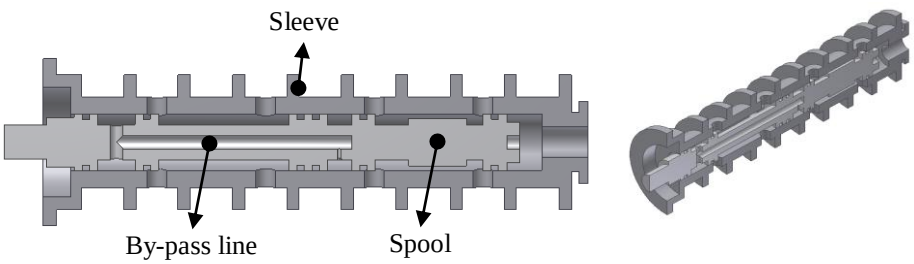

Figure 3-5 Sleeve and spool assembly

When supply pressure is given to the actuator the spool moves till the end of the mechanical stop and connects the pistons through the fixed orifice and flapper-nozzle system. When the pilot turn off the shut off valve of pitch trim actuator, the pistons of the actuator is interconnected via by-pass line exist in the spool.

3.2.4. Pistons

The hydraulic flow acts on the pistons of pitch trim actuator, named as “push-push” assembly in [42], and sets a trim detent position. There is preloaded spring under the pistons. The pistons are made of stainless steel. To prevent hydraulic lock, there are several grooves on pistons. These pistons are moving inside stainless steel sleeves. The pistons are worked smoothly with sleeves to minimize the leakage. In Figure 3-6, the picture of pistons, piston springs and trim lever is shown.

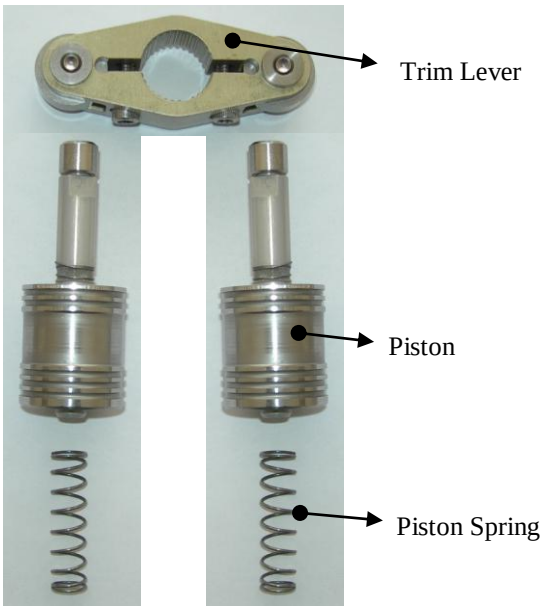

Figure 3-6 Pistons, pistons springs and trim lever

3.2.5. Gradient Spring and Trim Lever Assembly

Trim lever assembly and the input arm are mechanically connected via a preloaded gradient spring. By the help of this spring, it is possible for pilot to override the trim

position. Pilots feel detent force at first and gradient force while moving the cyclic stick when the trim is engaged. The 3-D solid model of trim lever, gradient spring, and input arm assembly drawn by using Autodesk® Inventor software is shown in Figure 3-7. The 3-D solid model is used to calculate mass moment of inertia of rotating trim lever, gradient spring and input arm.

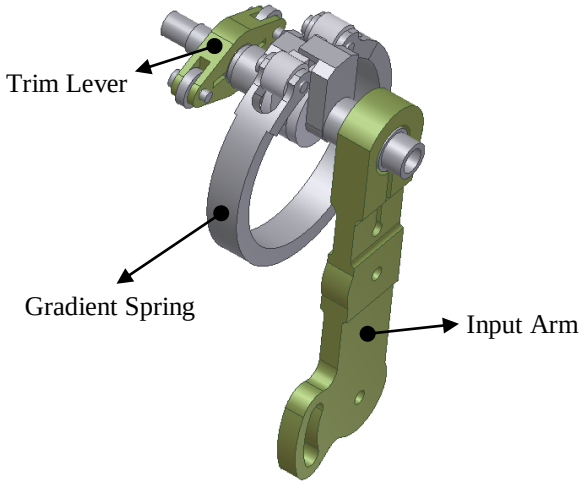

Figure 3-7 Gradient spring, trim lever and input arm assembly

3.2.6. Boost Actuator

The pitch boost actuator connects input arm and output arm and boosts the pilot mechanical input. A mechanical input to the input arm, pushing on or pulling on, drives the boost actuator and the actuator either moves to the right or to the left. The boost actuator is also used to prevent the output arm from back driving the input arm. With hydraulic power off the pitch boost actuator acts as a push-pull rod. In Figure 3-8, the schematic of pitch boost actuator is shown.

With the hydraulic power on, pressure causes a little movement to centering the control valve which closes off the port to chamber A causing a hydraulic lock. If the power piston is not being moved the 8.27 MPa (1,200 psi) relief valve opens pressure to return reducing the pressure. Pushing on the input causes the servo control valve to move right opening the port. The opened port allows fluid pressure in chamber A to

be ported to return through chamber C. The reduced pressure in chamber A will allow pressure in chamber B to move the power piston to the right until the input is stopped. When the input is stopped the power piston will over travel until the control valve is centered, closing the port. The servo is again hydraulically locked.

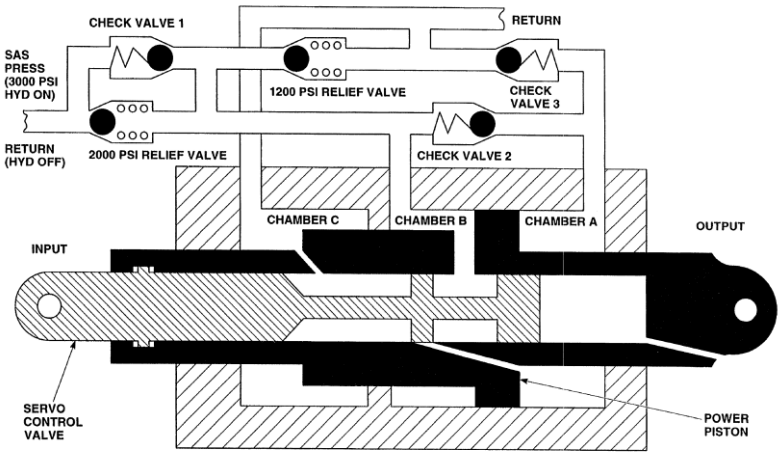

Figure 3-8 Schematic of pitch boost actuator [41]

Pulling on the input causes the servo control valve to be moved to the left opening the port. The opened port allows fluid pressure into chamber A from chamber B. Chamber A has a larger area piston than chamber B which causes a differential force between the two chambers. The greater force will drive the power piston to the left until the input is stopped. When the input is stopped the power piston will over travel until the control valve is centered, closing the port. The servo is again hydraulically locked.

3.2.7. Trim and Input Potentiometer

The trim lever and the input arm are connected to position detectors which simply comprise potentiometers connected to output of the trim actuator and arm. The stick trim position signal provided by position detector is indicative of the stick trim position; on the other hand, the signal at the output of the position detector being connected by the linkage of input arm directly to the pilot's stick, is indicative of the actual position of the stick. Whenever the pilot is not overriding the system, these

positions will be same. The stick position signal is not only provided for closed loop servo operation, but also provided to a track store unit.

3.2.8. Input Arm and Output Arm

Input arm is a mechanical linkage transfers pilots' cyclic stick movement to output arm via boost actuator. It has a connection to trim lever assembly with a gradient spring and transfers the trim reference to the cyclic stick. The output arm has a connection to pitch SAS actuator and besides the cyclic pitch movement of pilot, it also transfers the mechanical output of SAS actuator to aft and forward primary servo via pitch bias actuator and mixing unit.

3.3. Investigation on Pitch Trim Actuator

At the beginning of the study, the schematic representation given in [41] is used to identify the basic operation principles. By investigating the schematic representation shown in Figure 3-9, the basic operation principles of pitch trim actuator can be understood.

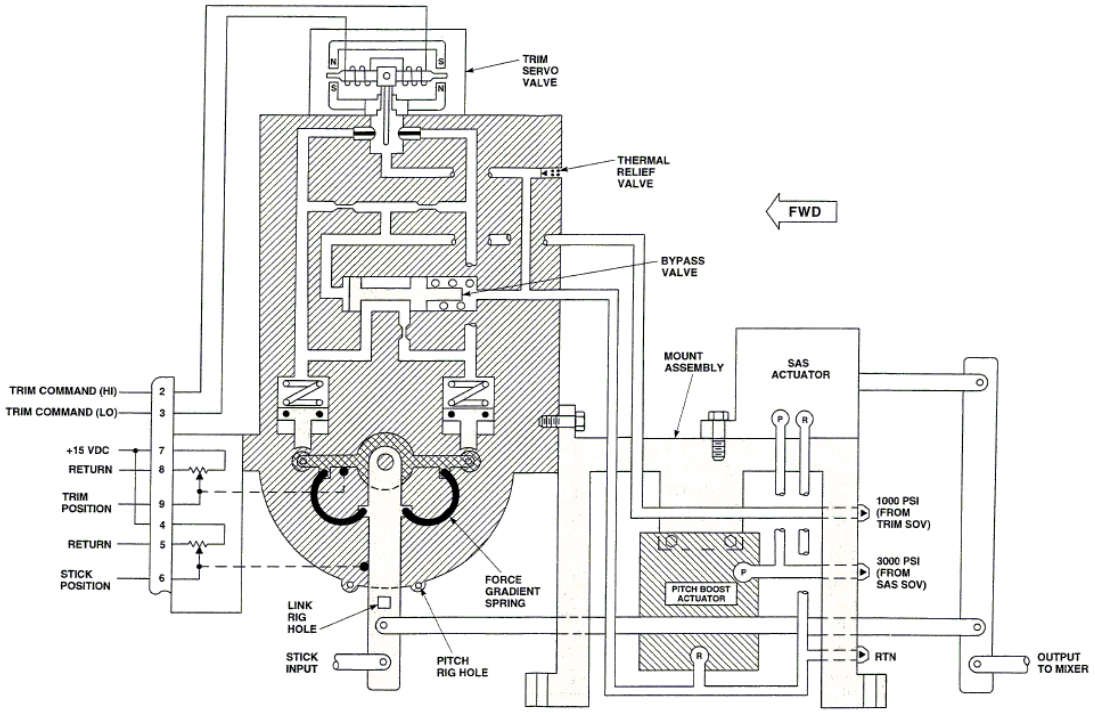

Figure 3-9 Pitch trim assembly operational schematic [41]

However, the schematic representation does not contain the details of sleeve spool assembly, the real hydraulic lines and some components such as visco jet which has a significant effect on functional behavior.

For proper establishment of mathematical equations, the hydraulic lines and components must be known. To achieve correct hydraulic circuit diagram of pitch trim actuator, X-ray is utilized for determination of transmission lines which are not obvious. Lead wire and numbers are used to identify the trajectory of hydraulic lines by X-ray. In Figure 3-10, the X-ray of pitch trim actuator is shown.

Figure 3-10 X-ray of pitch trim actuator

3.3.1. Visco Jet

In the part list given in [42], there is a hydraulic component named as visco jet. It is understood from the text, visco jet is a flow restrictor and the purpose is adjusting the pistons speed. When it is searched at the literature, it is found that the name "visco jet" is patented product of Lee Company [43]. However, the part number given in [42] could not be found on Lee Company's webpage. The visco jet used in pitch trim actuator is special production and the part number did not exist in standard product list. As it is stated in Lee Company Webpage [43], the visco jet adds the dimension of spin chambers for higher restriction.

In [42], the place of visco jet in hydraulic system is shown approximately. The visco jet is placed inside the structural body of pitch trim actuator through a hole and then

the hole is plugged. Since it is not possible to use destructive methods such as cutting or drilling on investigated pitch trim actuator, the place of visco jet could not be determined exactly. In Figure 3-11, the picture of visco jet is shown.

Figure 3-11 Visco jet [43]

3.3.2. Reconstruction of Hydraulic Circuit Representation

As it is known that the flapper nozzles and fixed orifices forms a hydraulic Wheatstone bridge circuit. To complete the bridge circuit, one hydraulic line is missing. In other words, the hydraulic line is not seen but it is known that there must be a hydraulic line for correct arrangement of hydraulic bridge circuit. Hydraulic line including visco jet is predicted according to this assumption.

After determination of hydraulic transmission lines, the schematic representation shown in Figure 3-9 is reconstructed by using AutoCAD® software. The new representation shown in Figure 3-12 includes the details of sleeve and spool assembly, all hydraulic lines. The place of visco jet and the predicted hydraulic line is shown in the figure. The hydraulic line including visco jet is between second cylinder and the right side hydraulic line of the Wheatstone bridge circuit.

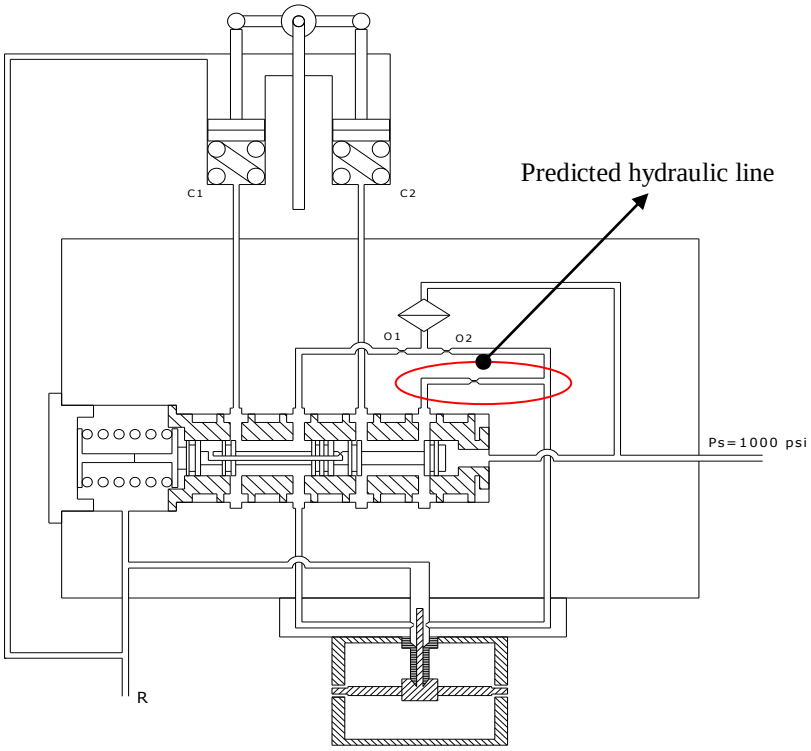

Figure 3-12 Schematic representation of pitch trim actuator

3.3.3. 3-D Model for Hydraulic Lines

To determine and understand the correct arrangement of hydraulic lines, 3-D solid model of hydraulic block shown in Figure 3-13 is drawn, known hydraulic lines are added to 3-D model and the place of visco jet is predicted. Also the 3-D model of sleeve spool assembly is added to this drawing. In Figure 3-13, the red color represents the pressurized hydraulic lines. Blue color is for return hydraulic lines. Orange color is for the hydraulic line to 1st cylinder and the purple color is for the hydraulic line to 2nd cylinder. From this 3-D model, the hydraulic circuit of pitch trim actuator is drawn.

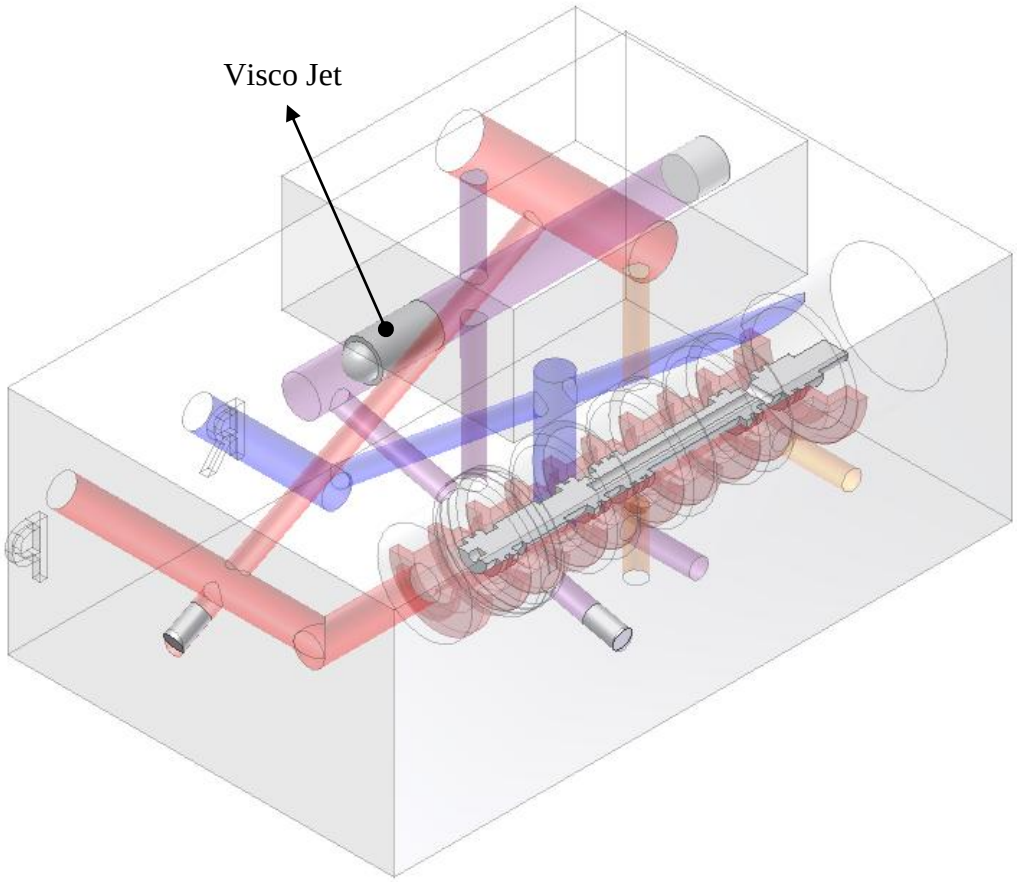

Figure 3-13 3-D solid model of hydraulic lines and spool assembly

3.3.4. Hydraulic Circuit of Pitch Trim Actuator

The hydraulic circuit of pitch trim actuator is shown in Figure 3-14. The circuit shows the hydraulic Wheatstone bridge including variable and fixed orifices. The place of visco jet is emphasized. Variable orifices are formed by two nozzles and the flapper of torque motor. In the figure, position of spool is drawn as in the pressurized system. The arrows show the positive direction for volumetric flow rates.

In Figure 3-14, only the hydraulic Wheatstone bridge circuit of pitch trim actuator is shown. The hydraulic lines for cylinders are not shown. The complete system representation is given in Figure 3-12.

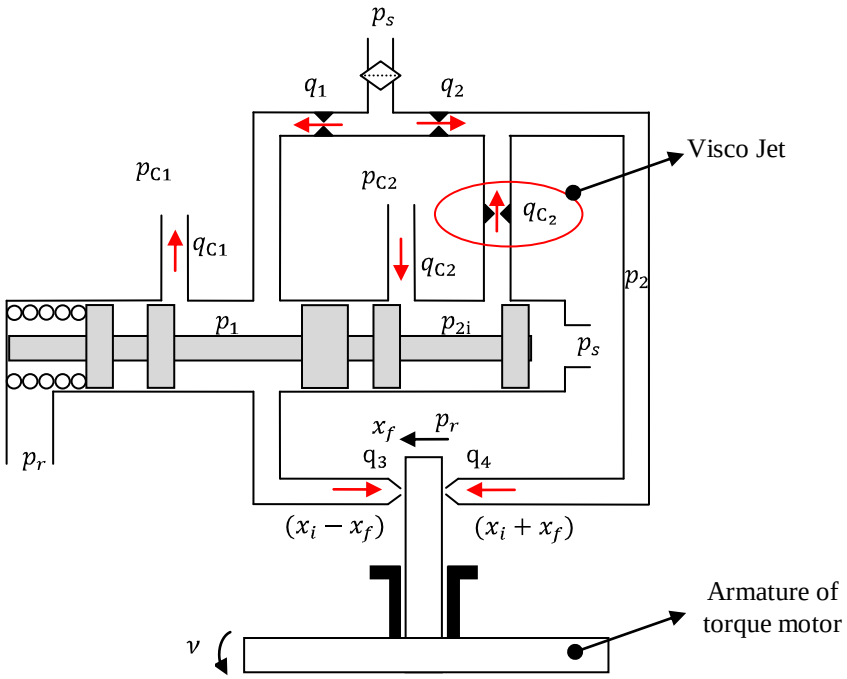

Figure 3-14 Hydraulic circuit of pitch trim actuator

As a result of these investigations, the basic operation principle of pitch trim actuator is completely comprehended and the hydraulic circuit is determined. The hydraulic components of the system are revealed. From this hydraulic circuit, volumetric flow rates equations are obtained and the mathematical model of pitch trim actuator is developed.

CHAPTER 4

MATHEMATICAL MODEL OF PITCH TRIM ACTUATOR

4.1. Electromagnetic Torque Motor

The torque generated in an electromagnetic torque motor is presented by Urata in [20]. For torque motors using permanent magnets, Merritt [8] developed a theory that has been widely distributed and followed by authors of books and research papers. Urata claims that the theory developed by Merritt gives totally erroneous results because it ignores the magnetic reluctance of permanent magnets and accompanying leakage flux. Urata submitted a corrected theory that agrees well with his experiment and is useful for the design of servo valves and the modeling of fluid power systems involving servo valves [20]. In this thesis study, the theory of Urata is used.

4.1.1. Torque Generated by Electromagnetic Forces

In [20], Urata developed a theory to express the torque generated in a torque motor that uses permanent magnets. The influence of magnets in the torque motor can be expressed using an experimental coefficient k_r. The magnetic reluctance and leakage flux have an essential influence on characteristics of a torque motor when it involves permanent magnets [20].

By the theory given in [20], torque generated by electromagnetic forces can be formulated as follows:

$$T_m = K_i i + K_m \alpha \tag{4.1}$$

where,

T_m : torque generated by electromagnetic forces (N.m)

K_i : torque motor current gain (N.m/A)

i : input current to torque motor (A)

K_m : torque motor electromagnetic spring constant (N.m/rad)

α : angular displacement of armature (rad)

The torque motor current gain K_i in Eqn. (4.1) is defined as,

$$K_i = \frac{N\, L_a\, \mu_0\, A_m\, M_m}{x_a^2\,(k_r + 1)} \tag{4.2}$$

The torque motor electromagnetic spring constant K_m in Eqn. (4.1) is defined as,

$$K_m = \frac{L_a^2\, \mu_0\, A_m\, M_m^2}{4\, x_a^3\,(k_r + 1)^2} \tag{4.3}$$

where,

N : number of coil turns

L_a : distance between poles at both ends of a yoke (m)

μ_0 : permeability of free space (= $4\,\pi/10^7$) (T.m/A)

A_m : sum of cross-sectional areas of permanent magnets (m^2)

M_m : magneto motive force of permanent magnets

x_a : length of air gap (m)

k_r : magnetic reluctance constant

The magneto motive force of permanent magnets M_m, is calculated by using equation,

$$M_m = \frac{l_m.\, B_r}{\mu_m} \tag{4.4}$$

where,

B_r : residual magnetic flux density of permanent magnet (T)

l_m : length of the permanent magnet (m)

μ_m : permeability of permanent magnet (T.m/A)

Magnetic reluctance constant k_r, is formulated as,

$$k_r = \frac{R_m}{R_a . k_l} \tag{4.5}$$

where,

R_m : permanent magnet reluctance

R_a : reluctance of air gap at null

k_l : coefficient of leakage flux, i.e. the flux through free space

The permanent magnet reluctance R_m, can be written as,

$$R_m = \frac{l_m}{A_m . \mu_m} \tag{4.6}$$

The reluctance of air gap at null R_a, can be written as,

$$R_a = \frac{x_a}{\mu_0 . A_a} \tag{4.7}$$

where,

A_a : cross-sectional area of air gap (m^2)

4.1.2. Equation of Rotational Motion for Torque Motor Armature

The resistances of variable orifices depend on the dynamics of torque motor armature. The rotation angle of armature can be determined by the equation of rotational motion. The rotation angle somehow depends on torque generated by torque motor, thus the current input. In this section, the equation of rotational motion for torque motor armature is obtained. From this equation, the rotation angle of armature and the displacement of flapper at the tip of the nozzles are calculated. In Figure 4-1, the free body diagram of armature is shown. The torques acting on the armature and forces due to pressure difference is shown in the figure.

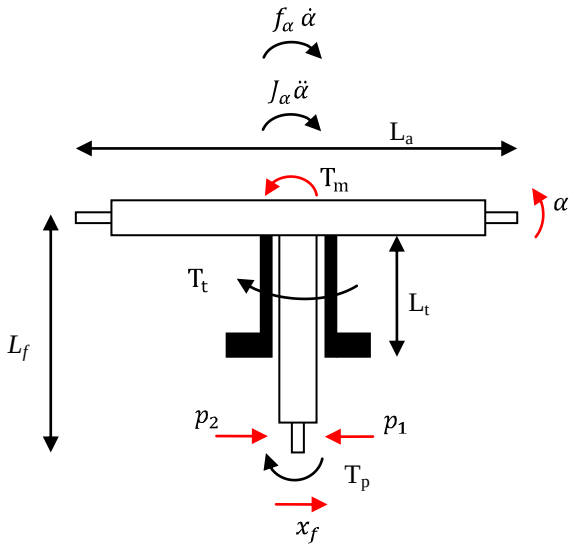

Figure 4-1 Free body diagram of armature

For the armature to be in rotational equilibrium, the total torque on the armature must be zero. The total torque on the armature is the vector sum of all the external torques.

$$J_\alpha \frac{d^2\,\alpha}{d^2\,t} + f_\alpha \frac{d\,\alpha}{d\,t} = T_m - T_t - T_p \tag{4.8}$$

Torque due to the pressure difference T_p can be written as,

$$T_p = \frac{\pi}{4}\, d_f^2\, (p_1 - p_2) L_f \tag{4.9}$$

Torque due to flexure tube T_t, can be written as,

$$T_t = K_t\, \alpha \tag{4.10}$$

From Eqn. (4.1), Eqn. (4.8), Eqn. (4.9) and Eqn. (4.10), the following equation representing the dynamics can be written,

$$J_\alpha \frac{d^2\,\alpha}{d^2\,t} + f_\alpha \frac{d\,\alpha}{d\,t} + (K_t - K_m)\,\alpha = K_i i - \frac{\pi}{4}\, d_f^2\, (p_1 - p_2) L_f \tag{4.11}$$

where,

J_α : mass moment of inertia of rotating armature (N.m.s^2/rad)

f_α : damping coefficient of armature (N.m.s/rad)

K_t : the rotational stiffness of flexure tube (N.m)

T_t : torque due to flexure tube (N.m)

T_p : torque due to the pressure difference (N.m)

d_f : nozzle diameter of flapper nozzle valve (m)

L_f : the length of flapper (m)

p_1 : pressure at the right side of the flapper (Pa)

p_2 : pressure at the left side of the flapper (Pa)

The displacement of flapper at the tip of the nozzles x_f, is defined as,

$$x_f = (L_f - L_t/2)\,\alpha \tag{4.12}$$

where,

x_f : the displacement of flapper at the tip of the nozzles (m)

L_t : the length of flexure tube (m)

α : angular displacement of armature (rad)

4.2. Spool Motion

There are two working modes of pitch trim actuator. When pilots want to change the trim reference of cyclic stick, they either press trim release button or use stick trim switch to set new cyclic reference. While trim release button is pressed, a signal send to the pressure shut off valve of pitch trim actuator and the pressure is set to 0. This gives pilot to change the trim reference of actuator without facing any spring force. When pilot stops pressing the trim release button, a signal sent to shut off valve is cut and the actuator engages the trim reference in 20 ms [42].

Mode 1: Trim Release Button is pressed or there is no supply pressure. $P_s = 0$;

The spool spring holds the spool at the bottom far end as shown in the Figure 4-2. At this position cylinders of piston are connected with by-pass passage exists in the spool. By the help of this by-pass passage, it is possible for pilot to give longitudinal cyclic input without facing any counter force. But there is an orifice at this by-pass line to damp the pilot input i.e., they cannot move the cyclic stick too fast.

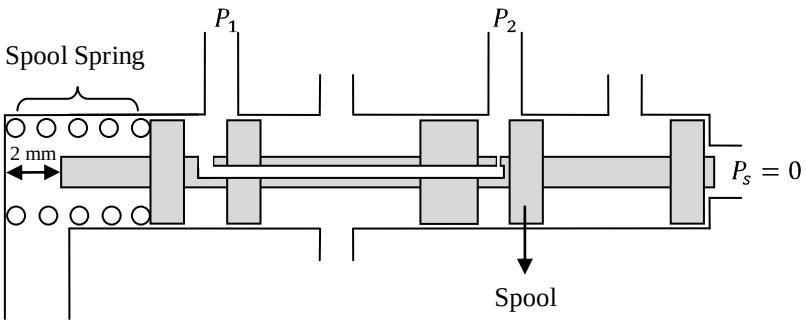

Figure 4-2 Schematic drawing of spool when Ps=0

Mode 2: The supply pressure is on. P_s = 1000 psi (6.89 MPa);

The supply pressure applied to bottom end of spool generates a force which overcomes the spool spring force and the spool moves to the other end as shown in the Figure 4-3. At this position the hydraulic fluid passes to cylinders of piston through the electro- hydraulic torque motor and fixed orifices.

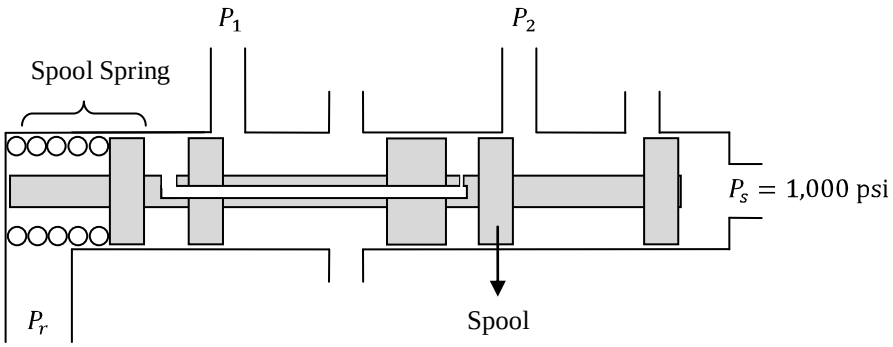

Figure 4-3 Position of spool when Ps=1,000 psi

Force acting on the spool can be written as,

$$F = \frac{\pi}{4} d_{sp}^2 \Delta P = K_{sp} x_{sp} \tag{4.13}$$

Table 4-1 Spool dimensions and pressure values

Diameter of spool	$d_{sp} = 5.14$ mm
Supply Pressure	$P_s = 6.89$ MPa (1,000 psi)
Return Pressure	$P_r = 0.35$ Mpa (50 psi)
Pressure difference	$\Delta P = P_s - P_r = 6.55$ MPa
Spool spring stiffness	$K_{sp} = 24.1$ N/mm

By using the values given in Table 4-1 and Eqn. (4.13), corresponding displacement of spool, x_{sp} is calculated as

$$x_{sp} = 5.64 \text{ mm}$$

However, because of the installation, the maximum allowable travel for the spool is 2 mm. The calculated value is greater than the allowable displacement, so,

$$x_{sp} = 2 \text{ mm}$$

Therefore, the spool moves till the mechanical stop as shown in Figure 4-3. Because of that the spool can be considered as an on-off hydraulic switch for the pitch trim actuator. After the actuator is pressurized, the spool opens the ports and cylinders are connected via hydraulic Wheatstone bridge formed by the torque motor flapper nozzle valves and fixed orifices.

4.3. Volumetric Flow Rates through Orifices

The design and construction of hydraulic circuit of pitch trim actuator is shown in Figure 3-14. There are two fixed orifices and two variable orifices created by the annular area between nozzle and flapper. These orifices are placed to form hydraulic Wheatstone bridge. The torque motor controlled by current rotates the flapper. As the displacement of the flapper, the size of orifice change to control the pressure at the cylinders. By using Figure 3-14, the symbolic representation of hydraulic Wheatstone bridge circuit shown in Figure 4-4 is drawn. In Figure 4-4, the electrical

analogy is used. The orifices are represented as resistance to hydraulic fluid flow. The notation and direction of volumetric flow rates are given.

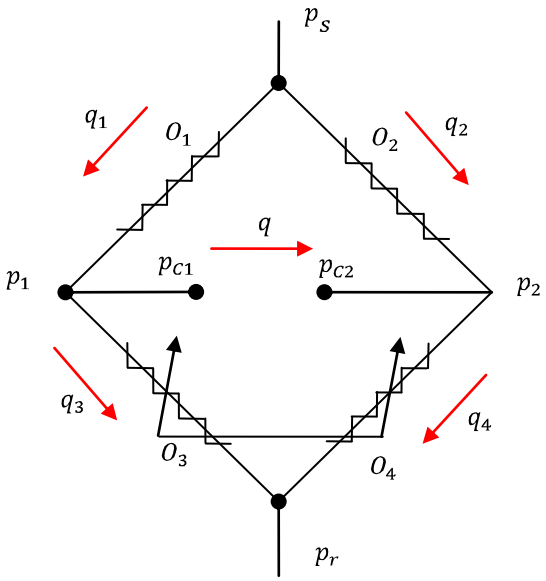

Figure 4-4 Symbolic drawing of hydraulic Wheatstone bridge circuit

Orifices are basic means for the control of fluid power. Flow characteristics of orifices play a major role in the design of many hydraulic control devices [8]. The relation between hydraulic fluid volumetric flow rate and pressure drop at any orifice can be defined as;

$$q = C_d A \sqrt{\frac{2}{\rho} \Delta P} \tag{4.14}$$

Volumetric flow rates equations for fixed orifices are as follows:

$$q_1 = C_{do} A_o \sqrt{\frac{2}{\rho} (p_s - p_1)} \tag{4.15}$$

$$q_2 = C_{do} A_o \sqrt{\frac{2}{\rho} (p_s - p_2)} \tag{4.16}$$

Volumetric flow rates through variable orifices can be defined as follows:

$$q_3 = C_{dn}\pi\, d_f(x_i - x_f)\sqrt{\frac{2}{\rho}\,(p_1 - p_r)} \tag{4.17}$$

$$q_4 = C_{dn}\pi\, d_f(x_i + x_f)\sqrt{\frac{2}{\rho}\,(p_2 - p_r)} \tag{4.18}$$

where,

q_1 : volumetric flow rate through fixed office at the left (m^3/s)

q_2 : volumetric flow rate through fixed office at the right (m^3/s)

q_3 : volumetric flow rate through variable office at the left (m^3/s)

q_4 : volumetric flow rate through variable office at the right (m^3/s)

p_s : supply pressure (Pa)

p_r : return pressure (Pa)

C_{do} : discharge coefficient of fixed orifices

C_{dn} : discharge coefficient of variable orifices

A_o : area of fixed orifices (m^2)

d_f : nozzle diameter of flapper nozzle valve (m)

x_i : the initial flapper distance to nozzle and flapper displacement limit (m)

x_f : the flapper displacement at the tip of the nozzles (m)

In this thesis study, discharge coefficients of left and right variable orifice are assumed equal. This assumption is justified in [24].

4.4. Pressure Losses and Effect of Oil Compressibility

The dynamic behavior of hydraulic transmission lines is affected by the hydraulic inertia, compressibility, and resistance [10]. Friction is the main cause of the loss of fluid energy as the fluid flows through a hydraulic transmission line. Because of friction, some fluid energy is converted to heat energy and exchanged into the surrounding atmosphere [44]. Hydraulic inertia refers to the energy stored within a fluid by virtue of its kinetic energy. The hydraulic inertia affects the transient response of the hydraulic transmission lines, but it has no significant effect on its

steady state behavior. The liquid compressibility is defined as the ability of liquid to change its volume when its pressure varies. Oil compressibility makes an important contribution to the dynamic behavior of the hydraulic control systems. The transient pressure variations, and consequently the transient variation of flow rates, forces, and accelerations, are highly affected by the oil compressibility [10].

The losses are considered in the pipes from spool to cylinder, and electrical analogy used for the calculation of losses in pipe system. The compressibility of hydraulic oil is also considered for the pipe volume.

4.4.1. Mathematical Model for Hydraulic Line of First Cylinder

In Figure 4-5, the electrical analogy for hydraulic line of first cylinder is shown. The losses due to hydraulic resistance and inertia are considered. The effect of compressibility of hydraulic fluid is taken into account.

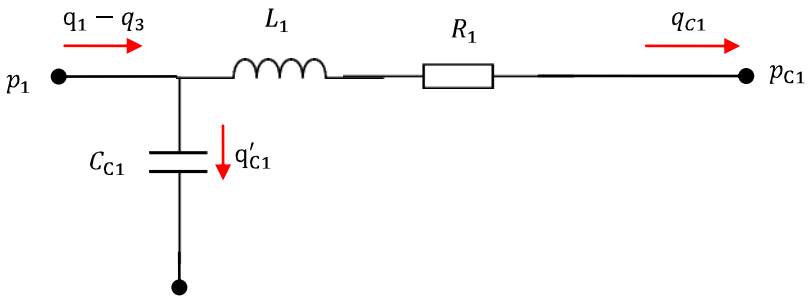

Figure 4-5 Electrical analogy for hydraulic line of first cylinder

If the flow in hydraulic line is assumed as laminar, the Hagen-Poiseuille equation can be used for calculating the resistance of hydraulic line. Loss due to resistance can be written as follows:

$$\Delta P_{R1} = R_1 q_{C1} = \frac{128\ \mu\ L_{pipe}}{\pi\ d_{pipe}^{\ 4}}\ q_{C1} \tag{4.19}$$

The following relations describe the motion of the hydraulic fluid under the action of its inertia. The effect of hydraulic inertia I, can be formulated as follows:

$$\Delta P_{I1} = I_1 \frac{dq_{C1}}{dt} = \frac{\rho L_{pipe}}{A_{pipe}} \frac{dq_{C1}}{dt} = \frac{\rho L_{pipe}}{\frac{\pi}{4} d_{pipe}^{\ 2}} \frac{dq_{C1}}{dt} \tag{4.20}$$

Considering the effect of hydraulic fluid compressibility (hydraulic capacitance) C, the following relation can be written;

$$q'_{C1} = C_{C1} \frac{dp_1}{dt} = \frac{V_1}{B} \frac{dp_1}{dt} \tag{4.21}$$

The continuity equation for first hydraulic line is as follows:

$$q_{C1} = (q_1 - q_3) - q'_{C1} \tag{4.22}$$

By combining Eqn. (4.20) and Eqn. (4.21), the volumetric flow to the first cylinder can be written as;

$$q_{C1} = (q_1 - q_3) - \frac{V_1}{B} \frac{dp_1}{dt} \tag{4.23}$$

By combining Eqn. (4.18) and Eqn. (4.19), the total pressure loss for hydraulic line of first cylinder can be written as;

$$\begin{aligned} \Delta P_{T1} &= \Delta P_{R1} + \Delta P_{I1} = R_1 q_{C1} + I_1 \frac{dq_{C1}}{dt} \\ \Delta P_{T1} &= p_1 - p_{C1} = \frac{128\,\mu L_{pipe}}{\pi d_{pipe}^{\ 4}} q_{C1} + \frac{\rho L_{pipe}}{\frac{\pi}{4} d_{pipe}^{\ 2}} \frac{dq_{C1}}{dt} \end{aligned} \tag{4.24}$$

where,

ΔP_{R1} : pressure loss due to resistance of first hydraulic line

ΔP_{I1} : pressure loss due to hydraulic inertia

ΔP_{T1} : total pressure loss at first hydraulic line

R_1 : hydraulic resistance for the hydraulic line of first cylinder

I_1 : hydraulic inertia for the hydraulic line of first cylinder

C_{C1} : hydraulic capacitance for the hydraulic line of first cylinder

V_1 : the volume of fluid in hydraulic line of first cylinder (m^3)

$q_{C1}{}'$: flow rate due to the compressibility of hydraulic fluid (m^3/s)

q_{C1} : flow rate to the 1st cylinder (m^3/s)

p_1 : pressure at the inlet of 1st hydraulic line (Pa)

p_{C1} : pressure at the 1st cylinder inlet (Pa)

μ : Dynamic viscosity of hydraulic fluid (Pa.s)

4.4.2. Mathematical Model for Hydraulic Line of Second Cylinder

In the hydraulic line of second cylinder, there exists the visco jet. At first the visco jet is modeled as orifice with very small area. So, the resistance of is visco jet is too high; therefore steady state flow rate through visco jet is very low. Simulation of Simulink model, which includes visco jet as an orifice, could not be run because of pressure higher than supply pressure. As a result of fluid compressibility, high pressure is built up at the inlet of visco jet. In Figure 4-6, the electrical analogy for hydraulic line of second cylinder is shown.

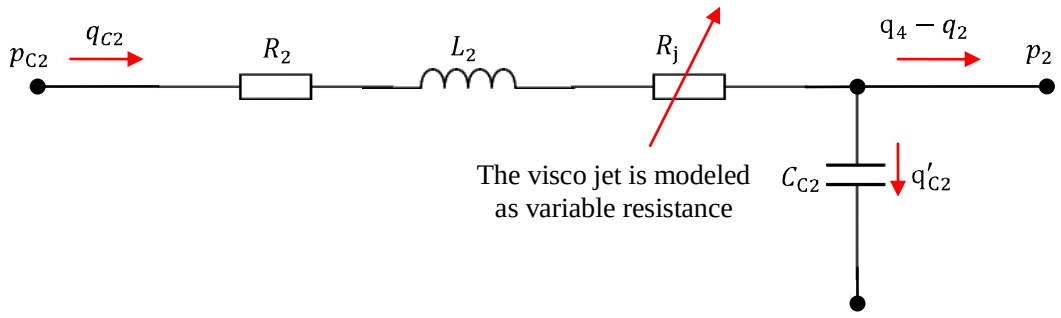

Figure 4-6 Electrical analogy for hydraulic line of second cylinder

While forming the mathematical model of the pipe system, the effect of hydraulic oil compressibility is taken into account. So, the transient flow rates are high enough to build up pressure at the inlet of visco jet higher than the supply pressure. Due to negative pressure difference, Simulink could not simulate the resulting mathematical model. As it is known from [42], the purpose of visco jet is to restrict the flow for adjusting the speed of input arm. So, it is decided to model the visco jet as a variable resistance. The term "variable" is used, because the resistance is changing according to pressure difference between the ports of visco jet.

As same in Section 4.4.1, the Hagen-Poiseuille equation can be used for calculating the resistance of hydraulic line. The lengths of two hydraulic lines L_{pipe} and the inner diameter of hydraulic lines d_{pipe}, are assumed equal.

Loss due to resistance of 2nd hydraulic line can be written as follows:

$$\Delta P_{R2} = R_2 q_{C2} = \frac{128\ \mu\ L_{pipe}}{\pi\ {d_{pipe}}^4}\ q_{C2} \tag{4.25}$$

The effect of hydraulic inertia *I*, can be formulated as follows:

$$\Delta P_{I2} = I_2\ \frac{dq_{C2}}{dt} = \frac{\rho\ L_{pipe}}{A_{pipe}}\ \frac{dq_{C2}}{dt} = \frac{\rho\ L_{pipe}}{\frac{\pi}{4}\ {d_{pipe}}^2}\ \frac{dq_{C2}}{dt} \tag{4.26}$$

Considering the effect of hydraulic fluid compressibility, the following relation can be deduced;

$$q'_{C2} = C_{C2}\ \frac{dp_2}{dt}\ = \frac{V_2}{B}\ \frac{dp_2}{dt} \tag{4.27}$$

The continuity equation for second hydraulic line is as follows:

$$q_{C2} - q'_{C2} = (q_4 - q_2) \tag{4.28}$$

By combining Eqn. (4.27) and Eqn. (4.28), the volumetric flow to the second cylinder can be written as;

$$q_{C2} = (q_4 - q_2) + \frac{V_2}{B}\ \frac{dp_2}{dt} \tag{4.29}$$

By combining Eqn. (4.25) and Eqn. (4.26), the total pressure loss for hydraulic line of second cylinder can be written as;

$$\begin{aligned} \Delta P_{T2} &= \Delta P_{R2} + \Delta P_{I2} = R_2 q_{C2} + I_2 \frac{dq_{C2}}{dt} \\ \Delta P_{T2} &= p_{C2} - p_2 = \frac{128\ \mu\ L_{pipe}}{\pi\ {d_{pipe}}^4}\ q_{C2} + \frac{\rho\ L_{pipe}}{\frac{\pi}{4}\ {d_{pipe}}^2}\ \frac{dq_{C2}}{dt} \end{aligned} \tag{4.30}$$

where,

ΔP_{R2} : pressure loss due to resistance of second hydraulic line

ΔP_{I2} : pressure loss due to hydraulic inertia

ΔP_{T2} : total pressure loss at second hydraulic line

R_2 : hydraulic resistance for the hydraulic line of second cylinder

I_2 : hydraulic inertia for the hydraulic line of second cylinder

C_{C2} : hydraulic capacitance for the hydraulic line of second cylinder

V_2 : the volume of fluid in hydraulic line of second cylinder (m^3)

q_{C2}' : flow rate due to the compressibility of hydraulic fluid (m^3/s)

q_{C2} : flow rate to the 2nd cylinder (m^3/s)

p_2 : pressure at the inlet of 2nd hydraulic line (Pa)

p_{C2} : pressure at the 2nd cylinder inlet (Pa)

μ : Dynamic viscosity of hydraulic fluid (Pa.s)

4.4.3. Cylinders Flow Equations

In Figure 4-7, the motion of pistons, nomenclature and the directions of flow rates are shown. Pitch trim actuator

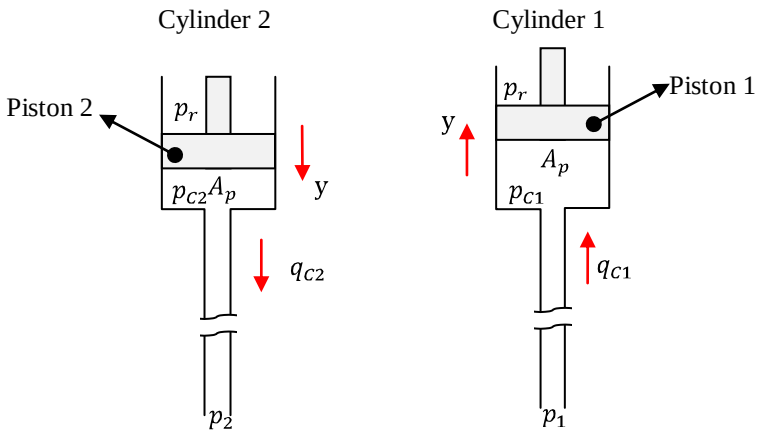

Figure 4-7 Motion of pistons and cylinder flow

If the leakages at the pistons are neglected, the continuity equation for hydraulic fluid flow through the cylinders can be written as follows:

$$q_{C1} = A_p \frac{dy}{dt} + \frac{V_o + A_p y}{B} \frac{dP_{C1}}{dt} \tag{4.31}$$

$$q_{C2} = A_p \frac{dy}{dt} - \frac{V_o - A_p y}{B} \frac{dP_{C2}}{dt} \tag{4.32}$$

where,

y : displacement of the pistons (m)

A_p : cross-sectional area of pistons (m^2)

V_o : volume of the cylinder at null position (m^3)

p_{C1} : pressure in the 1st cylinder(Pa)

p_{C2} : pressure at the 2nd cylinder (Pa)

4.5. Equations of Translational and Rotational Motion

The fundamental law governing mechanical systems is Newton's second law. Force acting on pistons due to the pressure difference between cylinders causes translational motion of pistons and the rotational motion of trim lever, gradient spring and input arm. In Figure 4-8, the schematic drawing of cylinders, pistons, trim lever and input arm is illustrated. There are springs under both pistons and the rods of pistons are always in contact between trim lever bearings. Trim lever is assumed as a rigid body. Thus, a vertical translational motion of one piston in a direction is directly transferred to the other piston in reverse direction. Translational motion of pistons causes rotational motion of input arm. The angular displacement of input arm is assumed equal to angular displacement of trim lever, because stiffness of the gradient spring is high enough to assume rigid connection for no-load condition.

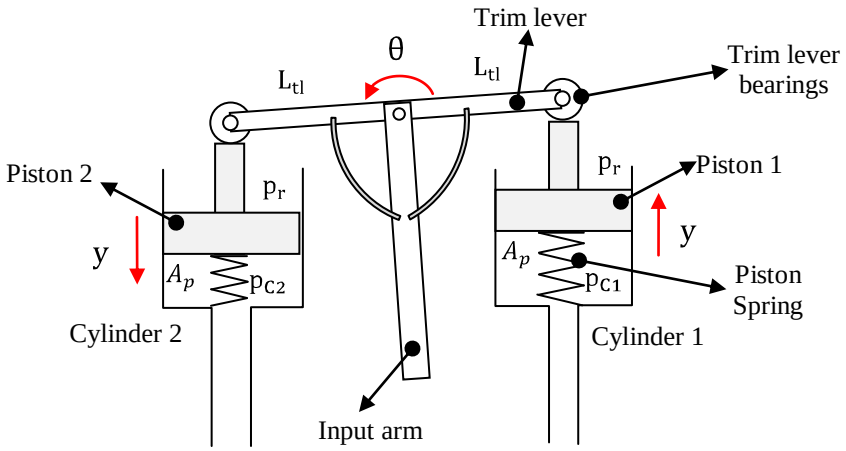

Figure 4-8 Schematic drawing of cylinders, pistons, trim lever and input arm

4.5.1. Equation of Translational Motion Pistons

To write the equation of motion of pistons, the free body diagrams of pistons are drawn. In Figure 4-9, the free body diagrams of pistons are shown.

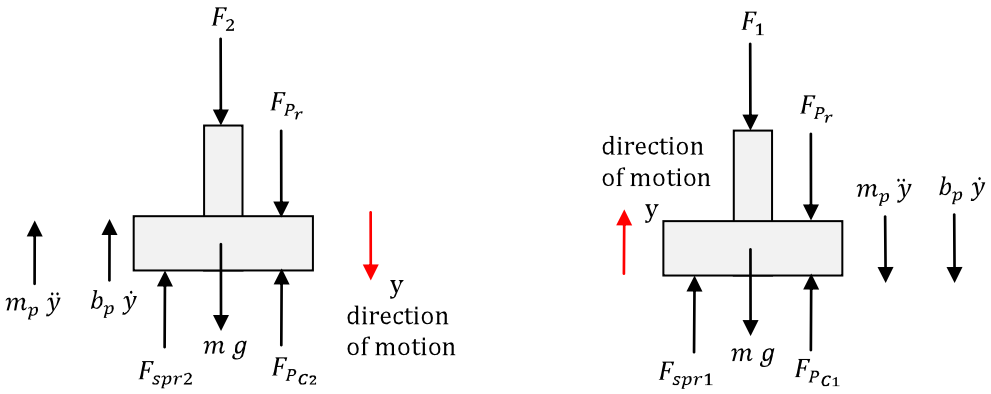

Figure 4-9 Free body diagram of pistons

Summing the forces acting on first piston and utilizing Newton's second law yields

$$\mathrm{m_p}\,\ddot{\mathrm{y}} + \mathrm{b_p}\,\dot{\mathrm{y}} = \mathrm{F_{P_{C_1}}} + \mathrm{F_{spr1}} - \mathrm{F_{P_r}} - \mathrm{F_1} - \mathrm{mg} \tag{4.33}$$

The spring force acting on first piston can be written as,

$$\mathrm{F_{spr1}} = \mathrm{K_p}(\mathrm{y_i} - \mathrm{y}) \tag{4.34}$$

Force due to first cylinder pressure can be formulated as,

$$\mathrm{F_{P_{C_1}}} = \mathrm{A_p P_{C1}} \tag{4.35}$$

Force due to return pressure can be written as,

$$\mathrm{F_{P_r}} = \mathrm{A_p P_r} \tag{4.36}$$

Combining Eqn. (4.34), Eqn. (4.35), and Eqn. (4.37) with Eqn. (4.33), equation of motion for 1st piston can be written as;

$$\mathrm{m_p}\,\ddot{\mathrm{y}} + \mathrm{b_p}\,\dot{\mathrm{y}} = \mathrm{A_p}(\mathrm{p_{C1}} - \mathrm{p_r}) - \mathrm{F_1} + \mathrm{K_p}(\mathrm{y_i} - \mathrm{y}) \tag{4.37}$$

The illustrated forces in Figure 4-9 acting on second piston are summed and Newton's second law is utilized. The equation of motion for 2nd piston can be written as;

$$m_p \ddot{y} + b_p \dot{y} = F_2 + F_{P_r} - F_{P_{C2}} - F_{spr2} + mg \tag{4.38}$$

The spring force acting on first piston can be written as,

$$F_{spr2} = K_p(y_i + y) \tag{4.39}$$

Force due to second cylinder pressure can be formulated as,

$$F_{P_{C2}} = A_p P_{C2} \tag{4.40}$$

Force due to return pressure can be written as,

$$F_{P_r} = A_p P_r \tag{4.41}$$

Combining Eqn. (4.39), Eqn. (4.40), and Eqn. (4.41) with Eqn. (4.38), equation of motion for 2nd piston can be written as;

$$m_p \ddot{y} + b_p \dot{y} = F_2 - A_p(p_{C2} - p_r) - K_p(y_i + y) \tag{4.42}$$

where,

F_{P_r} : force due to return pressure (N)
$F_{P_{C1}}$: force due to first cylinder pressure (N)
$F_{P_{C2}}$: force due to second cylinder pressure (N)
F_{spr1} : spring force acting on first piston (N)
F_{spr2} : spring force acting on second piston (N)
K_p : spring constant of piston spring (N/m)
y_i : initial compression of piston spring (m)
F_1 : reaction force acting on first piston (N)
F_2 : reaction force acting on second piston (N)
m_p : mass of the pistons (kg)
b_p : viscous damping coefficient of pistons (N.s/m)
y : displacement of the pistons (m)

4.5.2. Equation of Rotational Motion of Trim Lever and Input Arm

For no load condition, the gradient spring, which exists between trim lever and input arm, can be assumed as rigid connection. So, the trim lever and input arm assumed as single part. Translational motion of pistons causes rotational motion of trim lever and input arm. The free body diagram of trim lever and input arm is shown in Figure 4-10.

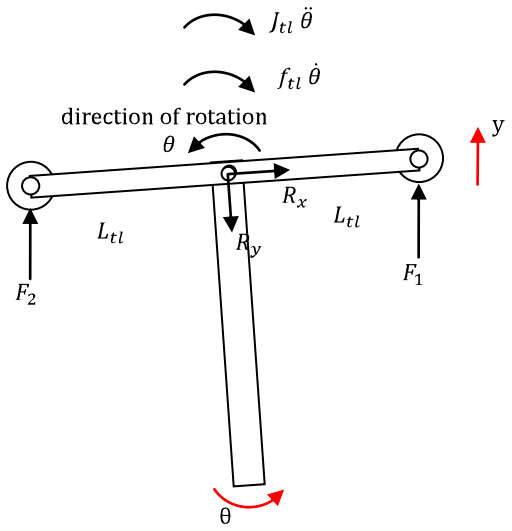

Figure 4-10 Free body diagram of trim lever and input arm

From free body diagram of trim lever and input arm, the equation of rotational motion;

$$J_{tl}\ddot{\theta} + f_{tl}\dot{\theta} = (F_1 - F_2)\,L_{tl} \tag{4.43}$$

where,

L_{tl} : the half length of trim lever (m)

θ : angular displacement of trim lever (rad)

$\dot{\theta}$: angular velocity of trim lever (rad/s)

$\ddot{\theta}$: angular acceleration of trim lever (rad/s^2)

J_{tl} : mass moment of inertia of rotating trim lever, gradient spring and input arm (N.m.s^2/rad)

f_{tl} : damping coefficient of rotating parts (N.m.s/rad)

Combining Eqn. (4.37), Eqn. (4.42) with Eqn. (4.43) and after some simplifications, it can written as follows:

$$J_{tl}\ddot{\theta} + f_{tl}\dot{\theta} = \left(A_p(P_{C1} - P_{C2}) - 2\, m_p\, \ddot{y} - 2\, b_p\, \dot{y} - 2\, K_p y\right)L_{tl} \tag{4.44}$$

From geometric relation;

$$y = L_{tl} \sin(\theta) \tag{4.45}$$

For small θ, $\sin(\theta) = \theta$, from Eqn. (4.45), it can be written

$$\theta = \frac{1}{L_{tl}}\, y \tag{4.46}$$

$$\dot{\theta} = \frac{1}{L_{tl}}\, \dot{y} \tag{4.47}$$

$$\ddot{\theta} = \frac{1}{L_{tl}}\, \ddot{y} \tag{4.48}$$

By inserting the above equations into Eqn. (4.44), we get

$$\left(\frac{J_{tl}}{L_{lt}^2} + 2\, m_p\right)\ddot{y} + \left(\frac{f_{tl}}{L_{tl}^2} + 2\, b_p\right)\dot{y} + 2\, K_p y = A_p(p_{C1} - p_{C2}) \tag{4.49}$$

4.6. Visco Jet as a Variable Resistance

For coarse approach, when compressibility of fluid and leakage in the pistons are neglected, from Eqn. (4.31) and Eqn. (4.32), it can be written;

$$q_{C_1} = q_{C_2} = A_p\, \dot{y} \tag{4.50}$$

If the losses at hydraulic lines are neglected, from Eqn. (4.24) and Eqn. (4.30), it can be written;

$$P_{C1} = P_1 \tag{4.51}$$

$$P_{C2} = P_2 \tag{4.52}$$

Flow rate for visco jet can be written as;

$$q_{C_1} = q_{C_2} = q_j = C_{do}\, A_j \sqrt{\frac{2}{\rho}\,(P_1 - P_2\,)} = A_p \dot{y} \tag{4.53}$$

For steady state response, acceleration term in Eqn. (4.49) can be neglected. Since the damping of rotational parts is too small when compared with damping effect of visco jet, it can be also neglected. Combining Eqn. (4.51) and Eqn. (4.52) and after simplifications, for the null position of pistons, Eqn. (4.49) can be rewritten as;

$$A_p(P_1 - P_2) = 2\, b_p \dot{y} \tag{4.54}$$

From Eqn. (4.53) and Eqn. (4.54),

$$A_p(P_1 - P_2) = 2\, b_p \frac{1}{A_p} C_{do}\, A_j \sqrt{\frac{2}{\rho}\,(P_1 - P_2)} \tag{4.55}$$

If variable damping coefficient caused by visco jet written as $b_j = 2\, b_p$, from Eqn. (4.55), it can be written;

$$b_j = 2\, b_p = \frac{A_p^2 \sqrt{|P_1 - P_2|}}{C_{do}\, A_j \sqrt{\frac{2}{\rho}}} \tag{4.56}$$

where,

b_j : damping coefficient caused by visco jet (N.s/m)

4.7. Conclusion

In this chapter, the mathematical model of pitch trim actuator is developed. To achieve realistic model, the effect of hydraulic fluid compressibility and losses at the transmission lines is taken into account. Equations for torque generated by electromagnetic forces, equation of rotational motion for torque motor armature, equations of volumetric flow rates through orifices, cylinders flow equations, equation of translational motion for pistons, equation of rotational motion for trim lever and input arm is established. By using these equations, the Simulik model of pitch trim actuator is constructed. To simulate the pitch trim actuator on Simulink environment, all the parameters used in mathematical model must be known or determined.

CHAPTER 5

EXPERIMENTAL STUDY

Experimental studies are carried out for parameter identification and to validate the Simulink model.

For identification of parameters, such as nozzle diameters, initial gap between flapper and nozzles, current gain, the stiffness of flexure tube of electromagnetic torque motor, particular tests are carried out. To use Simulink Parameter Estimation Toolbox, separate model of torque motor including the flow rates at one of the variable orifices is constructed. The input for this model is constant current and the output is flow rate at one of the variable orifices. It is planned to record flow rates for a constant pressure difference and for different constant current inputs. In these tests, two torque motors are tested. It is expected that the results of these two tests would be similar. However, different results are obtained. So, it is decided to determine the characteristics of torque motor together with the hydraulic system including fixed orifices.

For better evaluation, the torque motor is tested on structural body of pitch trim actuator with hydraulic system including fixed orifices. To conduct these tests, components of cylinders are removed from pitch trim actuator. For sealing the cylinder and boost ports of the actuator, piston like aluminum parts, dummy SAS actuator and plugs are designed and manufactured. To measure the pressures, small holes are drilled on the pipes of cylinders and pipes with connection nipple are soldered to these small holes. After these modifications, servovalve of the pitch trim actuator with four ports (C1, C2, Supply, and Return) could be tested separately. These tests are carried out on servovalve circuit of hydraulic test stand. For constant

supply pressure (6.89 MPa (1,000 psi)), different constant amplitude current inputs are given to the servovalve and the pressure and flow rate responses are measured. From these measured data, displacement of flapper, initial gap between flapper to nozzles, diameter of visco jet, and nozzle diameters are calculated by using mathematical models.

The experimental tests for data acquisition are done on two configurations. The first configuration is pitch trim actuator as an assembly without measuring pressures at cylinder inlet. The second configuration is pitch trim actuator with pressure measuring ports added on cylinder pipes. For first configuration, only the displacements of input arm of pitch trim actuator are measured for various current inputs. For both configuration square wave (step changes) and sine wave current inputs at different frequencies and amplitudes are given to torque motor. Square wave (step changes) current inputs with low frequency are used to measure transient and steady state behavior. Sine wave current inputs are used to determine frequency response of pitch trim actuator. For second configuration, the displacement of input arm and the pressures at the cylinder pipes are measured for different square and sine wave current inputs.

Due to visco jet, the flow rate through cylinder pipes is too small. Long hydraulic lines in order to measure pressures on cylinder pipes have adverse effects on the response time of the actuator. Thus, the experimental data could not be used to validate transient response. Adverse effect of long hydraulic lines is included to Simulink model by increasing the initial volume of the cylinders.

5.1. Experimental Setup

The experimental setup for testing and designating defects on pitch trim actuator is based on [42]. The systems used for functional test of pitch trim actuator are also used for experimental study. The test conditions are given in Table 5-1.

Table 5-1 Experimental test conditions [42]

Hydraulic Fluid :	MIL-PRF-83282
Actuator Hydraulic Supply Pressure	6.62-7.17 MPa (960 - 1,040 psig)
Boost Hydraulic Supply Pressure	19.65-21.72 MPa (2,850 - 3,150 psig)
Hydraulic Return Pressure	0-1.38 MPa (0 - 200 psig)
Hydraulic Fluid Temperature	21° to 49°C (70° to 120°F)
Hydraulic Fluid Filtration	3 micron per MIL-F-8815
Ambient Temperature	16° to 38°C (60° to 100°F)
Ambient Pressure	0.95-1.05 bar (28 - 31 inches Hg)
Relative Humidity	90% maximum

5.1.1. Hydraulic Test Stand

The hydraulic test stand used in experiments is manufactured by AAI/ACL Company. The model number of hydraulic test stand is 9770. The maximum flow rate of hydraulic pump is 946 cm^3/s (15 gpm). The maximum pressure supply of hydraulic stand is 34.5 MPa (5,000 psi). Tubing material for high pressure line is stainless steel and for low pressure line is aluminum. The schematic diagram of the servovalve circuit of the hydraulic test stand is shown in Figure 5-1.

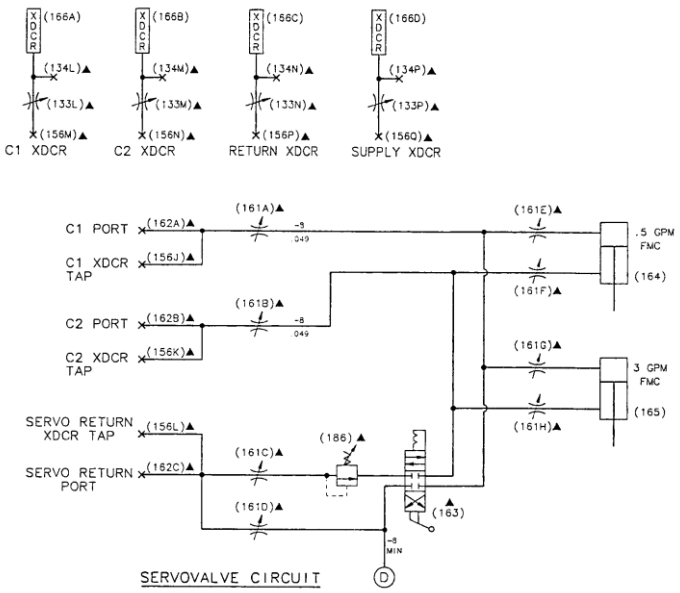

Figure 5-1 The schematic diagram of servovalve circuit of hydraulic test stand

This servovalve circuit is for testing 4-way servovalves. C1 port and C2 port can be connected with calibrated cylinders for flow measurements. There are two cylinders; one of which is to measure flow rates lower than 31.5 cm^3/s (0.5 gpm), the other is to measure higher flow rates (maximum 189 cm^3/s (3 gpm)). There are four pressure transducers to measure the pressures at ports C1, C2, Return, and Supply.

The overall material of base frame, cabinet and panel is stainless steel. The picture of hydraulic test stand taken from the hydraulic workshop of 5^{th} MMC is given in Figure 5-2

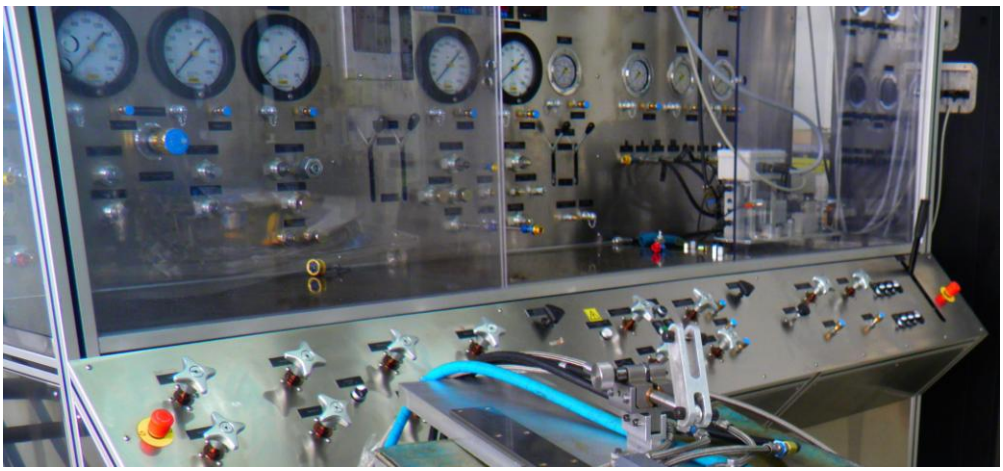

Figure 5-2 Hydraulic test stand

5.1.2. Electronic Console

Electronic console of hydraulic test stand shown in Figure 5-3 consists of six main parts. These are touch screen, PC controller, keyboard, Image® controller, printer, and power supplies and transformer. As a user interface, the electronic console utilizes special software named as Image®. Image® software gives ability for users to set currents, solenoids or control the signal generator by using buttons on the screen. Electronic console can be controlled using the touch screen and the keyboard or by using just the keyboard by itself. The keyboard is used in conjunction with the touch screen for entry of numerical data.

The main screen of Image® software is shown in Figure 5-3. By touching the buttons on the screen, the user can set current input, plot the output of transducer etc. It is possible for user to zoom, to window the plot after test, but the software does not have saving capability.

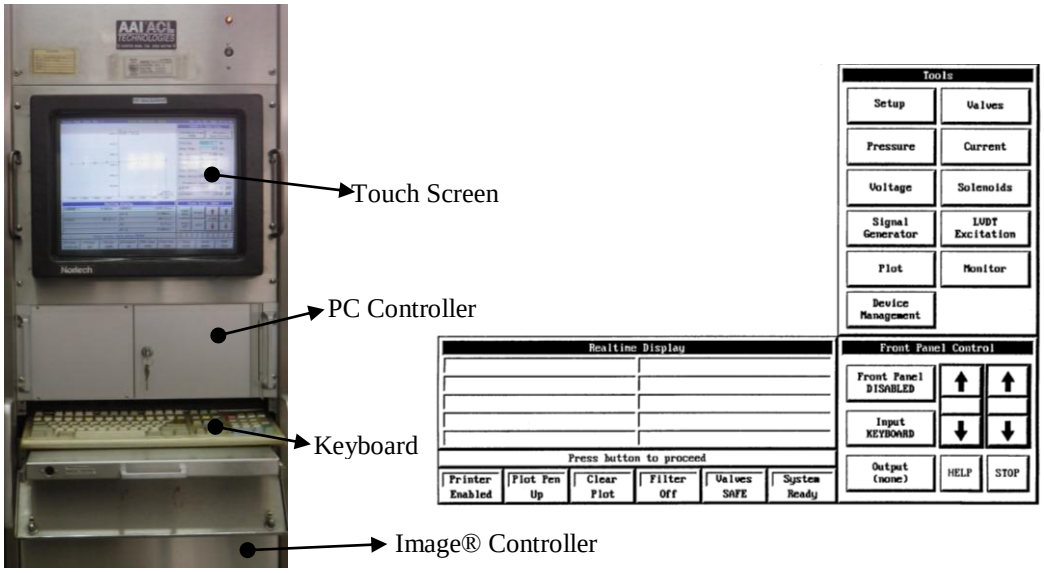

Figure 5-3 Electronic console and main screen of Image software

The results are shown on a graphical screen. The recording is possible by printing the plot. Because of that to acquire the experimental data for validation, electronic console is used only as current input device. For storing the data, another acquisition system is used. The details of data acquisition system are described in Section 5.1.4.

5.1.3. Test fixture

A test fixture is designed for experimental studies. The test fixture consists of servo position actuator for giving automated input, load cell for measuring input force, sliding mechanism to convert rotational motion into translational motion, position transducer to measure input displacement and velocity, dummy SAS actuator for supporting output arm, friction device to simulate forces due to flight controls, pressure block to connect pitch trim actuator to hydraulic test bench, fixture table to support all the equipment, cables and connectors.

For the experimental test, servo positioning part of the test fixture is not used. The displacement measurement is taken from sliding mechanism by position transducer compatible with KAM-500 system. The 3-D drawing and the components of test fixture are shown in Figure 5-4.

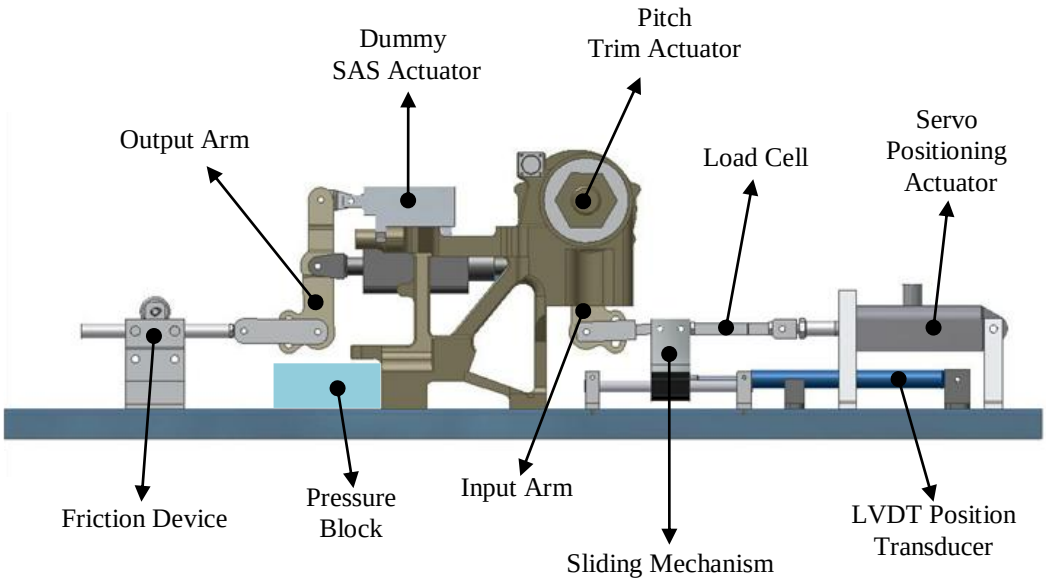

Figure 5-4 Designed test fixture

The picture of manufactured test fixture is given in Figure 5-5. The test fixture is currently used for testing pitch trim actuator subsequent to maintenance, repair or overhaul. In addition to this text fixture, there is a specific test software and electronic console to carry out the tests stated in [42]. The picture of electronic console for pitch trim actuator tests is shown in Figure 5-6.

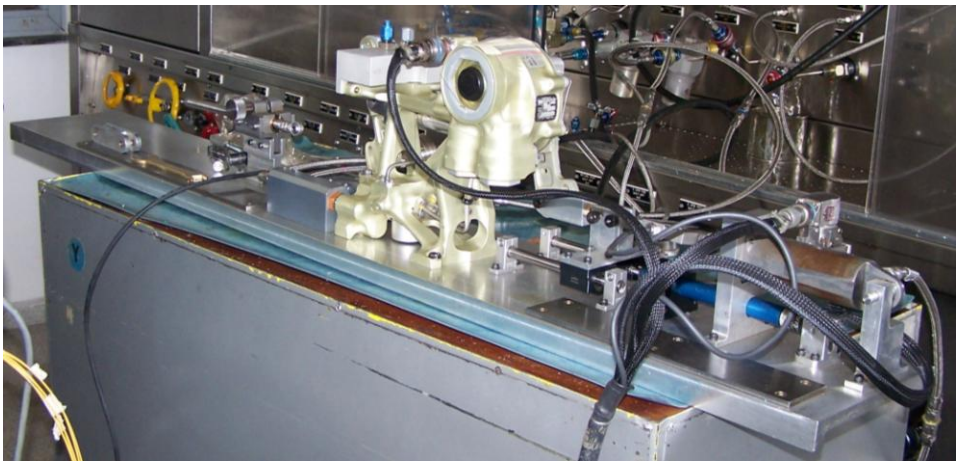

Figure 5-5 Manufactured test fixture

The software of pitch trim actuator test system is written by 5th MMC personnel. For routine tests, it gives instructions to operator and done the test automatically. By the help of this software, it is also possible to do manual tests.

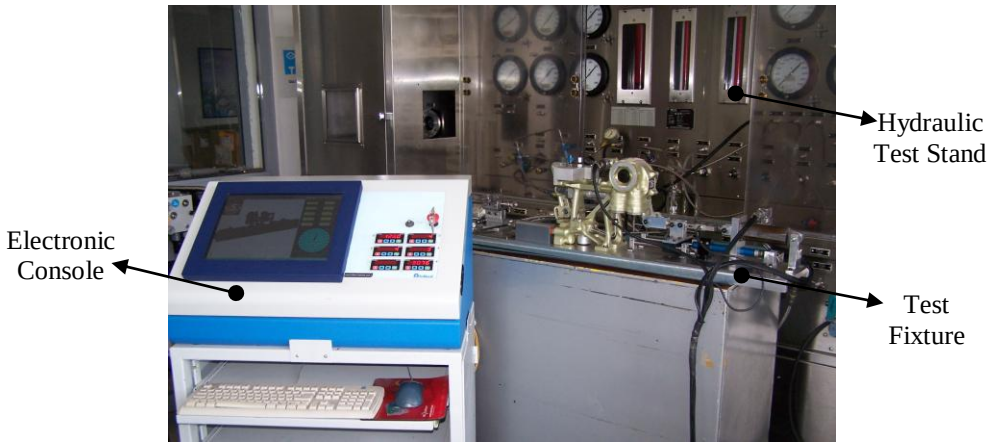

Figure 5-6 Electronic console and test fixture

5.1.4. Data Acquisition System

Experimental data acquired by commercially available data acquisition system known as KAM-500, which is manufactured by ACRA Control of Dublin, Ireland. The KAM-500 is a small, rugged, modular, lightweight data acquisition system with a relatively low power consumption that is designed for remote operation in harsh environments. Its operational temperature range is from -40 °C to +85 °C (-40 °F to +185 °F), and it can withstand 100 g shock loads. The KAM-500 is programmable from a remote computer; the data channel selection, data sampling rates, filter cut-off frequencies, channel gains and offsets, bridge excitation voltages, and PCM format are some of the options that can be set from a ground based computer. The programming information can be transferred via hard-wire from the computer to the data acquisition system at any time. In Figure 5-7, the picture of KAM-500 data acquisition system and the computer is shown.

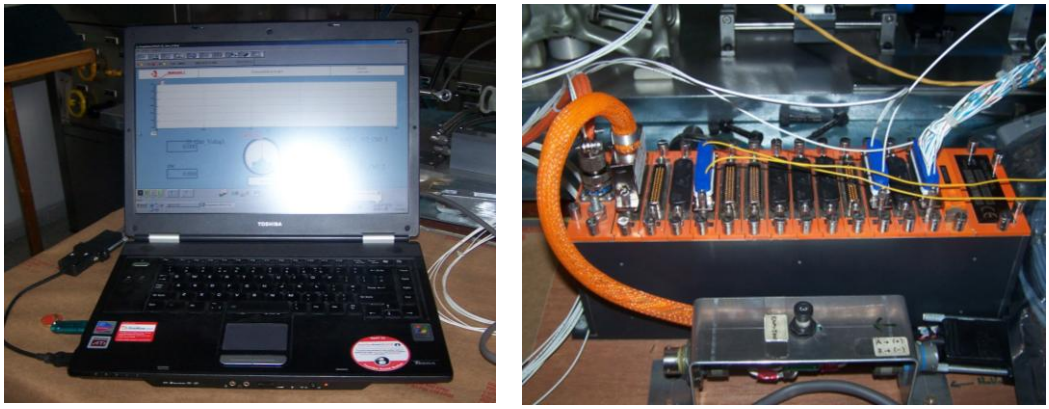

Figure 5-7 KAM-500 data acquisition system

5.1.5. Data Acquisition Software

The KAM-500 system uses Magali GSX-500 graphical user interface software to store, analyze, post-process, and visualize the data. A screen shot of software is shown in Figure 5-8.

Figure 5-8 Magali GSX-500 software

By using Magali GSX-500 software, channel names and sampling frequencies can be entered. The real time data acquisition screen can be prepared. The data can be stored in specified directory set by the user.

5.1.6. Position Transducer

The displacement of input arm is measured by commercially available position transducers, which is manufactured by Spaceage Control Inc. The range of position transducers is 165 mm (6.5 inches). The type is one-turn conductive plastic potentiometer. The transducer includes a minimum of 305 mm (12 inches) of displacement cable, pull ring for connection to the application, and a minimum of 457 mm (18 inches) Teflon insulated electrical cable. The picture of position transducer is shown in Figure 5-9 (a).

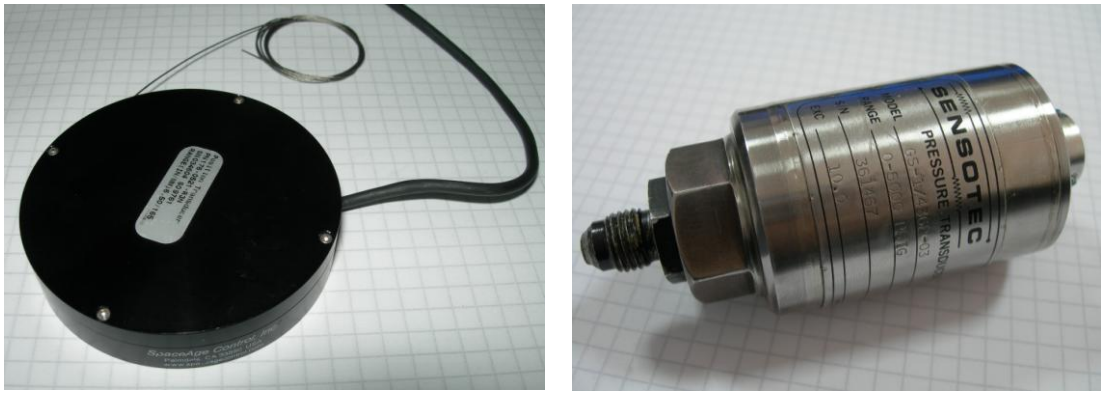

(a) (b)

Figure 5-9 (a) Position transducer, (b) Pressure transducer

5.1.7. Pressure Transducers

The pressures of ports are measured by commercially available pressure transducers shown in Figure 5-9 (b), which are manufactured by Sensotec. The transducer uses resistive type, balanced, and bonded fully active strain gage bridge. The pressure range of the transducers is 0-34.5 MPa (0-5000 psi). Nominal bridge resistance of transducer is 350 Ohm. Excitation voltage is 10 VDC. The non-linearity of transducer is 0.15% of the rated output. In Figure 5-9 (b), the picture of pressure transducer is shown.

5.2. Sub-Assembly Tests

The dynamic characteristic of pitch trim actuator depends on the electromagnetic torque motor. To achieve a realistic model of the torque motor, the parameters such as current gain, stiffness of flexure tube, diameter of nozzles, initial gap between flapper and nozzles must be determined. These parameters affect the displacement of torque motor flapper. The flow rates through variable orifices and the pressures depend on flapper displacement. The variable orifices consist of two nozzles and the torque motor flapper. When the flapper moves towards a nozzle, the area of hydraulic passage decreases. As a result, the resistance to flow of hydraulic fluid increases and the pressure at this side of hydraulic circuit increases. On the other side of hydraulic circuit, the flapper moves away from nozzle, thus the resistance to flow of hydraulic fluid decreases and the pressure at this side of hydraulic circuit decreases. To calculate the displacement of flapper, it is important to determine the parameters mentioned above accurately.

To determine these parameters, electromagnetic torque motor is tested particularly. The aim of these tests is to calculate the parameters of torque motor. If the Eqn. (4.11), Eqn. (4.12), and Eqn. (4.17) are revisited as shown below, to calculate flow rate q_3, for a current input i, the values of K_i, J_α, f_α, $(K_t - K_m)$, K_i, d_f, L_f, L_t, p_1, p_r, C_{dn} must be known or determined.

$$J_\alpha \frac{d^2\,\alpha}{d^2\,t} + f_\alpha \frac{d\,\alpha}{d\,t} + (K_t - K_m)\,\alpha = K_i i - \frac{\pi}{4} . d_f^2\,(p_1 - p_2) L_f \qquad (4.11)$$

$$x_f = (L_f - L_t/2)\,\alpha \qquad (4.12)$$

$$q_3 = C_{dn} \pi\, d_f (x_i - x_f) \sqrt{\frac{2}{\rho}\,(p_1 - p_r)} \qquad (4.17)$$

In experimental study for torque motor, for constant pressure values, the current input is changed. It is expected that steady state flow rate from one side of torque motor is proportional to current. For a test for port 1, pressure at port 2, p_2 and return pressure, p_r is set to zero. The current, i and pressure, p_1 are the inputs, and flow rate at port 1 is measured as an output. The mass moment of inertia of rotating armature, J_α is calculated by 3-D CAD program. The values of damping coefficient of

armature, f_α and discharge coefficient at nozzle, C_{dn} are assumed. The length of flapper, L_f, the length of flexure tube, L_t are measured. The density of hydraulic fluid, ρ is known. The unknown values are current gain, K_i, difference between stiffness of flexure tube and electromagnetic spring constant $K_t - K_m$, nozzle diameter, d_f, initial gap between flapper and nozzles, x_i.

For determining x_i, the current input is set to zero, pressures at both side of the flapper are equal. The pressure is set to a value and the total flow rate is measured from return port for this given pressure value. If the discharge coefficient at variable orifices is assumed as constant, for a value of nozzle diameter, d_f, the initial gap between flapper and nozzles, x_i can be calculated. The displacement of flapper at the tip of nozzles, x_f is derived from Eqn. (4.16).

From Eqn. (4.12), armature angular displacement, α could be calculated by using known values. For steady state value of α, the angular acceleration and angular velocity term of Eqn. (4.12) is neglected. From this simplified equation for a known pressure difference, the values of current gain, K_i, difference between stiffness of flexure tube and electromagnetic spring constant, $K_t - K_m$ and nozzle diameter, d_f could be calculated.

5.2.1. Electromagnetic Torque Motor Test

The aim of the tests is to measure flow rates for different pressures and for different current inputs. From these flow rates, it is intended to calculate the displacement of flapper, stiffness of flexure tube and torque motor current gain.

To test the electromagnetic torque motor, an aluminum manifold is manufactured to connect the ports of torque motor to hydraulic test stand. In Figure 5-10, the test setup for electromagnetic torque motor is shown. As it is seen from the figure, there are three ports of electromagnetic torque motor; C1, C2 and return ports.

The flow rates are measured by a 250 ml graduated cylinder and a chronometer. The procedure for measuring the volumetric flow rates is as follows:

1. Set pressure to a certain value at one port.
2. Record port name and pressure value.
3. Set the pressure zero for the other port. Record port name.
4. Set current to a certain value.
5. Record the current value.
6. Wait for approximately 10 second to obtain steady state flow.
7. Collect the hydraulic fluid from return port in a 250 ml graduated cylinder. At the same time, start the chronometer.
8. Stop the chronometer when 250 ml is filled. Record the time.
9. Change the current input, repeat steps 5-8.
10. Repeat steps 1-9 by swapping the ports.
11. Repeat steps 1-10 for a different pressure value.

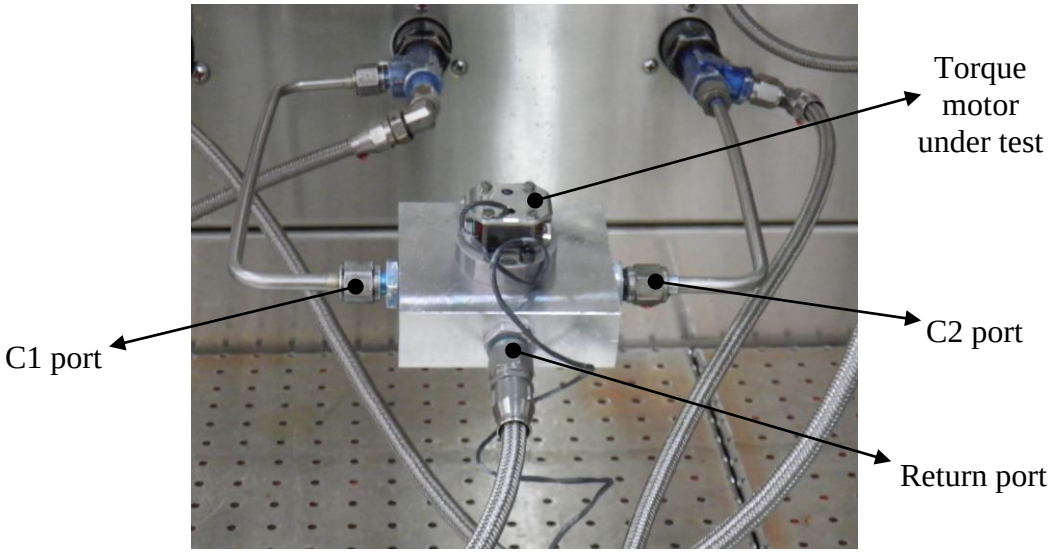

Figure 5-10 Test setup for electromagnetic torque motor

In these tests, two torque motors are tested. From these tests, initial gap between flapper and nozzles, x_i and nozzle diameter, d_f is determined. For the other parameters, it is expected that the results of these two tests would be similar. However, different results are obtained. So, it is decided to determine the

characteristics of torque motor together with the hydraulic system including fixed orifices.

5.2.2. Torque Motor Tests Together with Hydraulic System Including Fixed Orifices

To test electromagnetic torque motor together with hydraulic system including fixed orifices, the frame of pitch trim actuator is used. The pistons of pitch trim actuator are replaced by manufactured piston like aluminum block and the cylinder ports are sealed. Ports for pressurizing pitch SAS actuator and the ports for pitch boost actuator are plugged with aluminum blocks. In Figure 5-11, modifications done on pitch trim actuator is shown.

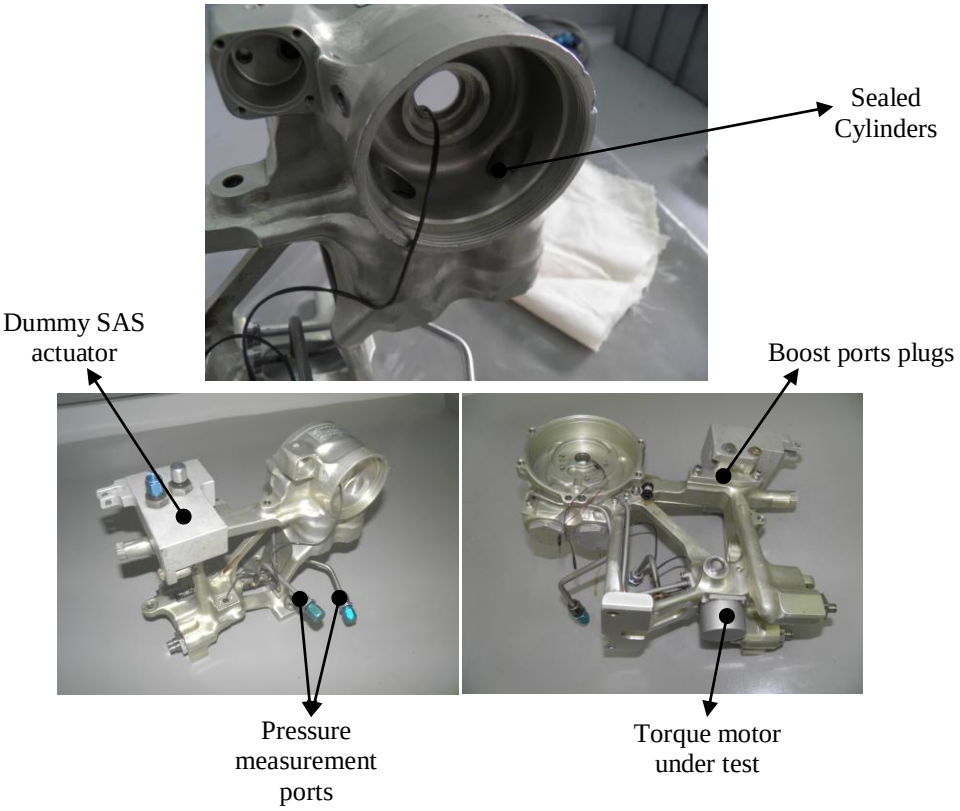

Figure 5-11 Torque motor and fixed orifice test setup

To measure the pressures, small holes is drilled on the pipes of cylinders and pipes with connection nipple are soldered to these small holes. After these modifications,

servovalve of the pitch trim actuator with four ports (C1, C2, Supply, and Return) could be tested separately. These tests are carried out on servovalve circuit of hydraulic test stand. For constant supply pressure (6.89 MPa (1,000 psig)), different constant amplitude current inputs are given to the servovalve and the pressure and flow rate responses are measured. Figure 5-12 shows a sample plots from result of test for ± 4 mA constant current input. The graphs of test resultsare given in Appendix.

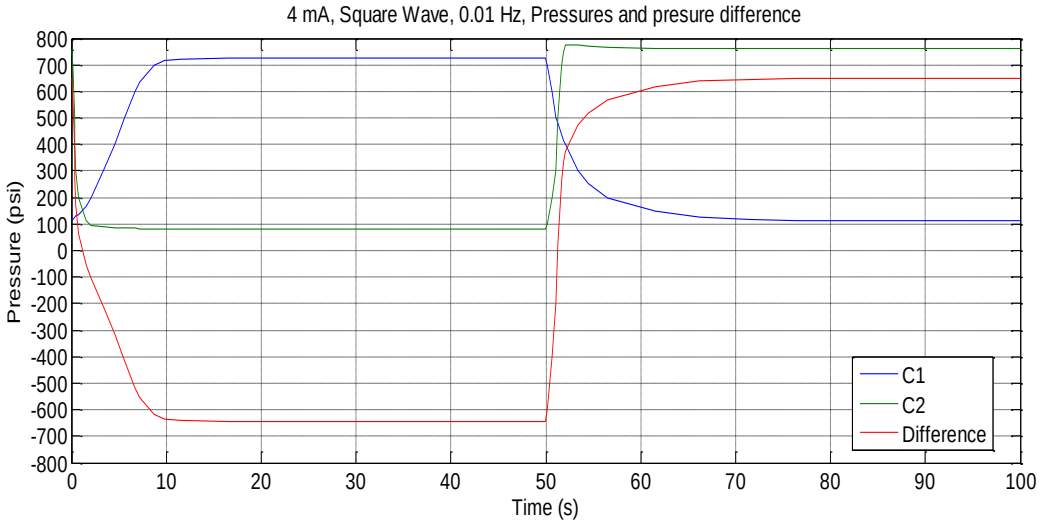

Figure 5-12 Sample plot for servovalve test

5.3. Procedure for Acquiring Validation Data

The channel names, channel configuration and sampling frequency is set on Magali GSX-500 software before the acquisition. The pitch trim actuator is mounted on test fixture. The supply pressures,P_s is set to 6.89 MPa (1,000 psi) and the return pressure,P_r is set to 0.35 MPa (50 psi). The amplitude, frequency and type (sine, square wave) of current input signal is set at electronic console. The position of pitch trim actuator input arm is taken to midpoint manually. The acquisition name is changed at Magali GSX-500 software. The current is sent to pitch trim actuator, at the same time the acquisition is started manually. The acquired data is exported to MATLAB via text file. The voltage data is converted to physical values (mA, psi, Pa, inch, mm etc.)

5.4. Determination of Physical Values

To determine the values of parameters, different methods are used. The first method is direct measurement if it is possible. The second method is calculation by using the result of experimental study or known values. CAD program is utilized to calculate mass moment of inertia of rotating parts. With the results of particular tests mentioned in Section 5.2, Simulink Parameter Estimation Toolbox is used to predict the values of parameters such as current gain, K_i and difference between stiffness of flexure tube and electromagnetic spring constant, $K_t - K_m$. M-files containing the values of all parameters used in mathematical model are given in Appendix B.

5.4.1. Electromagnetic Torque Motor

The torque motor used on pitch trim actuator is permanent magnet type. From electromagnetic equations given in Section 4.1.1, the torque motor current gain K_i and torque motor electromagnetic spring constant K_m are calculated.

Table 5-2 Properties of electromagnetic torque motor

Material	Alnico8
Residual Induction, Br	0.83 T
Coercive Force, Hc	131,340 A turn/m
Constant of leakage flux in air gap, kl	0.27
Permanent magnet permeability, μm	6.32×10^{-6} H/m
Air Gap permeability, μ0	1.26×10^{-6} H/m
Length of permanent magnet, lm	10×10^{-3} m
Width of permanent magnet, wm	18×10^{-3} m
Cross sectional area of magnet, A_m	1.8×10^{-4} m2
Cross sectional area of air gap, A_a	2×10^{-5} m2
Number of turns of each coil, N	3,000

By using values given in Table 5-2, from Eqn. (4.2), Eqn. (4.3), Eqn. (4.4), and Eqn. (4.5), the following values are calculated.

$$M_m = 1313 \ [A.turn]$$

$$k_r = 1.129$$

$$K_i = 15.536 \ [N.m/A]$$

$$K_m = 79.88 \ [N.m/rad]$$

CHAPTER 6

SIMULINK MODEL

6.1. The Structure of the Model

The pitch trim actuator Simulink model shown in Figure 6-1 consists of four subsystems. The first subsystem is as "Input system". It is used to test the model with different inputs and to easily change the current input given to the system. The second subsystem is named as "Torque Motor" which includes the model of the electromagnetic torque motor. The third subsystem is named as "Flow Rates & Pressures" which includes the model of the hydraulic Wheatstone bridge, flow rates and resultant pressures. The fourth subsystem is "Pistons & Rotational components". It is used to model the cylinder motion and input arm rotation.

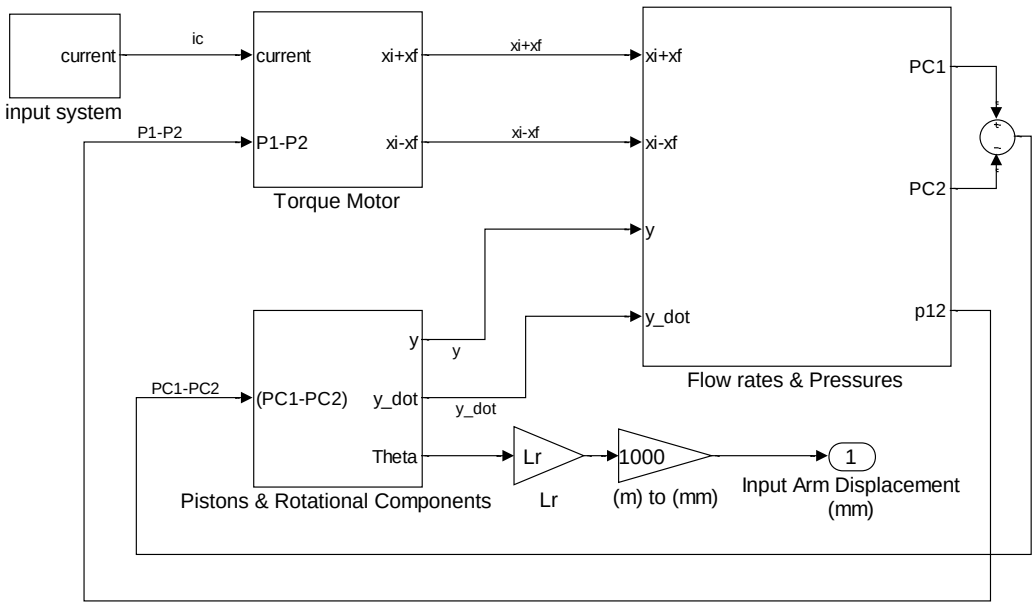

Figure 6-1 Pitch trim actuator Simulink model

6.2. Torque Motor Model

"Torque Motor" subsystem shown in Figure 6-2 is constructed based on torque equation mentioned in Section 4.1.2. It includes switch block to simulate the limiting action of nozzles. The inputs of subsystem are current and pressure difference at the tip of the flapper and the outputs of the subsystem are two distances between flapper and nozzles.

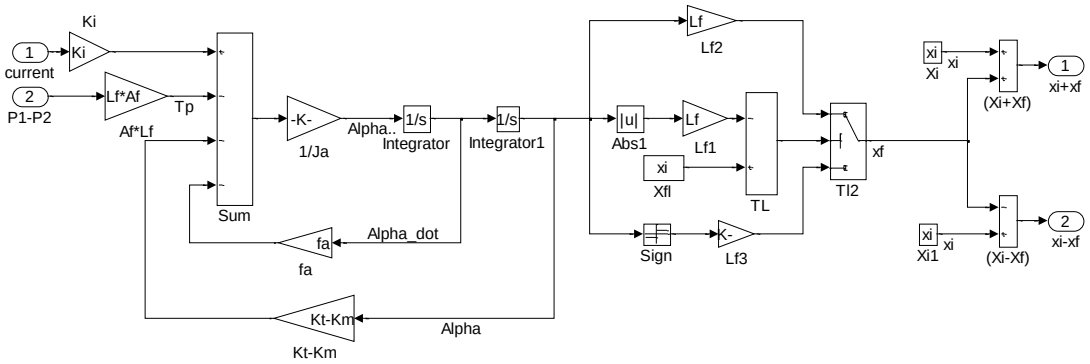

Figure 6-2 The Simulink model of electromagnetic torque motor

6.3. Fixed and Variable Orifice System and Cylinder Hydraulic Model

"Flow Rates & Pressures" subsystem of the model shown in Figure 6-3 includes flow rates equation, models of hydraulic lines, and pressures at the cylinder. The inputs of this subsystem are two distances between flapper and the outputs of the subsystem are pressures of cylinders. The detail of flow rates subsystem is given in Appendix C.

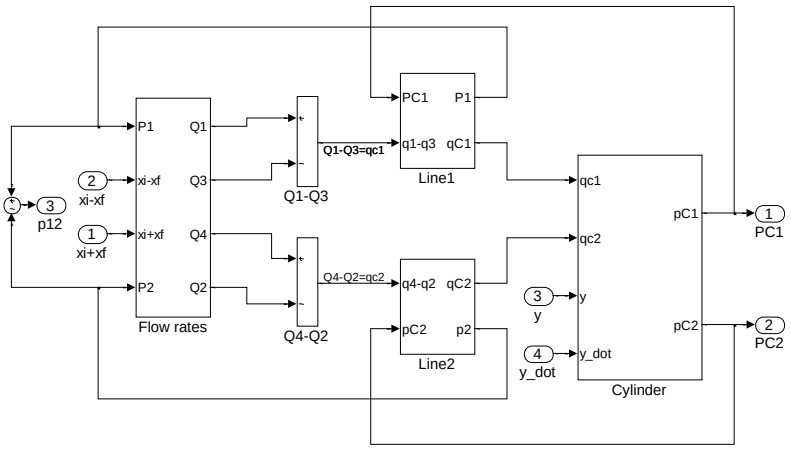

Figure 6-3 The Simulink model of Wheatstone bridge and cylinder pressure

As it is mentioned in Section 4.4, electrical analogy is used to model the hydraulic pipe lines. The subsystem names as “Line 1” shown in Figure 6-4 includes the hydraulic line model for first cylinder based on the equation given in Section 4.4.1. The inputs of subsystem are flow rate difference and pressure of 1st cylinder and the outputs of the subsystem are pressure at the inlet of 1st line and flow rate to 1st cylinder.

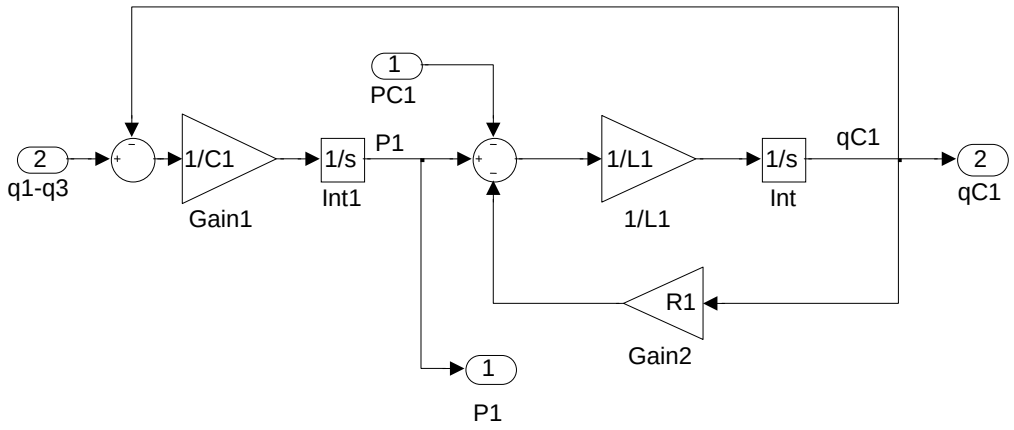

Figure 6-4 Simulink model for hydraulic line of first cylinder

The subsystem names as “Line 2” shown in Figure 6-5 includes the hydraulic line model for second cylinder based on the equation given in Section 4.4.2. The inputs of subsystem are flow rate difference and pressure of 2nd cylinder and the outputs of the subsystem are pressure at the inlet of 2nd line and flow rate to 2nd cylinder.

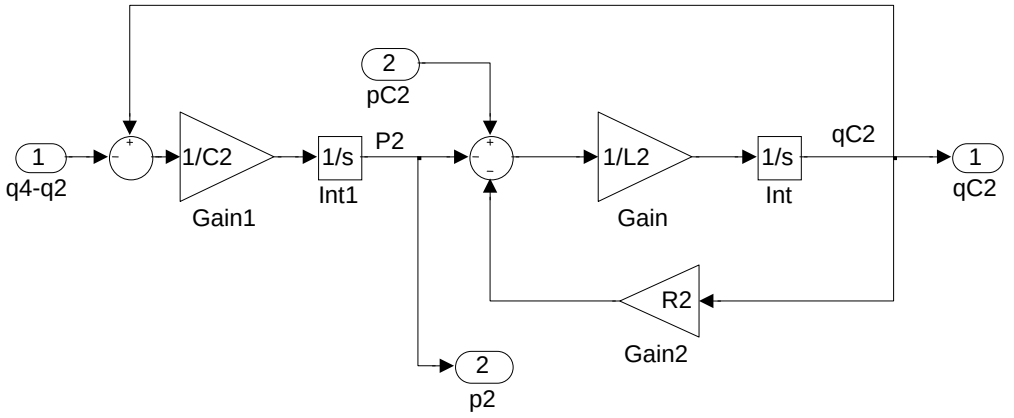

Figure 6-5 Simulink model for hydraulic line of second cylinder

6.3.1. Cylinder Pressure and Flow Rate Model

The cylinder pressures are found by considering the compressibility of fluid and flow rates to the cylinders. The cylinder volume is important to calculate the cylinder pressures. During validation of Simulink model, it is recognized that the volume of pipelines, added on pitch trim actuator to measure the pressures at cylinders, has a great influence on system response time since the flow rate is very small. Due to the high response time, transient response of pitch trim actuator could not be measured well especially for high frequency. The model for cylinder flow and pressures is given in Figure 6-6 based on the equation in Section 4.4.3.

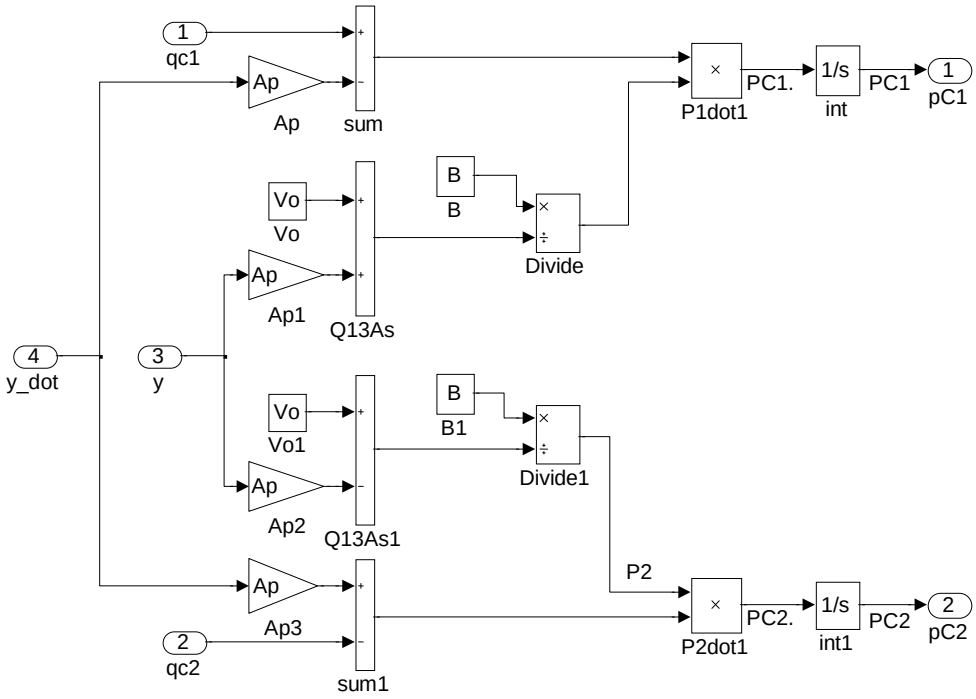

Figure 6-6 The Simulink model of cylinder pressures

6.4. Pistons, Trim Lever and Input Arm Motion Model

The subsystem named as “Pistons & Rotational components” is based on motion and rotation equations developed in Section 4.5. As it is mentioned in Section 4.6, effect of visco jet is modeled as variable resistance. The damping coefficient due to visco jet is included to model. In Figure 6-7, the Simulink model for motion of pistons and rotation of input arm is given.

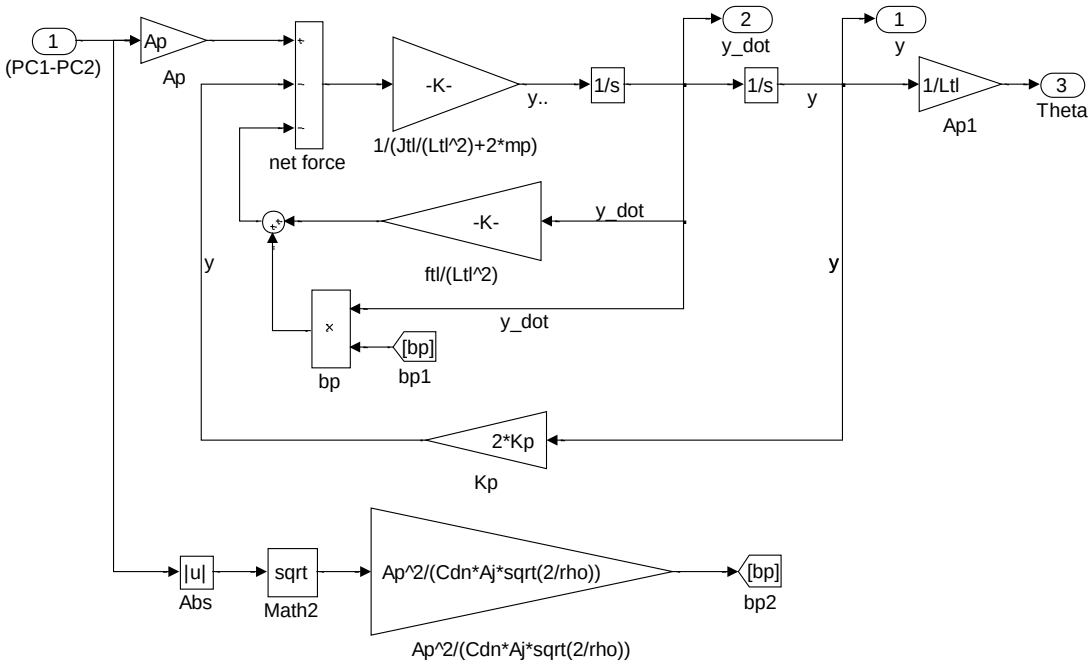

Figure 6-7 The Simulink model for motion of pistons and rotation of input arm

CHAPTER 7

EXPERIMENTAL EVALUATION OF MODELS

7.1. Data Acquisition Method

For validation of Simulink model, data such as current input, input arm displacement, pressures at the inlet of the cylinder, supply pressure are acquired by using KAM-500 data acquisition system.

The experimental data acquisitions are carried out on two configurations. The first configuration is pitch trim actuator as an assembly without measuring pressures at cylinder inlet. The test matrix for this configuration is given in Appendix D (Table D-1). For these current inputs the displacement of input arm of pitch trim actuator is measured as output by position transducer and by trim position potentiometer.

The second configuration is pitch trim actuator with pressure measuring ports added on cylinder pipes. To plot Bode diagram for pitch trim actuator; systematic sine wave response of pitch trim actuator is acquired. Test matrix for Bode diagram is given in Appendix D (Table D-2). For these current inputs, the displacement of input arm, pressures at the cylinder pipes are measured as outputs.

From the measured displacement of input arm, the velocity is calculated by using MATLAB built in "`diff`" command for each frequency given in Table D-2. Amplitudes of velocities are converted to dB for plotting Bode diagram. The Bode diagram is shown in Figure 7-1.

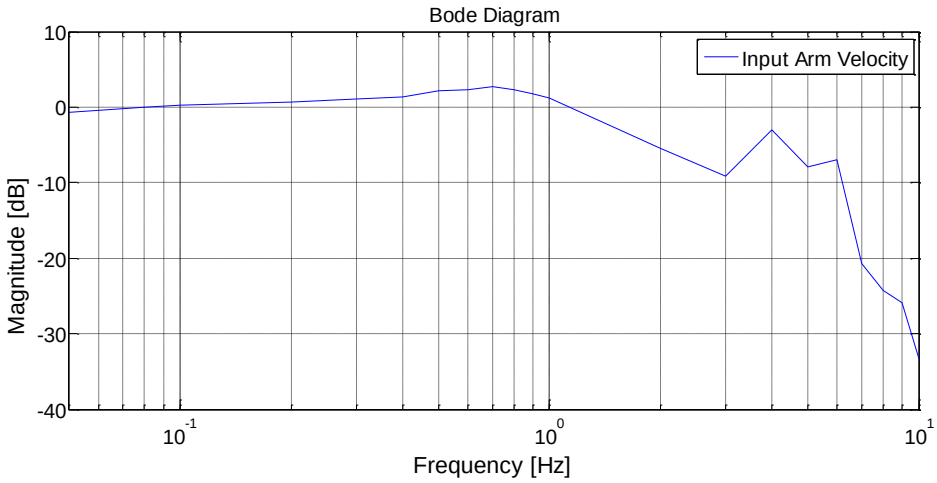

Figure 7-1 Bode diagram of displacement of input arm

The magnitude of the frequency response is -3 dB at 1.55 Hz excitation frequency, indicating the bandwidth of the system. This is not an expected result. The frequency response of torque motor is much higher. However, volumetric flow rate is too low due to visco jet, so, frequency response of pitch trim actuator is too low. Also, long hydraulic line added to measure pressures affect the frequency response of the system. It is seen from the Bode diagram that there is an increase in magnitude around 0.7 Hz. This could be the resonance frequency of the system with hydraulic lines added.

7.2. Data Post Processing and Scaling

The KAM-500 system uses Magali GSX-500 software to store, analyze, post-process, and visualize the data. The Magali GSX-500 software gives opportunity for user to export the data to text file. The processing tools of Magali GSX-500 software are limited and it is time consuming to work with GSX-500. Because of that the data is exported to MATLAB via text files. There are 41 acquisitions with 7 channels each. For faster data processing and scaling, a simple m-file is written. The M-files used to scaling and processing the acquired data is given in Appendix E.

7.3. Model Update and Estimation of Unknown Parameters

Although the current gain of torque motor is calculated according to electromagnetic magnetic theory, the model of torque motor includes some nonlinearity due to air gap inequalities of torque motor [21], [22] and fluid temperature [12]. The current gain of torque motor and the stiffness of flexure tube are found by using Simulink Parameter Estimation Toolbox. According to results of parameter estimation the following values used in Simulink model;

The current gain; $\mathrm{K_i} = 15.81\ \mathrm{N.m/A}$

The stiffness of flexure tube; $\mathrm{K_m} = 87.28\ \mathrm{N.m/rad}$

7.4. Numerical Solution of Wheatstone bridge Flow Rates by Using MATLAB

The pressure difference and flow rates can be calculated, if the values of parameters such as x_f, x_i, d_f, d_o, d_j, C_{do}, C_{dn}, ρ is known. The results obtained from experimental study in Section 5.2.2 can be used to verify the values of parameters. The graphs of the test results used for comparison are given in Appendix F.

The non-linear systems of equations resulting from hydraulic Wheatstone bridge circuit of variable and fixed orifices shown in Figure 7-2 are solved by MATLAB "`fsolve`" function.

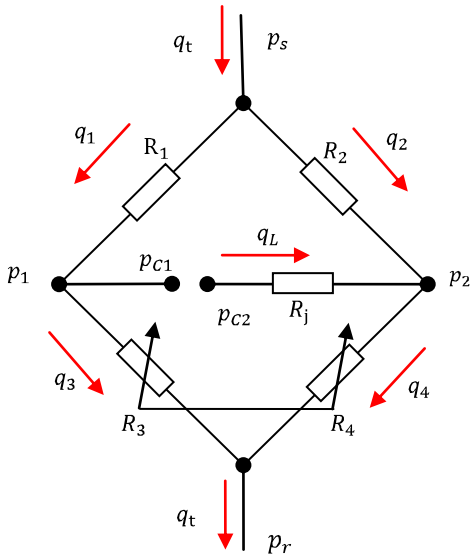

Figure 7-2 Symbolic drawing of hydraulic Wheatstone bridge circuit

For simplicity, if the leakage, compressibility and losses are neglected, p_1 is equal to p_{C1}. For no-load condition and constant velocity, the cylinder pressures are p_{C1} and p_{C2} are equal. As a result, it can be written $p_1 = p_{C1} = p_{C2}$. From hydraulic Wheatstone bridge, the following non-linear system of equations can be written.

Flow continuity equations are as follows:

$$q_1 + q_2 - q_t = 0 \tag{7.1}$$

$$q_L + q_3 - q_1 = 0 \tag{7.2}$$

$$q_4 - q_L + q_4 = 0 \tag{7.3}$$

From equation $q = C_d\, A \sqrt{\frac{2}{\rho}\, \Delta P}$, if ΔP is derived, it can be written as follows:

$$\Delta P = \left(\frac{1}{C_d\, A \sqrt{\frac{2}{\rho}}} \right)^2 q^2 = R\, q^2 \tag{7.4}$$

From Figure 7-2, the equality of pressure differences can be written as follows:

$$-R_2 q_2^2 + R_1 q_1^2 + R_j q_L = 0 \tag{7.5}$$

$$R_3 q_3^2 - R_4 q_4^2 - R_j q_L^2 = 0 \tag{7.6}$$

$$-P_s + R_1 q_1^2 + R_3 q_3^2 + P_r = 0 \tag{7.7}$$

where,

$$R_1 = \left(\frac{1}{C_{do}\, A_o \sqrt{\frac{2}{\rho}}} \right)^2 \tag{7.8}$$

$$R_2 = \left(\frac{1}{C_{do}\, A_o \sqrt{\frac{2}{\rho}}} \right)^2 \tag{7.9}$$

$$R_3 = \left(\frac{1}{C_{dn} \pi\, d_f\, (x_i - x_f) \sqrt{\frac{2}{\rho}}} \right)^2 \tag{7.10}$$

$$R_4 = \left(\frac{1}{C_{dn} \pi \, d_f \, (x_i + x_f) \sqrt{\frac{2}{\rho}}} \right)^2 \tag{7.11}$$

$$R_j = \left(\frac{1}{C_{do} \, A_j \sqrt{\frac{2}{\rho}}} \right)^2 \tag{7.12}$$

After determination of flow rates, the velocity of piston and velocity of input arm can be calculated by the following equations.

$$q_L = A_p \, \dot{y} \quad \text{and} \quad \dot{x} = \frac{L_r}{L_{tl}} \, \dot{y} \tag{7.13}$$

The system of equation is solved by MATLAB "`fsolve`" function for different x_f.

Table 7-1 The numerical values of parameters

$x_i = 100 \text{ x } 10^{-6}$ m
$d_f = 0.0001586$ m
$d_o = 0.0001586$ m
$d_j = 117 \text{ x } 10^{-6}$ m
$C_{do} = 0.783$
$C_{dn} = 0.64$
$P_s = 6.89$ MPa $= 1{,}000$ psi
$P_r = 0.35$ M Pa $= 50$ psi

By using numerical values of parameter given in Table 7-1, the results of "`fsolve`" function for different x_f values, are listed in Table 7-2. In Figure 7-3, the graph of x_f versus pressures is shown.

Table 7-2 Results of numerical solution

Numerical Solution of Flow Rates and Pressures with respect to flapper displacement (xf)							
xf (mm)	7.63E-02	3.82E-02	1.91E-02	0.00	-1.91E-02	-3.82E-02	-7.63E-02
q1 (m^3/s)	9.44E-07	1.51E-06	1.63E-06	1.68E-06	1.71E-06	1.74E-06	1.78E-06
q2 (m^3/s)	1.78E-06	1.74E-06	1.71E-06	1.68E-06	1.63E-06	1.51E-06	9.44E-07
q3 (m^3/s)	3.58E-07	1.18E-06	1.42E-06	1.68E-06	1.91E-06	2.08E-06	2.37E-06
q4 (m^3/s)	2.37E-06	2.08E-06	1.91E-06	1.68E-06	1.42E-06	1.18E-06	3.59E-07
qL (m^3/s)	5.85E-07	3.33E-07	2.02E-07	2.73E-18	-2.02E-07	-3.33E-07	-5.85E-07
qt (m^3/s)	2.72E-06	3.26E-06	3.33E-06	3.35E-06	3.33E-06	3.26E-06	2.73E-06
p1 (psi)	720.1	358.6	268.4	226.2	197.6	167.3	128.1
p2 (psi)	128.1	167.3	197.6	226.2	268.3	358.6	720.1
p2i (psi)	720.1	358.7	268.4	226.2	197.6	167.3	128.1
y_dot (m/s)	1.15E-03	6.57E-04	3.99E-04	0.00	-3.99E-04	-6.57E-04	-1.16E-03
x_dot (ips)	0.239	0.136	0.082	0.00	-0.082	-0.136	-0.239

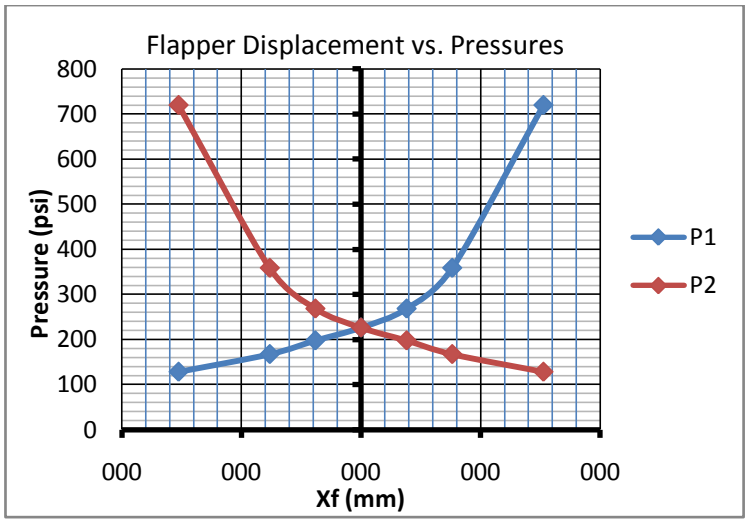

Figure 7-3 The graph of numerical solution (x_f vs. P1&P2)

7.5. Implementation of Experimental Data to Simulink Model

In order to obtain comparable the results, the data must start from zero. For this purpose a special routine is used in MATLAB. For validation acquired current data is used as input and the measured input arm displacement is compared with the simulated value for input arm displacement. The comparisons of experimental data and the output of Simulink model simulation are given. The red line represents the

simulated output for input arm displacement and the blue line represents the measured input arm displacement.

Figure 7-4 shows the comparison of simulated and the measured input arm displacement for 1 Hz square wave current input which has 3 mA amplitude. The red line represents the simulated output for input arm displacement and the blue line represents the measured input arm displacement. As it is seen from the graph, the simulated output is harmonious with the measured values. Figure 7-5 shows the error of simulation. The maximum absolute error is less than 0.2 mm. For comprehensible comparison, the maximum absolute error is divided by maximum displacement of input arm for this current input to calculate normalized error. For 3 mA square wave current input at 1 Hz frequency, the normalized error is 0.08.

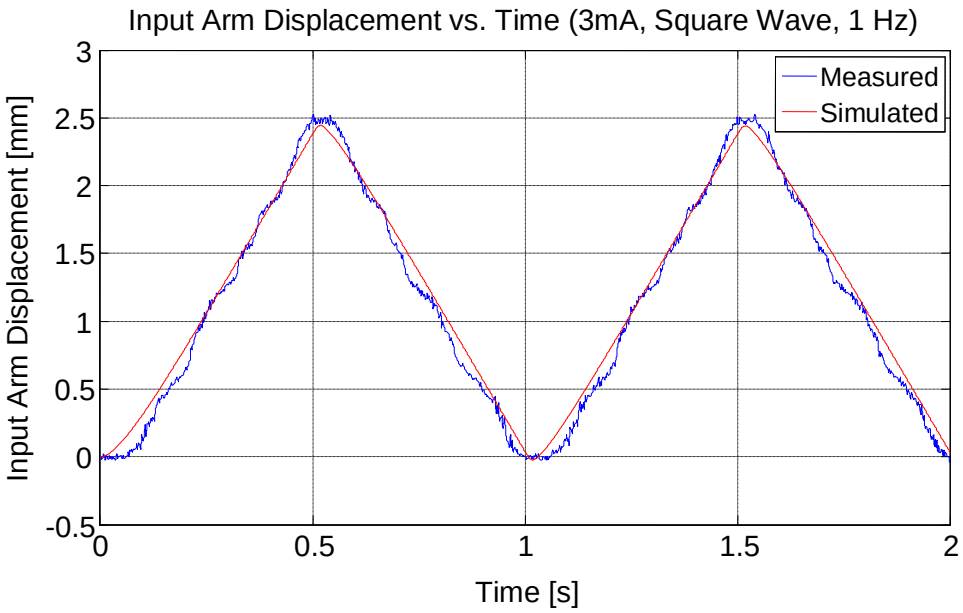

Figure 7-4 The plot of Simulated and Measured Input Arm Displacement

Input Current: 3 mA, Square Wave, 1Hz

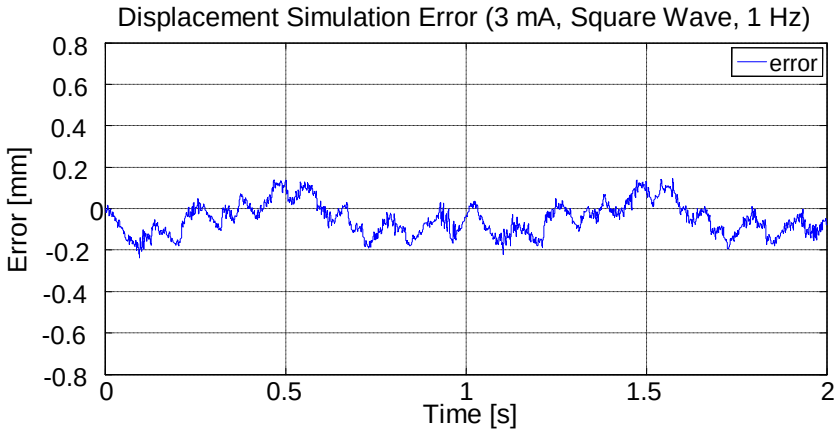

Figure 7-5 The error of simulated model (mm).

Input Current: 3 mA, Square Wave, 1Hz

Figure 7-6 shows the comparison of simulated and the measured input arm displacement for 3 mA square wave current input at 0.5 Hz frequency. As same in Figure 7-4, the red line represents the simulated output for input arm displacement and the blue line represents the measured input arm displacement. Figure 7-7 shows the error of simulated output. The maximum absolute error is less than 0.43 mm. For 3 mA square wave current input at 0.5 Hz frequency, the normalized error is 0.081.

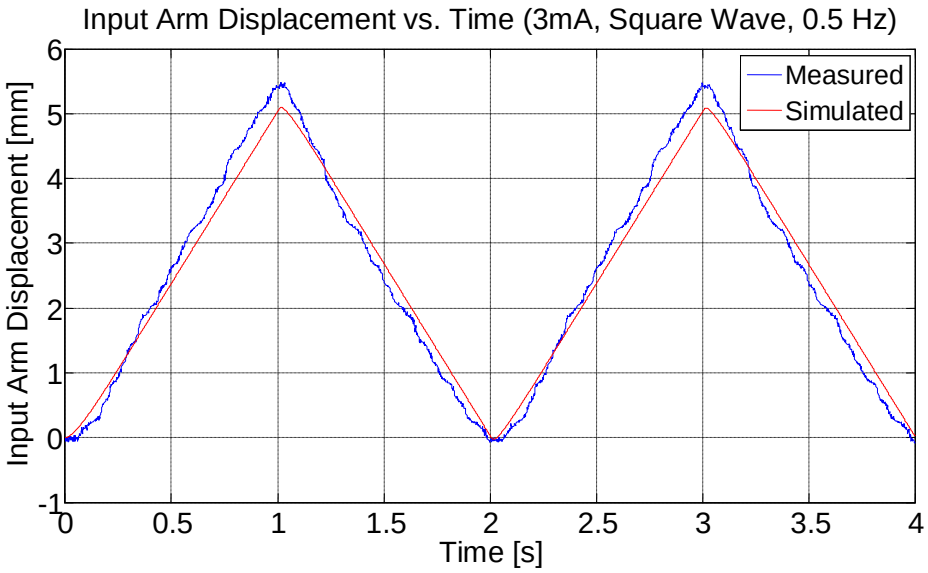

Figure 7-6 The plot of Simulated and Measured Input Arm Displacement

Input Current: 3 mA, Square Wave, 0.5 Hz

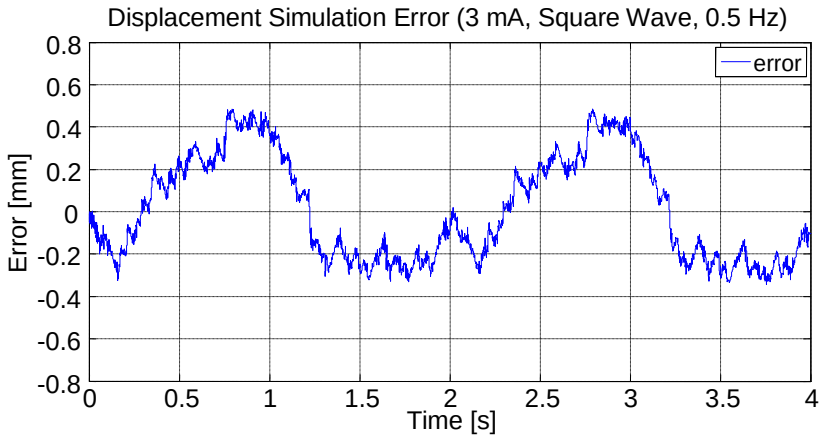

Figure 7-7 The error of simulated model (mm).

Input Current: 3 mA, Square Wave, 0.5 Hz

Figure 7-8 shows the comparison of simulated and the measured input arm displacement for 3 mA sine wave current input at 0.5 Hz frequency. As it is seen from the figure, the Simulink model gives the order of magnitude but did not simulate the system good enough especially for low speed region. For low currents the velocity of input arm is nearly zero. Therefore, the pitch trim actuator has a dead zone for low current values. Figure 7-9 shows the error of simulated output. The maximum absolute error is less than 0.68 mm for 3 mA sine wave current input at 0.5 Hz frequency, the normalized error is 0.26.

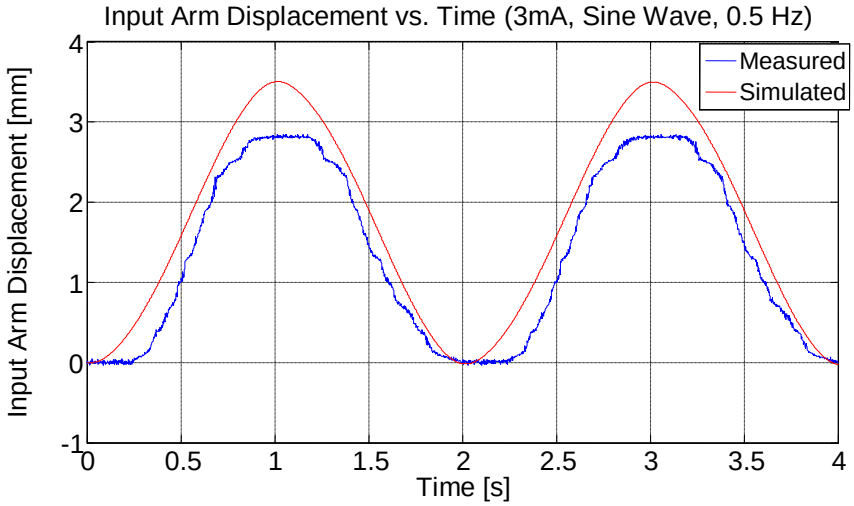

Figure 7-8 The plot of Simulated and Measured Input Arm Displacement

Input Current: 3 mA, Sine Wave, 0.5 Hz

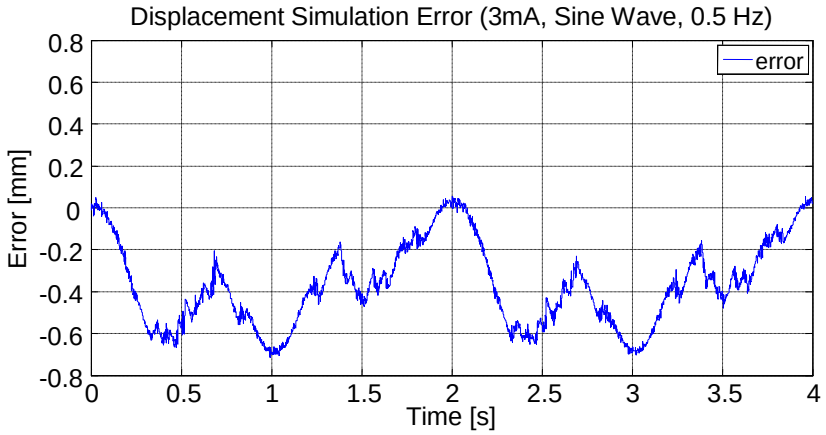

Figure 7-9 The error of simulated model (mm).

Input Current: 3 mA, Sine Wave, 0.5 Hz

Figure 7-10 shows the comparison of simulated and the measured input arm displacement for 3 mA sine wave current input at 1 Hz frequency. When the frequency of the sine wave is increased, the model gives erroneous results. Figure 7-11 shows the error of simulated output for 1 Hz sine wave. As it can be seen from figure the maximum absolute error is 0.6 mm. The normalized value for 3 mA sine wave current input at 1 Hz frequency is 0.5.

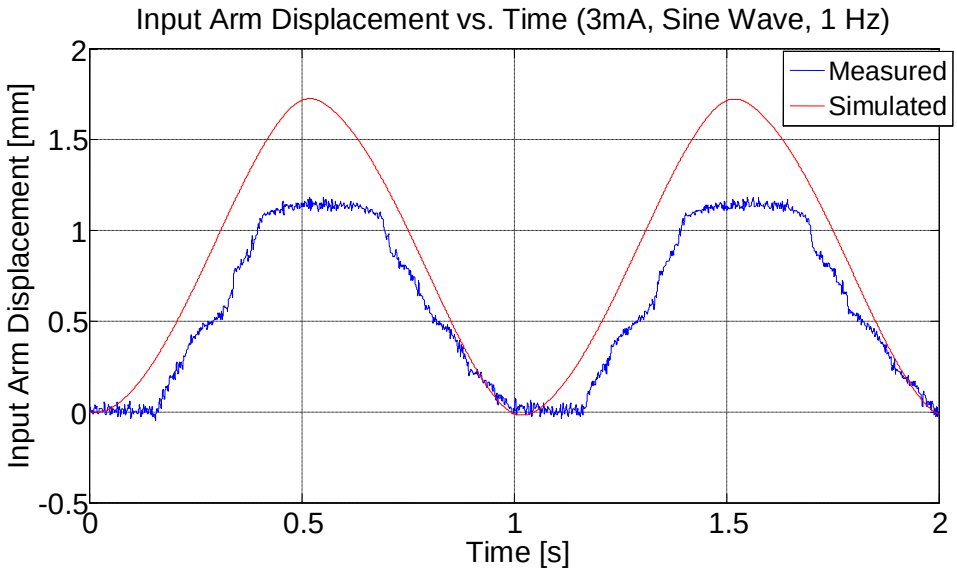

Figure 7-10 The plot of Simulated and Measured Input Arm Displacement

Input Current: 3 mA, Sine Wave, 1 Hz

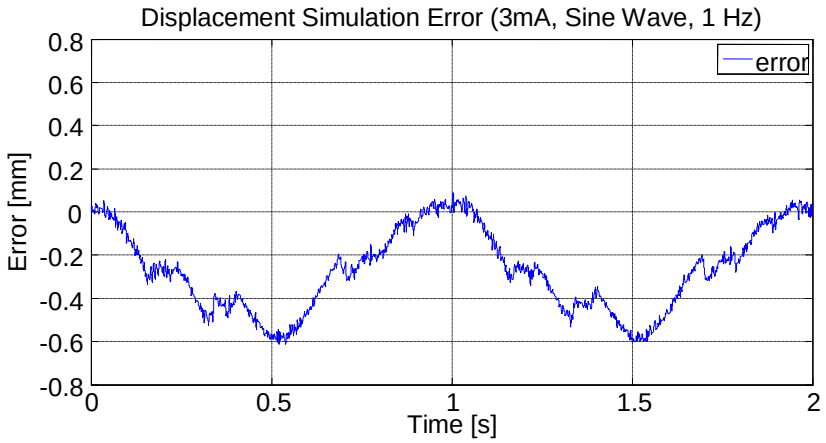

Figure 7-11 The error of simulated model (mm).

Input Current: 3 mA, Sine Wave, 1 Hz

CHAPTER 8

CONCLUSION AND FUTURE WORK

8.1. Conclusion

The pitch trim actuator is a hydraulic powered electro-mechanical flight control device of UH-60 helicopters which converts a mechanical input and an electrical command into a mechanical output with trim detent capabilities. In this thesis study, pitch trim actuator is investigated and its mathematical model is developed. From these mathematical equations, actuator is modeled in MATLAB Simulink environment. To achieve the realistic model for torque motor, tests are carried out and the values of torque motor current gain and flexure tube stiffness and the flapper displacement are calculated. To verify the Simulink model, experimental data is collected with data acquisition system. A test fixture is designed for collecting the experimental data. To verify the consistency of Simulink model, the experimental data is implemented to Simulink environment. The output of Simulink model simulation and the experimental results are compared.

As it is seen from the figures given in Chapter 7, the simulation and the experimental results are quite similar and the error of simulation is in the acceptable limits for step changes (square wave).

However, simulated output for sine wave current input at high frequencies is not consistent with the measured input arm displacement, especially when velocity changes sign. This could be caused by modeling visco jet as a variable resistance. Another reason could be the variation of discharge coefficient with the Reynolds

number. This phenomenon is mentioned in [25] and [24]. The effect of variable discharge coefficient can be included in the Simulink model.

For constant current input, the steady state response of pitch trim actuator can be simulated by the model. The results of comparison verify that the model is good enough for steady state response simulation, but for the transient and low current response, the Simulink model can be modified in order to include the non-linearities of the system.

Understanding the working principles of such flight safety critical part is very important while testing, maintaining or repairing. During the tests of components, when a trouble or malfunction is found which did not exist in troubleshooting instructions, it is easier to fix the trouble without making a lot of trial and error process for the technician or the engineer who knows the working principles of the components. The best way to understand the working principles of a system is to model it mathematically. In this thesis study, the actuator part of the pitch trim assembly is modeled. The working principles and the duties of the components are understood. This study leads the overhaul and maintenance capability of pitch trim actuator.

In this thesis study, servo actuator part of pitch trim assembly is modeled. The effect of boost actuator is not included. For the future work, the mathematical model of boost actuator with pilot input can be developed. The pitch trim actuator functional tests described in [42] can be carried out in Simulink environment. A control algorithm can be developed to control the position of pitch trim actuator output arm.

REFERENCES

[1] Kebede, E., "Technical Assessment of Hydraulic Systems used in Mi-24 and Mi-35 Helicopters", Addis Abada University, Ethiopia, 2008.

[2] Boulet, J., "History of the Helicopter: As Told by its Pioneers, 1907-1956", Editions France-Empire, 1984.

[3] Sikorsky, I.I., "Direct Lift Aircraft", Sikorsky Aircraft Corporation, US 1,994,488, 1935.

[4] Leishman, J.G., "Principles of Helicopter Aerodynamics", Cambridge University Press, 2006.

[5] Viswanath, S., Nagarajan, R., "Helicopter Hydraulic System (Design, Component Selection, Modular Construction, Integration & Testing)", ICAS 2002, Toronto, Canada, September 2002.

[6] Chaturvedi, D.K., "Modeling and Simulation of Systems using MATLAB and Simulink", CRC Press, 2010.

[7] The MathWorks Inc., "Simulink Documentation (Version 7.0 (R2007b) Simulink Software)", 2007.

[8] Merritt, H.E., "Hydraulic Control Systems", Wiley, New York, 1967.

[9] Gordic, D., Babic, M., Jovocic, N., "Modelling of Spool Position Feedback Servovalves", International Journal of Fluid Power, 5, 37-50, 2004.

[10] Rabie, M.G., "Fluid Power Engineering", McGraw-Hill, New York, 2009.

[11] Dongjie, M., Changchun, L., "A new mathematical model of twin flapper-nozzle servo valve based on input-output linearization approach", Artificial Intelligence, Management Science and Electronic Commerce (AIMSEC), Zhengzhou, China, August 2011.

[12] Zhang, X., Yin, Y., Huang, W., "Influence of temperature on null position pressure characteristics of flapper-nozzle servo valve", Computer Design and Applications (ICCDA), Shaanxi, China, June 2010.

[13] Lin, S.J., Akers, A., "The Predicted Performance of a Flapper-Nozzle Valve: Comparison with Experiment", American Control Conference (ACC), Atlanta, USA, June 1988.

[14] Lin, S.J., Akers, A., "A Non-Linear Model of a Flapper-Nozzle Valve", American Control Conference (ACC), Pittsburgh, USA, June 1989.

[15] Ghasemi, E., Jazayeri, S.A., Moosavian, S., "Model Improvement for a Servovalve with Force Feedback and Back Pressure", Robotics, Automation and Mechatronics (RAM), Chengdu, China, September 2008.

[16] Jinsheng, R., Xiaoyang, L., Tongmin, J., Hong, W., "Double-nozzle flapper-style hydraulic servovalve simulation based on sphere wear", Reliability, Maintainability and Safety (ICRMS), Guiyang, China, June 2011.

[17] Cheng, J., Liu, W., Zhang, Z., "Modeling and simulation for the electro-hydraulic servo system based on Simulink ", Consumer Electronics, Communications and Networks, (CECNet), Xianning,China, April 2011.

[18] Thayer, W J, "Specification Standards for Electrohydraulic Flow Control Servovalves", Moog Inc. Tecnhical Bulletin, 1962.

[19] Johnson, B, "Hydraulic Servo Control Valves",Wright Air Development Center, USAF, Aeronautical Research Laboratory, WADC Tech.Rep 55-29, 1957.

[20] Urata, E., "On the torque generated in a servo valve torque motor using permanent magnets ", Proc. Inst. Mech. Eng. Part C, 221, 519-525, 2007.

[21] Urata, E., "Influence of unequal air-gap thickness in servo valve torque motors ", Proc. Inst. Mech. Eng. Part C, 221, 1287-1297, 2007.

[22] Gordic, D., Babic, M., Jovicic, N., Milovanovic, D., "Effects of the Variation of Torque Motor Parameters on Servovalve Performance", Journal of Mechanical Engineering , 54, 12, 866-873, 2008.

[23] Lichtarowicz, A., "Flow and Force Characterisitics of Flapper Valves", 3rd. International Fluid Power Symposium, Torino, Italy, May 1973.

[24] Babic, M., Dusan, G., Sustersic, V., "Determination of Values for Flow Coefficients of First Stage Orifices in Two-Stage Electrohydraulic Servovalves", Heavy Machinery (HM), Kraljevo, Yugoslavia, June 2002.

[25] Bergada, J.M., Codina, E., "Discharge Coefficients for a Four Nozzle Two Flapper Servovalve", Procedings of the 46th National Conference on Fluid Power, Anaheim, California, March 1994.

[26] Wright, S.C., Murphy, R.D., Adams, D.L., "Incorporation of Pitch Bias Actuator Function into an Existing AFCS", United Technologies Corporation, US 4,580,223, 1986.

[27] Wright, G.P., Adams, D.L., "Speed and Collective Pitch Bias of Helicopter Longitudinal Cyclic Pitch", United Technologies Corporation, US 4,168,045, 1979.

[28] Verzella, D.J., Fischer, W.C., Adams, D.L., Wright, S.C., "Non-Saturating airspeed/attitude Controls", United Technologies Corporation, US 4,385,356, 1983.

[29] Verzella, D.J., Fischer, W.C., Adams, D.L., Wright, S.C., "Pitch Stick Force Inhibit of Aircraft Automatic Outer Loop", United Technologies Corporation, US 4,382,283, 1983.

[30] Tefft, F.A., Adams, D.L., Cotton, L.S., "Helicopter Pitch Rate Feedback Bias for Pitch Axis Maneuvering Stability and Load Feel", United Technologies Corporation, US 4,127,245, 1978.

[31] Guojian, L., Yunhua, L., Liman, Y., "Accurate mathematical model for describing electrohydraulic loading system of helicopter pitch adjusting hydromechanical servos", Robotics, Automation and Mechatronics (RAM), Singapore, June 2010.

[32] Clelford, D.H., Murphy, R.D., "Helicopter Attitude and Airspeed Acquisition and Retention System", United Technologies Corporation, US 4,382,283, 1983.

[33] Howlett, J.J., "UH-60A Black Hawk Engineering Simulation.Program: Volume I - Mathematical Model (United Technologies Sikorsky Aircraft)", NASA Ames Research Center, California, 1981.

[34] Howlett, J.J., "UH-60A Black Hawk Engineering Simulation.Program: Volume II-Background Report (United Technologies Sikorsky Aircraft)", NASA Ames Research Center, California, 1988.

[35] Langworthy, W., "Seahawk Helicopter Simulation", University of New South Wales, 2008.

[36] ACME Worldwide, Rotary Wing Dynamic Motion Seat http://www.acme-worldwide.com/dynamic_motion_seat_Rotary.htm, last visited on 17.01.2012.

[37] Federal Aviation Administration, U.S. Dept. of Transportation, "Rotorcraft Flying Handbook", Skyhorse Publishing, 2007.

[38] Sikorsky Aircraft Corporation, "TM-1-70-28-23 Aircraft Maintenance Procedures Manual", United Technologies Inc., 2009.

[39] Labows, S.J., "UH-60 Black Hawk Disturbance Rejection Study for Hover/Low Speed Handling Qualities Criteria and Turbulence Modeling", Naval Postgraduate School, Monterey, California, 2000.

[40] Sikorsky Aircraft Corporation, "UH-60 Airframe and Powertrain Systems Maintenance Course Student Guide", Volume I ed., United Technologies Inc., 1999.

[41] Sikorsky Aircraft Corporation, "UH-60 Airframe and Powertrain Systems Maintenance Course Student Guide", Volume II ed., United Technologies Inc., 1999.

[42] US Army Aviation and Missile Command, "DMWR 1-1650-385 Pitch Trim Actuator Assembly", United Technologies Inc., Redstone Arsenal, Alabama, 2003.

[43] The Lee Company, The Lee Company Presents http://www.theleeco.com/JETWEB2.NSF/$$JET!OpenView, last visited on 24 Jaunary 2012.

[44] Cundiff, J.S., "Fluid Power Circuits and Controls Fundamentals and Applications", CRC Press, Boca Raton, 2002.

APPENDIX A

AFCS BLOCK DIAGRAM

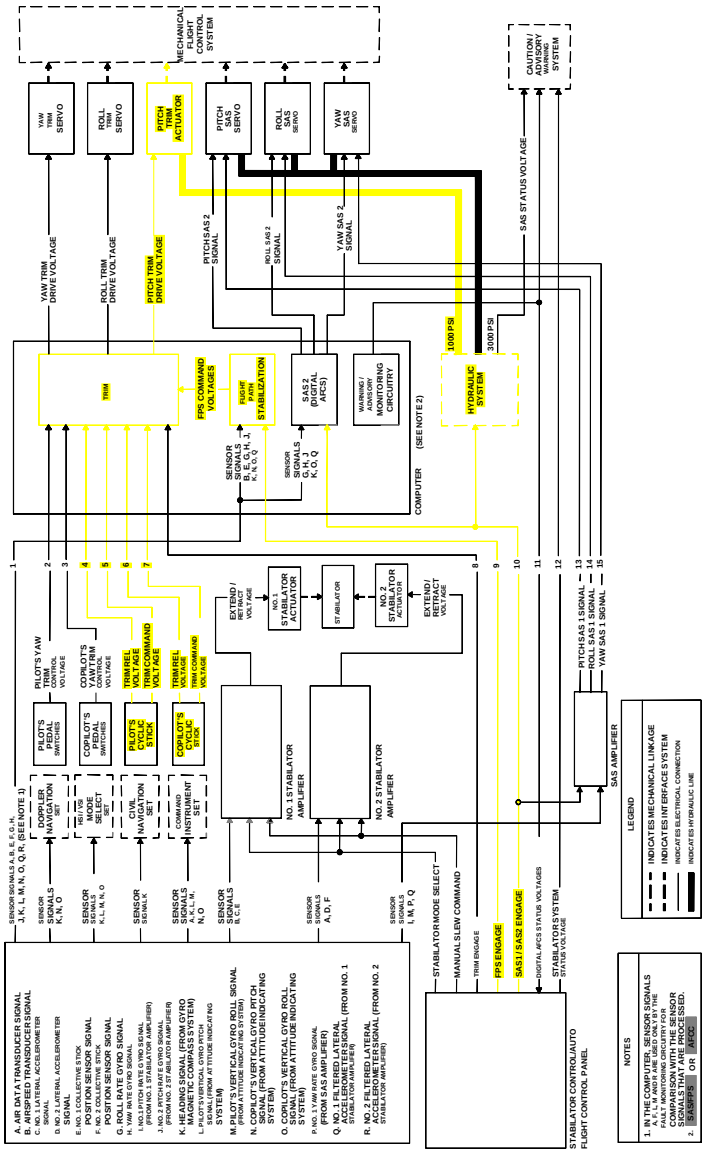

Figure A-1 AFCS Block Diagram [38]

APPENDIX B

MATLAB M-FILES

M-file Containing the Numerical Values

The following M-file is used to implement the numerical values of Simulink model parameters.

```
% Values Calculated by CAD program
% -------------------------------------
% Moment of inertia of rotor J(kg sqm)
Ja=1.58e-7; %(Calculated by CAD program)
% Moment of inertia of rotational components J(kg sqm)
Jtl=0.001949213; %(Jtl=0.110645651463961,
Estimation)(Jtl=0.001949213 Calculated by CAD program)

% Measured Values
% -----------------
% Flapper length Lf(m)
Lf=0.0104; %(Measured)
% Flexure tube length (m)
Lt=0.008;
% flapper rotation length (m)
Lfr=Lf-Lt/2;
% flapper thickness df(m)
tf=0.0186; %(Measured)
% Supply Pressure Ps (Pa)(1000 psi)
Ps=6894757; %(Measured)
% Return Pressure Pt (Pa)(50 psi)
Pr=344740; %(Measured)
% Diameter of piston dp(m)
dp= 0.0254; %(Measured)
% Piston mass mp (kg)
mp=0.0757; %(Measured)
% Trim lever Radius (inner Rotational link Length) Llt(m)
Ltl=0.0254; %(Measured)
% Rotational link Length Lr(m)
Lr=0.1332; %(Measured)
% Initial volume of piston chamber Vo (Cu m)
Vo=5.1e-6*8; %(measured and calculated)
% length of pipe (from spool to pistons) (m)
Lp=0.3; %(Measured)
% inner diameter of pipe (m)
```

```
dpipe=3e-3; %(Measured)
% mass of sliding mechanism (kg)
ms=0.5; %(Measured)

% Calculated after experiment
% ----------------------------
% Diameter of fixed orifice do(m) Orifice number:20 do=0.02 inch
do=0.0001586; %(calculated do=0.0001586)
% Hydraulic amplifier nozzles (orifices) N1 & N2 diameter df(m)
df=0.0001586; %(df=0.0001586)
% Diameter of viscojet orifice dj(m)
dj=117e-6; %(Assumption: dP_max=650psi, dX_max/dt=0.24ips)
% Flapper limiting displacement xi(m)
%xi=78.3483e-6 %(***Estimation)
%xi2=84.2926e-6 %(***Estimation)
xi=100e-6; %(calculated xi=86.77e-6; )

% Known Values
% -----------------
% pi
pi=3.14159;
% Oil density Ro (kg/Cum)
rho=851; %((Oil property, ref:MIL-PRF-83282D)
% Bulk modulus of oil B (Pa)
B=1.379e9; %(Oil property, ref:MIL-PRF-83282D)
%Viscosity of oil (at 40 centigrade degree)(Pa s)
mu=0.0119;
% Piston loading coefficient Ky Piston Spring Stiffness (N/m)
Kp=1050; %(Given by manufacturer)

% Assumed Parameters
% -------------------
% Discharge Coefficient Cd
Cdo=0.783; %(According to Gordic)
% Discharge Coefficient Cd, typically 0.6 to 0.65
Cdn=0.64; %(According to Gordic)

% Estimation Parameters
% ------------------------
% Current gain, Ki (Nm/A)
Ki=15.81; %(Ki=15.81 ***Estimation) (Ki=7.768, Calculated)
% Armature rotational angle torque gain Km
Km=79.88;  %Km=13.64(Calculated)
% Flexible tube rotational stiffness, Kt
Kt=87.28; %Kt=140(***Estimation)
% Armature rotational damping coefficient, fa
fa=0.01; %(***Estimation)
% rotational damping coefficient on rotational link, ftl
ftl=0.01; %(***Estimation)
% friction coefficient for sliding mechanism, bs
bs=0;

% coulomb friction force for sliding mechanism
Fsc=30;
```

```
% Calculated Values
% --------------------
% Flapper nozzle area Af (sq m)
Af=pi*df*df/4;
% Fixed orifices area Ao(sq m
Ao=pi*do*do/4;
% Flow Coefficients (in SI)
Cd1=Cdo*Ao*sqrt(2/rho);
Cd2=Cdn*sqrt(2/rho);
% Piston area Ap (Sq m)(piston diameter 0.0254 m)
Ap=pi*dp*dp/4;
% Visco Jet area Aj (Sq m
Aj=pi*dj*dj/4;

% Hydraulic impedances
l1=300*1e-3; % (m)
l2=300*1e-3; % (m)
al1=(2.5*1e-3)^2*pi/4;
L1=rho*l1/al1;
L2=rho*l2/al1;

% hydraulic capacitances
Vvalve1=(5^2-2.77^2)*pi/4*11.9*1e-9+(3^2*pi/4*300)*1e-9;
Vvalve2=(((5^2-2.77^2)*pi/4*4.55)+((5^2-4^2)*pi/4*5.26))*1e-
9+(3^2*pi/4*300)*1e-9;
C1=Vvalve1/B;
C2=Vvalve2/B;

% hydraulic resistances
R1=128*mu*Lp/(pi*dp^4);
R2=128*mu*Lp/(pi*dp^4);
Rj=(1/(Cdo*Aj*sqrt(2/rho)))^2;
```

APPENDIX C

SIMULINK MODELS FOR FLOW RATES

The subsystem names as “Flow rates” includes the Simulink models of flow rates through fixed and variable orifices

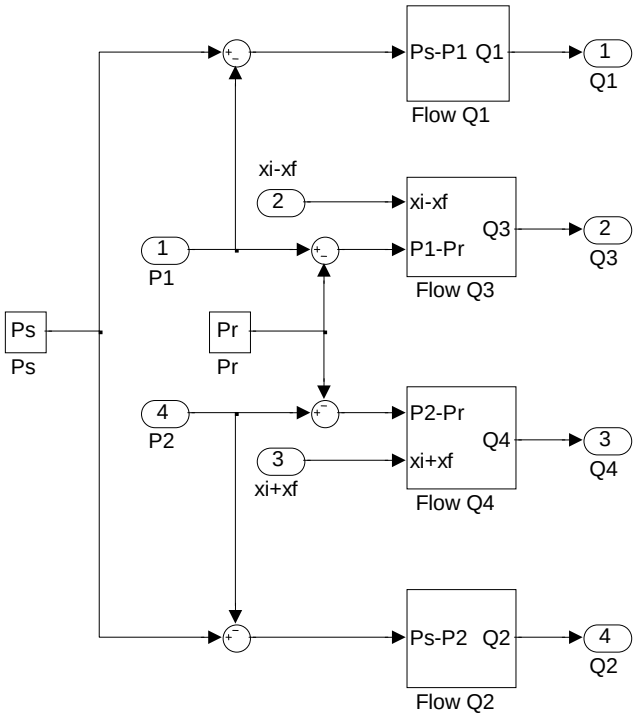

Figure C-1 Flow Rates Model

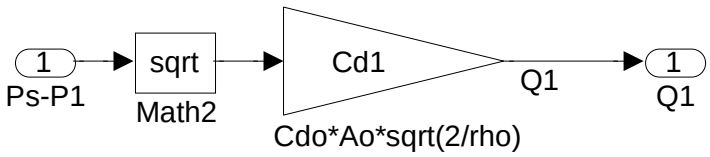

Figure C-2 Flow Rate at Orifice 1

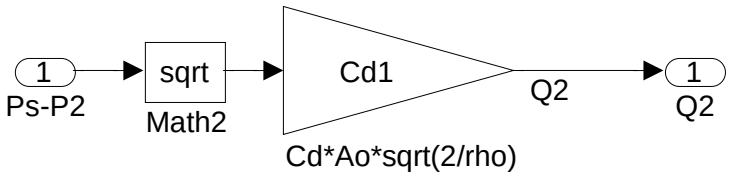

Figure C-3 Flow Rate at Orifice 2

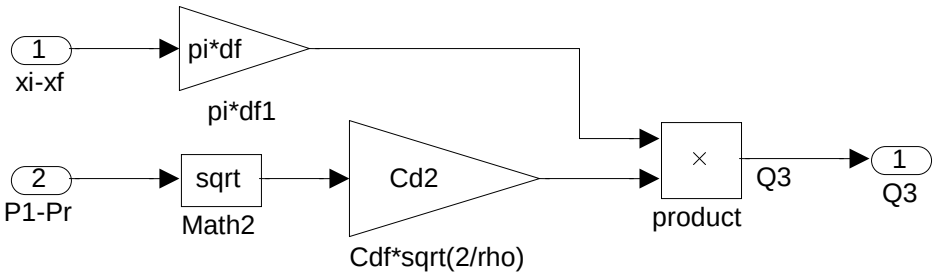

Figure C-4 Flow Rate at Variable Orifice 3

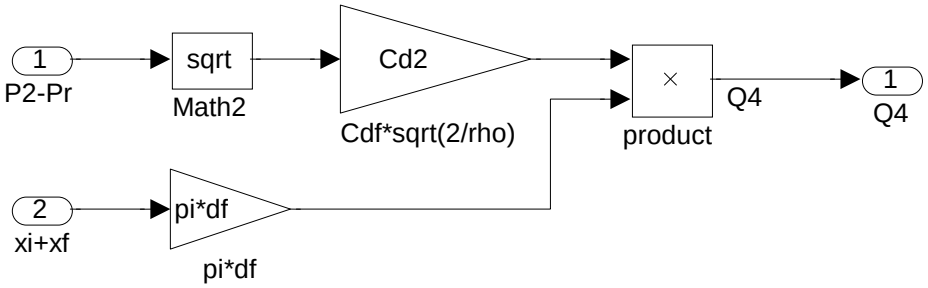

Figure C-5 Flow Rate at Variable Orifice 4

APPENDIX D

TEST MATRIX FOR DATA ACQUISITION

Table D-1 Test matrix for first configuration

Input Current Amplitude (mA)	Input Type	Frequency (Hz)
4	Sine Wave	0.04
4	Square Wave	0.04
4	Sine Wave	0.5
4	Sine Wave	10
4	Square Wave	10
3	Sine Wave	0.1
3	Square Wave	0.1
3	Sine Wave	0.2
3	Square Wave	0.2
3	Sine Wave	0.5
3	Sine Wave	1
3	Square Wave	2
3	Sine Wave	5
3	Sine Wave	10
3	Square Wave	10
1	Sine Wave	0.01
1	Square Wave	0.01
1	Sine Wave	0.5
1	Square Wave	0.5

Table D-2 Test matrix for Bode diagram

Input Current Amplitude (mA)	Input Type	Frequency (Hz)
3	Sine Wave	0.05
3	Sine Wave	0.08
3	Sine Wave	0.1
3	Sine Wave	0.2
3	Sine Wave	0.3
3	Sine Wave	0.4
3	Sine Wave	0.5
3	Sine Wave	0.6
3	Sine Wave	0.7
3	Sine Wave	0.8
3	Sine Wave	0.9
3	Sine Wave	1
3	Sine Wave	2
3	Sine Wave	3
3	Sine Wave	4
3	Sine Wave	5
3	Sine Wave	6
3	Sine Wave	7
3	Sine Wave	8
3	Sine Wave	9
3	Sine Wave	10

Table D-3 Test matrix for second configuration

Input Current Amplitude (mA)	Input Type	Frequency (Hz)
3	Square Wave	0.05
3	Square Wave	0.08
3	Square Wave	0.1
3	Square Wave	0.2
3	Square Wave	0.3
3	Square Wave	0.4
3	Square Wave	0.5
3	Square Wave	0.6
3	Square Wave	0.7
3	Square Wave	0.8
3	Square Wave	0.9
3	Square Wave	1
3	Square Wave	2
3	Square Wave	3
3	Square Wave	4
3	Square Wave	5
3	Square Wave	6
3	Square Wave	7
3	Square Wave	8
3	Square Wave	9
3	Square Wave	10

APPENDIX E

M-FILES USED FOR DATA SCALING AND PROCESSING

Function for data processing

```
function
[veri_sin,veri_sqr,veri_sin_trim_t,veri_sqr_trim_t,veri_sin_current_
t,veri_sqr_current_t]=data_isle(veri,name_m,t1,t2,t3,t4,N);
%[X3mA_0_05hz_sin,X3mA_0_05hz_sqr,X3mA_0_05hz_sin_trim_t,X3mA_0_05hz
_sqr_trim_t,X3mA_0_05hz_sin_current_t,X3mA_0_05hz_sqr_current_t]=dat
a_isle(X3mA_0_05hz,'3mA_0_05hz',187.5,231.6,4.79,46.5,125);
%veri_sin_A=Amplitude (veri_sin(1,10))
%veri_sin_offset=Akim verilerinin sifirdan sapmasi (veri_sin(2,10))
%veri_sin(:,8)=trim displacement
%veri_sin(:,9)=pressure difference
%veri_sqr_Vel=velocity obtained from sqr data (veri_sqr(:,10);
%veri_sqr(:,8)=trim displacement
%veri_sqr(:,9)=pressure difference

%sine verisinin bulunmasi
%-----------------------------------------------
%t1=187.5;
%t2=231.6;

%N=125 hiz hesaplamasi düzgünlestirilmis veriler kullaniliyor
oradaki katsayi
t_sin=find(veri(:,1)>t1 & veri(:,1)<t2); %Sinus dalga için indisler
veri_sin=veri(t_sin,:); %yeni indislerle matrix olusturma
veri_sin(:,1)=veri_sin(:,1)-veri_sin(1,1); %zamani sifirdan
baslatmak için
veri_sin(:,3)=veri_sin(:,3)-mean(veri_sin(:,3)); %verilerin 0
etrafina alinmasi
veri_sin(:,3)=veri_sin(:,3)/1000; %mesafenin "inch" e çevrilmesi
veri_sin(:,7)=-veri_sin(:,7); %voltaj yön notasyon degerini
degistirilmesi [(-) akim (-) velocity]
veri_sin(:,7)=veri_sin(:,7)/1055; %voltajin akima(A) dönüstürülmesi
veri_sin_offset=mean(veri_sin(:,7)); %zero offset
veri_sin(:,7)=veri_sin(:,7)-mean(veri_sin(:,7)); %akimin DC
bilesininin sifirlanmasi
veri_sin(:,8)=(veri_sin(:,2)-5.922567)*0.3041; %trim displacement
(inch)
veri_sin(:,8)=veri_sin(:,8)*25.4; %trim displacement (mm)
veri_sin(:,8)=veri_sin(:,8)-veri_sin(1,8); %trim displacement'i
sifirdan baslatmak için
veri_sin(:,9)=veri_sin(:,5)-veri_sin(:,4)-17;
```

```
figure;
set(gcf,'Name',name_m);
subplot(5,1,1);
plot(veri_sin(:,1),veri_sin(:,7)); %sin akim verisinin grafigi
title('Current Input');
%xlabel('Time(s)');
ylabel('Current(mA)');
%text(12.5,0,' \leftarrow Current Input','FontSize',10);
subplot(5,1,2);
plot(veri_sin(:,1),veri_sin(:,3)); %konum verisinin grafigi
title('Displacement Response');
%xlabel('Time(s)');
ylabel('Displacement(inch)');
veri_sin_A=(max(veri_sin(:,3))+abs(min(veri_sin(:,3))))/2; %Genlik
hesaplanmasi (max+abs(min)))/2
veri_sin(1,10)=veri_sin_A;
veri_sin(2,10)=veri_sin_offset;

%kare dalga(sqr) verisinin bulunmasi
%-----------------------------------------------
%t3=4.79
%t4=46.5
t_sqr=find(veri(:,1)>t3 & veri(:,1)<t4); %kare dalga için indisler
veri_sqr=veri(t_sqr,:); %yeni indislerle matrix olusturma
veri_sqr(:,1)=veri_sqr(:,1)-veri_sqr(1,1); %zamani sifirdan
baslatmak için
veri_sqr(:,3)=veri_sqr(:,3)-mean(veri_sqr(:,3)); %verilerin 0
etrafina alinmasi
veri_sqr(:,3)=veri_sqr(:,3)/1000; %mesafenin "inch" e çevrilmesi
veri_sqr(:,7)=-veri_sqr(:,7); %akim yön notasyon degerini
degistirilmesi [(-) akim (-) velocity]
veri_sqr(:,7)=veri_sqr(:,7)/1055; %voltajin akima dönüstürülmesi
veri_sqr(:,8)=(veri_sqr(:,2)-5.922567)*0.3041; %trim displacement
(inch)
veri_sqr(:,8)=veri_sqr(:,8)*25.4; %trim displacement (mm)
veri_sqr(:,8)=veri_sqr(:,8)-veri_sqr(1,8); %trim displacement'i
sifirdan baslatmak için
disp_N=smooth(veri_sqr(:,3),N,'lowess'); %verilerin
düzgünlestirilmesi
veri_sqr_Vel=diff(disp_N)/0.002; %Hiz verisinin hesaplanmasi
veri_sqr(:,9)=veri_sqr(:,5)-veri_sqr(:,4)-17;
t=length(t_sqr);
veri_sqr(2:t,10)=veri_sqr_Vel;
veri_sqr(1,10)=0;

%figure;
subplot(5,1,3);
plot(veri_sqr(:,1),veri_sqr(:,7)); %kare akim verisinin grafigi
title('Current Input');
%xlabel('Time(s)');
ylabel('Current(mA)');
subplot(5,1,4);
plot(veri_sqr(:,1),veri_sqr(:,3)); %konum verisinin grafigi
title('Displacement Response');
%xlabel('Time(s)');
ylabel('Displacement(inch)');
subplot(5,1,5);
plot(veri_sqr(1:t-1,1),veri_sqr_Vel); %hiz verisinin grafigi
```

```
title('Velocity Response');
xlabel('Time(s)');
ylabel('velocity(ips)');

%text(pi,0,' \leftarrow sin(\pi)','FontSize',18)
[veri_sin_trim_t,veri_sqr_trim_t,veri_sin_current_t,veri_sqr_current
_t]=trimcurrent(name_m,veri_sqr,veri_sin);

End
```

Function for data implementation

```
function
[veri_sin_trim_t,veri_sqr_trim_t,veri_sin_current_t,veri_sqr_current
_t]=trimcurrent(name_m,veri_sqr,veri_sin);
veri_sqr_current(:,2)=veri_sqr(:,7);
veri_sqr_current(:,1)=veri_sqr(:,1);
veri_sqr_trim(:,1)=veri_sqr(:,1);
veri_sqr_trim(:,2)=veri_sqr(:,8);

veri_sin_current(:,2)=veri_sin(:,7);
veri_sin_current(:,1)=veri_sin(:,1);
veri_sin_trim(:,1)=veri_sin(:,1);
veri_sin_trim(:,2)=veri_sin(:,8);

veri_sin_trim_t=veri_sin_trim';
veri_sqr_trim_t=veri_sqr_trim';
veri_sin_current_t=veri_sin_current';
veri_sqr_current_t=veri_sqr_current';

name_file=strcat(name_m,'_sin_current');
save(name_file,'veri_sin_current_t');
name_file=strcat(name_m,'_sqr_current');
save(name_file,'veri_sqr_current_t');
name_file=strcat(name_m,'_sin_trim');
save(name_file,'veri_sin_trim_t');
name_file=strcat(name_m,'_sqr_trim');
save(name_file,'veri_sqr_trim_t');
end
```

APPENDIX F

TORQUE MOTOR TEST RESULTS

The results of experimental study described in Section 5.2.2 are given below.

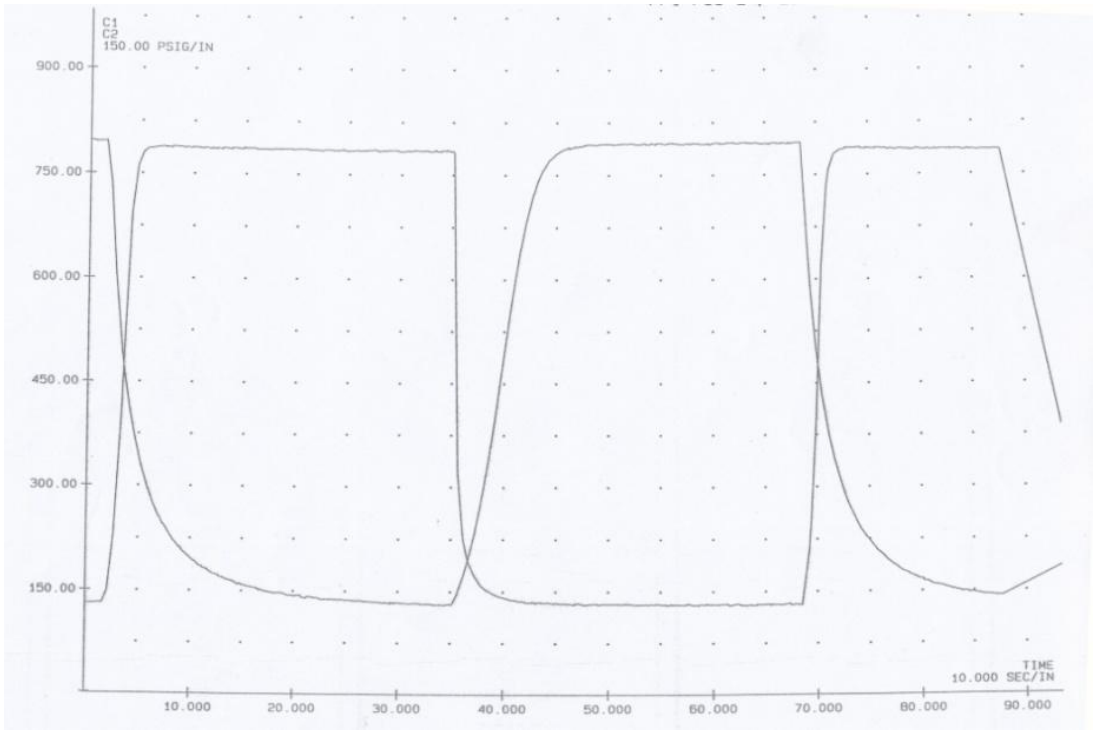

Figure F-1 Test result for 4 mA square wave current input

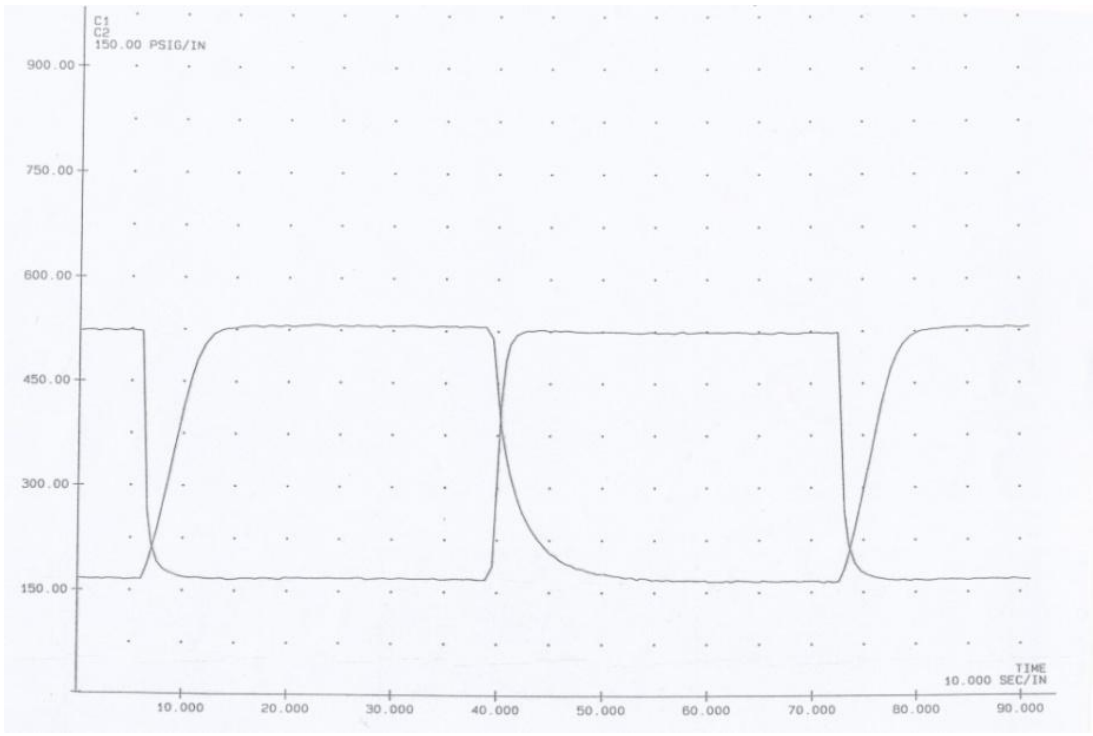

Figure F-2 Test result for 3 mA square wave current input

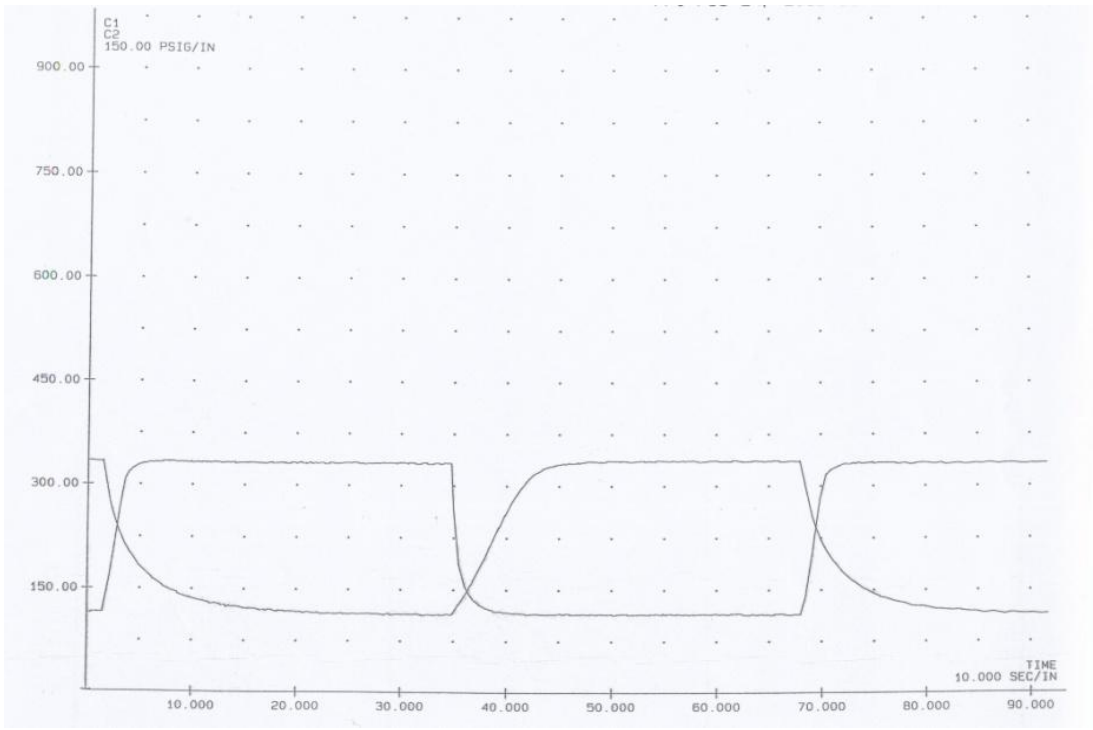

Figure F-3 Test result for 2 mA square wave current input

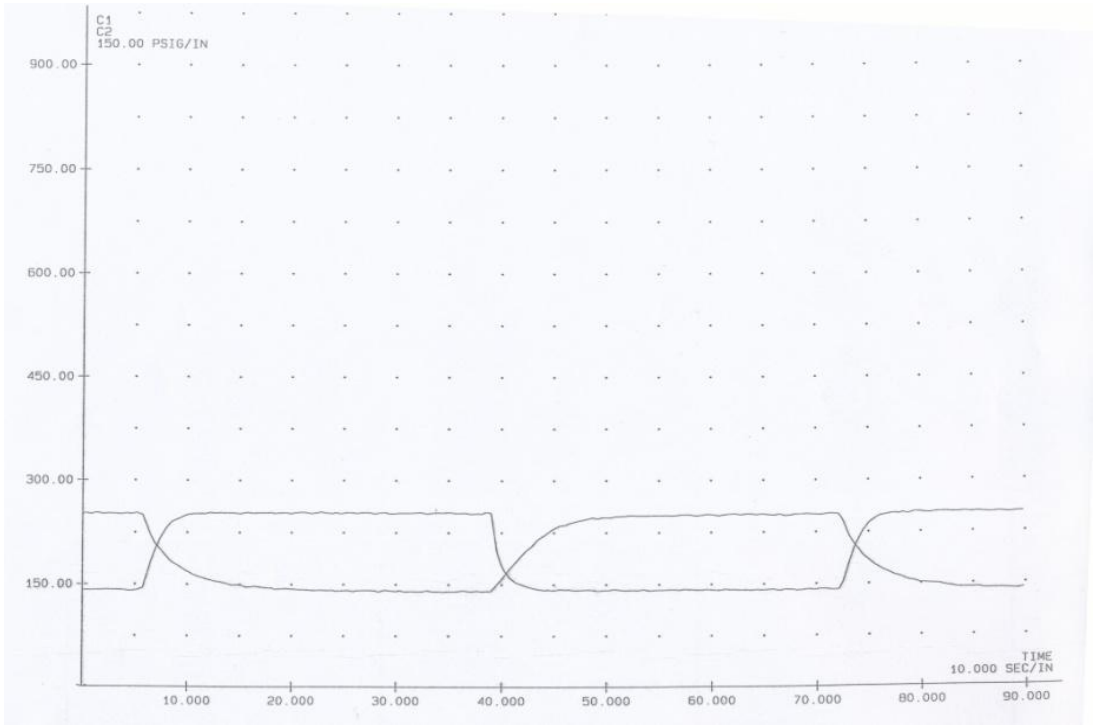

Figure F-4 Test result for 1 mA square wave current input

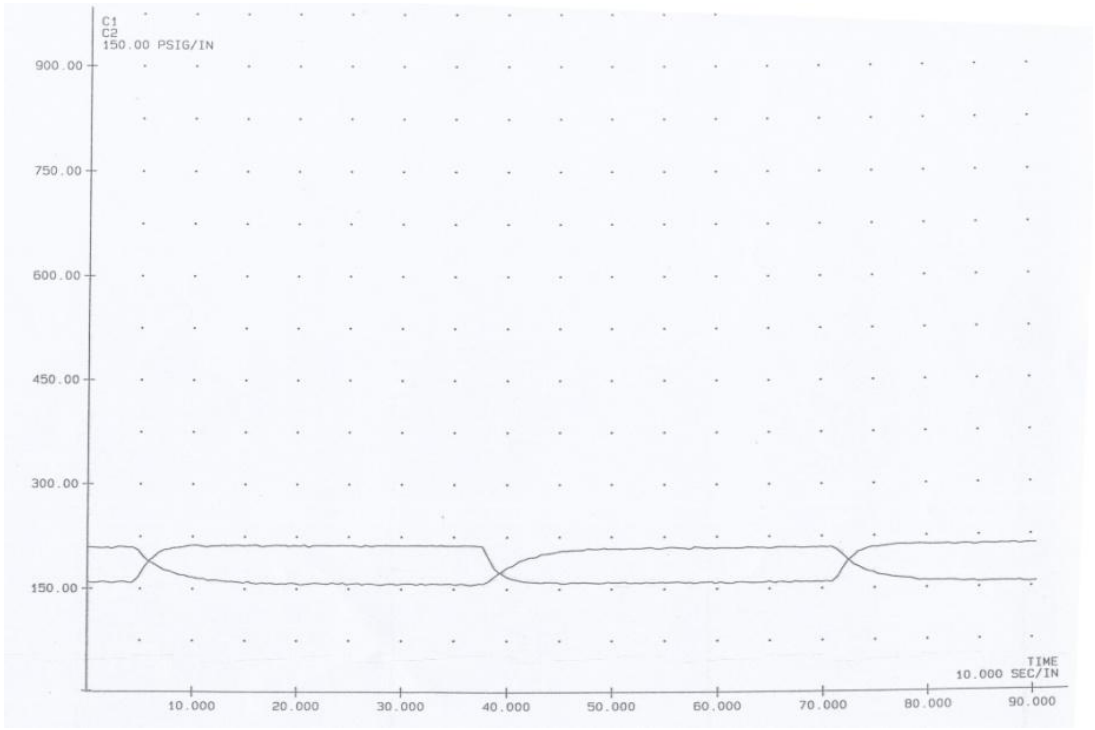

Figure F-5 Test result for 0.5 mA square wave current input